Departamento de Biología Molecular

Facultad de Ciencias

Universidad Autónoma de Madrid

Role of MASTL in mammals: Molecular functions and physiological relevance

Belén Sanz Castillo

Degree in Biotechnology

Thesis Directors:

Dr. Marcos Malumbres

Dra. Mónica Álvarez Fernández

Centro Nacional de Investigaciones Oncológicas (CNIO)

Madrid, 2017

Marcos Malumbres Martínez, Jefe del Grupo de División Celular y Cáncer del Centro Nacional de Investigaciones Oncológicas (CNIO) y, Mónica Álvarez Fernández, Investigadora del Grupo de División Celular y Cáncer del CNIO.

Certifican: que Belén Sanz Castillo ha realizado bajo su dirección el trabajo de Tesis Doctoral titulado: "Role of MASTL in mammals: Molecular functions and physiological relevance" en el Centro Nacional de Investigaciones Oncológicas y tutelada en el departamento de Biología Molecular de la Universidad Autónoma de Madrid.

Revisado el presente trabajo, considera que reúne todas las condiciones requeridas por la legislación vigente y la originalidad y calidad científica para su presentación y defensa con el fin de optar al grado de Doctor.

Y para que conste donde proceda, firmamos el presente certificado.

Dr. Marcos Malumbres Martínez

Dra. Mónica Álvarez Fernández

A mi familia

"Tu llegada allí es tu destino. Mas no apresures nunca el viaje. Mejor que dure muchos años y atracar, viejo ya, en la isla, enriquecido de cuanto ganaste en el camino"

Constantino Cavafis

Acknowledgements

Esta tesis hubiera sido completamente imposible sin la ayuda y apoyo de muchas personas. En primer lugar Marcos, muchas gracias por haberme acogido en tu laboratorio, aún recuerdo cuando llegué cargada de ilusión y ahora pienso que no podría haber escogido un sitio mejor. Gracias por tu entusiasmo, pasión y fuerza que nos transmites a cada uno de los que trabajamos contigo. Por supuesto quiero agradecerte haberme dado la oportunidad de trabajar en este apasionante proyecto junto a Mónica. No podía haber tenido una mejor co-directora de tesis, ella ha sido mi gran apoyo y todo esto hubiera sido completamente imposible sin tu trabajo, ayuda, compresión, y apoyo incondicional. Gracias por escucharme, por nuestras innumerables discusiones, ideas, y por estar siempre ahí. No tengo palabras para agradecerte todo lo que me has apoyado, así que simplemente mil gracias y porque has conseguido sacar lo mejor de mí. No ha sido fácil encontrar el camino pero al final, como dice Guille, "todo esfuerzo tiene su recompensa". Y es verdad, Guille es una fuente de sabiduría, en todos los sentidos. El otro gran pilar de este laboratorio, incansable e insaciable por la ciencia, siempre dispuesto a ayudar, a colaborar y a tenderte una mano en todo lo que necesitas. María Salazar, gran científica y mejor persona. Aportas serenidad, siempre son brillantes ideas, muchas gracias por tus consejos y tu ayuda en este proyecto. Bego, siempre con una sonrisa dispuesta a ayudar, por la alegría que transmites, y por todo lo que me has enseñado y ayudado también con los ratoncillos. Carol, muchas gracias por escucharme, ayudarme y preocuparte por mí. De vosotros he aprendido que no hay que rendirse nunca.

A María Guirola gracias por cuidar del labo y hacernos el trabajo mucho más sencillo. Y a la juventud del laboratorio, por el buen ambiente que creáis y vuestra alegría. Filipa, María Maroto, María Sanz y Diego, compañeros de tesis, juntos hemos aprendido mucho, gracias por vuestro apoyo y por ser como sois! Eli siempre con una sonrisa y por el buen rollo que transmites. No podía olvidarme de Aisha, la persona con más mano para los ratoncillos que conozco!, sabes que sin tu ayuda los experimentos de los ratoncillos hubiera sido imposible, hasta a mi me salvaste alguna vez ☺. Paloma, tu eres una más del labo, ha sido muy divertido pero por supuesto gracias siempre por tu ayuda. Alejandro por tu granito de arena con los mutantes, buen trabajo! Y a los que estáis recién llegados, Pepe y Bea, muchas gracias también. Que voy a deciros, creáis el mejor ambiente para trabajar y ha sido un placer trabajar con vosotros, esta tesis hubiera sido imposible sin vuestro apoyo!

No podía olvidarme de los que ya se fueron, pero que pasamos mucho tiempo juntos. Manu, Elena, Ale, Marianna, creía que no iba a llegar este momento pero ya estoy aquí!

Vosotros me acogisteis cuando llegué al labo y aprendí mucho de todos vosotros. Elena, gracias por tus consejos y Marianna, por tu fuerza, y consejos. A David, Iñaki y Eva, fue un placer trabajar con vosotros, al final estuvimos juntos casi 3 años, como pasa el tiempo… David, siempre dispuesto a ayudar, quiero agradecerte todo lo que nos ayudaste y a mi especialmente también con los ratoncillos. Iñaki por tu serenidad y Eva por esas risas. Y también me acuerdo de esas cervezas, botellines, cenas y esas risas que, de vez en cuando, nos hemos echado. Gracias a todos!

Summary/Resumen

MASTL is a Ser/Thr kinase first identified in *Drosophila* and *Xenopus* as a protein required for mitosis. MASTL inhibits, through phosphorylation of ENSA and ARPP19, the phosphatase PP2A in complex with the B55 family of regulatory subunits. In this work, we describe that Mastl is essential for mitotic progression in mouse embryonic fibroblasts (MEFs) derived from a conditional loss-of-function mouse model for *Mastl*, through inhibition of PP2A/B55 complexes. Mastl mediated inhibition of PP2A/B55 prevents premature dephosphorylation of CDK1 phosphosubstrates that are essential for chromosome condensation and segregation, and proper progression through mitosis. This proliferative role of Mastl is essential *in vitro* in cell culture and *in vivo*. Work done in a mouse model for Mastl shows that ablation of *Mastl* in young mice results in mitotic aberrations, severe proliferative defects and rapid death after *Mastl* depletion. Deletion of *Mastl* in elder mice, in contrast, causes less severe proliferative problems and improved survival. Nevertheless, Mastl depletion in adult mice also leads, in the long term, to impaired tissue regeneration, altered tissue homeostasis and eventual death of the mice.

Although PP2A/B55 is a phosphatase that regulates multiple cellular processes, the only function attributed so far to the PP2A/B55-inhibitory kinase MASTL in mammals is its role in mitosis. Aiming to identify new functions of MASTL, we have explored other potential cell cycle-dependent and independent functions of MASTL. Whereas Mastl was not required for S-phase entry or maintenance of the quiescence state, we have found a new and unexplored role for the MASTL-PP2A/B55 pathway in the control of insulin signaling downstream of mTORC1.

The mTORC1/S6K1 axis triggers a negative feedback loop that inhibits the upstream PI3K pathway, which in turn, is also important for controlling mTORC1 activity. We have found that MASTL-mediated PP2A/B55 inhibition prevents the activating dephosphorylation of the feedback target proteins, IRS1 and GRB10, and is required to fine-tune the feedback-mediated inhibition of the PI3K/AKT pathway and its metabolic consequences. Interestingly, MASTL activity is also modulated downstream of the mTORC1/S6K1 axis in conditions of feedback activity.

This feedback loop is physiologically relevant *in vivo* for metabolic diseases involving insulin resistance, such as obesity or type 2 diabetes. Importantly, we have found that depletion of *Mastl* improves glucose tolerance in a mouse model of high fat diet-induced obesity, and lowers basal glycaemia in old mice. This data together indicate that MASTL, through the inhibition of PP2A/B55, has a new mitotic-independent function in mammals in the control of PI3K/AKT-mTORC1 signaling and cooperates to control glucose homeostasis *in vivo*.

MASTL fue identificada por primera vez en *Drosophila* y *Xenopus* como una quinasa requerida para mitosis. MASTL inhibe, a través de la fosforilación de ENSA y ARPP19, los complejos de la fosfatasa PP2A con subunidades reguladoras de la familia B55. En este trabajo hemos demostrado que MASTL también es esencial para la progresión a través de mitosis en fibroblastos embrionarios de ratón del modelo condicional de pérdida de función de Mastl, mediante la inhibición de PP2A/B55. La inhibición de PP2A/B55 por MASTL previene la desfosforilación prematura de los epítopos fosforilados por CDK1, los cuales son esenciales para la condensación y segregación de los cromosomas, y la progresión a través de mitosis. Los estudios realizados en el modelo condicional demostraron que la eliminación de Mastl en ratones jóvenes resulta en aberraciones mitóticas y defectos proliferativos severos que comprometen la supervivencia rápidamente después de la eliminación de Mastl. Por el contrario, la depleción de Mastl en ratones adultos, resulta en defectos proliferativos menos severos y mayor supervivencia. La eliminación de Mastl a largo plazo resulta, sin embargo, en pérdida de capacidad regenerativa y homeostasis de los tejidos que finalmente provoca la muerte.

Aunque PP2A/B55 es una fosfatasa que regula múltiples procesos, la única función atribuida hasta la fecha a su quinasa inhibitoria, MASTL, es por ahora su papel en mitosis. Mientras que MASTL no es esencial para la entrada en fase S o para el mantenimiento de quiescencia, hemos encontrado una nueva función de la vía MASTL-PP2A/B55 en el control de la ruta de señalización de insulina regulada por mTORC1.

El módulo PI3K/AKT-mTORC1 acopla la presencia de nutrientes, energía y factores de crecimiento con el crecimiento, proliferación y metabolismo celular. mTORC1/S6K1 lanza un circuito de retroalimentación negativo (*negative feedback loop)* que inhibe la vía de PI3K/AKT después de su activación. Hemos descubierto que la inhibición de PP2A/B55 mediada por MASTL previene la desfosforilación de las proteínas fosforiladas por mTORC1/S6K1, IRS y GRB10, y es necesaria para regular la inhibición de AKT mediada por mTORC1 y sus consecuencias metabólicas. Además, la actividad catalítica de MASTL está regulada de manera dependiente de mTORC1/S6K1 en condiciones de inhibición de AKT.

La regulación retroactiva de la ruta PI3K/AKT-mTORC1 es importante *in vivo,* dado que su desregulación está implicada en enfermedades metabólicas de resistencia a la insulina, como obesidad o diabetes tipo 2. Nuestros resultados muestran que la eliminación de Mastl mejora la tolerancia a la glucosa en un modelo de ratón de obesidad inducida por dieta grasa y disminuye la glicemia basal en ratones adultos. En conjunto, estos resultados indican que MASTL desarrolla una función independiente de mitosis en mamíferos, en la que regula la vía de señalización de PI3K/AKT/mTORC1 y ayuda a mantener la homeostasis de la glucosa *in vivo.*

Index

Abbreviations

2-DG	2-Deoxy glucose
AGC	Protein kinase A, Protein kinase G, Protein kinase C - family
ATP	Adenosine Triphosphate
ATCC	American Type Culture Collection
B2M	Beta-2-Microglobulin
BCA	Bicinchoninic acid assay
CLS	Chronological Life Span
Cre	Cre DNA recombinase
Ctrl	Control
DAPI	4', 6-diamino-2-phenylindole
DMEM	Dubelcco's Modified Eagle's Medium
DOM	Duration of Mitosis
Dox	Doxycycline
ECAR	Extracellular Acidification Rate
EDTA	Ethylene Diamine Tetra acetic Acid
EdU	5-ethynyl-2'-deoxyuridine
EGTA	Ethylene Glycol Tetra acetic Acid
FBS	Fetal Bovine Serum
dFBS	Dialyzed Fetal Bovine Serum
GAP	Guanine Associated Protein
GEF	Guanine Exchange Factor
GFP	Green Fluorescent Protein
Glc	Glucose
GPCR	G-Protein Coupled Receptor
GSIS	Glucose-Stimulated Insulin Secretion
H2B	Histone 2B
HE	Haematoxylin and Eosin
HEP	Humane End Point
HFD	High Fat Diet
HM	Hydrophobic Motif
HPRT	Hypoxanthine Phosphoribosyl Transferase 1
HTM	High-throughput Microscopy
IF	Immunofluorescence
IHC	Immunohistochemistry
Ins	Insulin
IP	Immunoprecipitation
M	Mitosis
MEF	Mouse Embryonic fibroblast
mRFP	Monomeric Red Fluorescent Protein
NEB	Nuclear Envelope Breakdown
NES	Nuclear Export Signal
NLS	Nuclear Localization Signal
NMR	Nuclear Magnetic Resonance
Ns	Not significant
OA	Okadaic Acid
OCR	Oxygen Consumption Rate
OXPHOS	Oxidative phosphorylation
PAS	Periodic Acid Schiff
PBS	Phosphate Buffer Saline
PCR	Polymerase Chain Reaction
PDL	Population Doubling Levels
PFA	Paraformaldehyde
PI	Propidium Iodide
PM	Plasma Membrane
Rapa	Rapamycin
RT	Room temperature
RTK	Receptor Tyrosine Kinases
SAC	Spindle Assembly Checkpoint

Scr	Scramble
SD	Standard Deviation
SDS-PAGE	Sodium Dodecyl Sulfate Polyacrylamide Gel Electrophoresis
SEM	Standard Error of the Mean
sgRNA	Small guide RNA
shRNA	Short hairpin RNA
siRNA	Small interference RNA
TAM	Tamoxifen
TCA	Tricarboxylic Acid Cycle
TMSP	Sodium 3-Trymethylsilylpropionate
WB	Western Blot
WT	Wild Type

1. Introduction

1.1 MASTL-PP2A/B55 pathway in mammals

1.1.1 MASTL/Greatwall: a PP2A-inhibitory kinase with critical roles in mitosis

Cell cycle progression is controlled by multiple enzymatic activities including protein phosphorylation, which are coordinated by a network of kinases and phosphatases. Mitotic entry is driven by the activation of the cyclin-dependent kinase 1 (CDK1)-cyclin B complexes, which are activated at the G2-M transition and promote a broad range of protein phosphorylations that result in ordered structural rearrangements in the cell, such as nuclear envelope breakdown (NEB), chromosome condensation, and spindle formation. Entry and maintenance of the mitotic state depends on the inhibition of phosphatases to promote CDK1-cyclinB activity through an autocatalytic amplification loop, and to prevent the premature dephosphorylation of CDK substrates (Álvarez-Fernández & Malumbres, 2014; Lindqvist et al., 2009). In mammals, protein phosphatase 2A (PP2A) is the main phosphatase that dephosphorylates CDK1-cycB target proteins, including those involved in the CDK1 auto-amplification loop. Mitotic exit, on the contrary, requires inhibition of mitotic kinases, activation of phosphatases, and degradation of other critical regulators. PP2A/B55 activity as a major phosphatase that counteracts CDK-substrate phosphorylation, is essential for mitotic exit (Wurzenberger & Gerlich, 2011) (**Figure 1**).

PP2A is a major proline-directed Ser/Thr phosphatase involved in cell cycle regulation. It is a heterotrimeric complex composed of a catalytic subunit C, a structural subunit A, and a regulatory subunit B that confers substrate specificity. In mammals there are 4 subfamilies of B regulatory subunits (B55, B56, PR72 and PR93). The B55 family of regulatory subunits is composed of four isoforms (α, β, γ, and δ), and *in vitro* confers specificity toward CDK substrate consensus sequences (proline-directed Ser/Thr sites). PP2A/B55δ is essential for dephosphorylation of CDK1 substrates and mitotic exit in *Xenopus* extracts (Castilho et al., 2009; Mochida et al., 2009). Depletion of B55α in HeLa cells delays mitotic exit and the re-assembly of postmitotic structures, such as nuclear envelope and Golgi apparatus (Schmitz et al., 2010), whereas depletion of both B55α and B55δ induces mitotic exit of metaphase-arrested cells in mouse embryonic fibroblasts (MEFs) (Manchado et al., 2010).

Rencently, a new cell cycle kinase has emerged linking CDK1 and PP2A activities in mitosis. MASTL (microtubule-associated Ser/Thr kinase-like protein), also known as Greatwall (Gwl) in *Xenopus* and *Drosophila*, is activated by CDK1 during mitotic entry and inhibits the activity of PP2A/B55 complexes in mitosis to prevent premature dephosphorylation of CDK1 substrates and maintain the mitotic state (Castilho et al., 2009; Mochida et al., 2009) (**Figure 1**).

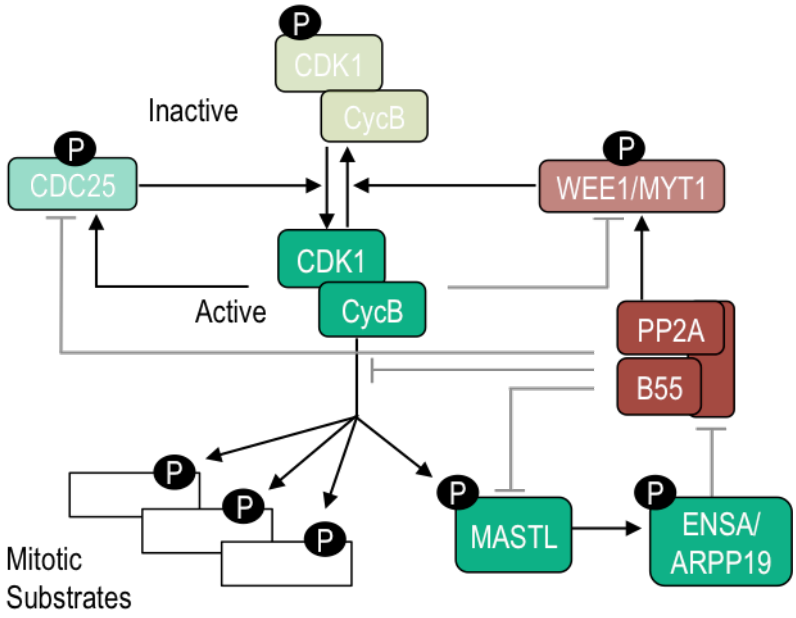

Figure 1. Regulatory interactions between CDK1 and PP2A and their control by MASTL/Gwl. CDK1 is inhibited by WEE1/MYT1-dependent phosphorylation and activated by CDC25 phosphatases that counteract inhibitory phosphorylation. Activity of these proteins is controlled by CDK1 and PP2A. CDK1 activate its activators and inhibits its inhibitors, and these processes are reverted by PP2A/B55 activity. MASTL, which is activated by CDK1 and inactivated by PP2A/B55, is able to inhibit PP2A/B55 complexes through direct phosphorylation of endosulfines. All these regulatory loops modulate the phosphorylation of a wide spectrum of substrates whose phosphorylation controls mitotic entry and progression. Adapted from (Álvarez-Fernández & Malumbres, 2014).

MASTL/Gwl was originally identified in *Drosophila* as a protein required for DNA condensation and normal progression through mitosis (Yu et al., 2004). Gwl mutant cells displayed a delayed entry into mitosis, with spindle aberrations and chromosome condensation and segregation defects, a function that was later on shown to be conserved in mammalian cells. RNA interference studies in cultured HeLa cells showed that depletion of MASTL results in inefficient mitotic entry, mitotic defects and deficient phosphorylation of CDK1 substrates, which can be partially rescued by PP2A inhibition (Burgess et al., 2010; Voets & Wolthuis, 2010). In contrast to fly and mammals, depletion of Gwl from *Xenopus* extracts prevents mitotic entry (J. Yu et al., 2006), and the concomitant inhibition of PP2A/B55 rescues defective mitotic entry (Vigneron et al., 2009). Additionally, studies in *Xenopus* oocytes and other organisms reported the involvement of Gwl in meiosis, as activation of Gwl promotes meiotic resumption through inhibition of PP2A/B55 (Vigneron et al., 2016).

1.1.2 MASTL inhibits PP2A through phosphorylation of ENSA and ARPP19

Studies in *Xenopus* egg extracts showed that MASTL/Gwl inhibits PP2A/B55 indirectly through phosphorylation of two substrates of the endosulfine family, α-endosulfine (ENSA) and cAMP-regulated phosphoprotein (ARPP19) (Aicha Gharbi-Ayachi et al., 2010; Mochida et al., 2010) (**Figure 1**). These two 20-kDa proteins share high homology and are phosphorylated by MASTL on a unique serine residue (S67 and S62 of human ENSA and ARPP19, respectively), in turn, this phosphorylation is counteracted by PP2A/B55. MASTL-mediated phosphorylation of ENSA and ARPP19 promotes their binding to the active site of PP2A/B55 complexes, and inhibits its phosphatase activity through a mechanism termed 'inhibition by unfair competition'. That means that ENSA/ARPP19, when phosphorylated, bind very efficiently but are very slowly dephosphorylated by PP2A/B55 compared to other substrates, until progressive dephosphorylation reduces its affinity and allow reactivation of the phosphatase and complete dephosphorylation and release of its inhibitor (Williams et al., 2014).

Besides MASTL/Gwl-dependent phosphorylation, ENSA and ARPP19 can be also phosphorylated by protein kinase A (PKA) and CDK1-cycB at different sites. In *Xenopus* egg extracts phosphorylation of endosulfines by CDK1 alone does not generate inhibitory activity against PP2A/B55 (Mochida, 2014), and mitotic entry is impaired in the absence of Gwl. In Starfish oocytes, by contrast, Cdk1-dependent phosphorylation of Arpp19 inhibits PP2A/B55 via a Gwl independent mechanism and is sufficient to promote mitotic entry. Whereas the role of PKA-mediated phosphorylation is not well understood, it is proposed that PKA-mediated phosphorylation of endosulfines could impair MASTL-mediated phosphorylation or decrease its binding affinity to PP2A/B55, since PKA inhibition promotes Cdk1-cyclinB re-activation and meiotic resumption (Dupre et al., 2014). Although the relative contribution of Cdk1 and PKA to the regulation of ENSA and ARPP19 is yet not fully understood, they might participate in the fine modulation of PP2A to confer the correct timing of inhibition under different *in vivo* conditions (Lorca & Castro, 2012; Mochida, 2014).

1.1.3 Regulation of MASTL activity

MASTL and its close relatives MAST1-4 constitute a poorly studied branch of the AGC kinase family. MASTL is an atypical member of the AGC family as it contains a non-conserved insertion of around 550 amino acids (termed non conserved middle region; NCMR) splitting the catalytic kinase domain into two separate N-terminal and C-terminal lobes. The mechanism by which MASTL is activated at mitotic entry is poorly understood (Blake-Hodek et al., 2012) (**Figure 2**).

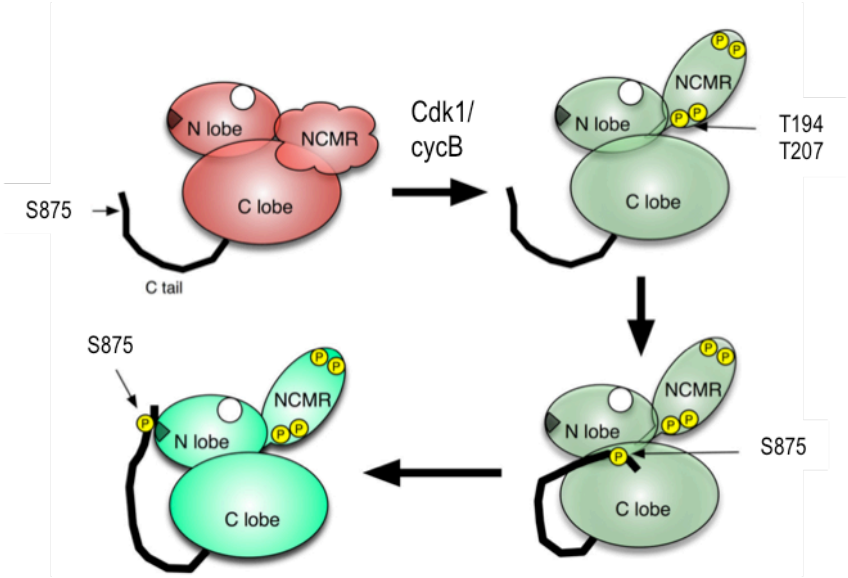

Figure 2. Model of MASTL activation. MASTL is depicted with four domains: the N-terminal lobe (N lobe), the C-terminal lobe (C lobe), the nonconserved middle region (NCMR), and the C-terminal tail (thick black line). During M phase entry, CDK1-cyclinB phosphorylates MASTL at the presumptive activation T-loop sites T194 and T207. After MASTL is primed by phosphorylation at the T-loop, S875 in the C-terminal tail can be autophosphorylated. It is likely that phosphorylated S875 can subsequently interact with a patch of basic residues in the N-lobe (dark triangle) to help stabilize active MASTL. The round hole in the N lobe depicts the putative conserved hydrophobic binding pocket, whose role is not yet clear. Adapted from (Blake-Hodek et al., 2012).

Activating phosphorylations in MASTL are located within its N-terminal region, including the T194 and T207, which probably function as activating T-loop phosphorylation and are targeted by CDKs, explaining at least in part how MASTL is turned on at mitotic entry (Blake-hodek et al., 2012). The C-terminal tail (known as the turn motif in PKA or the tail/Z site in growth factor-stimulated AGC kinases) is a critical region whose phosphorylation is normally required for conformational changes and kinase activity. In fact, autophosphorylation at S875 is considered a major pre-requisite for full activation of MASTL, and mutations of this residue to alanine impairs MASTL activity (Blake-Hodek et al., 2012; Vigneron, Gharbi-ayachi, et al., 2011). This phosphorylated residue in the C-tail probably interacts with a basic patch on the enzyme's N-terminal lobe to help stabilize the active conformation. Apart for the already described regulation of MASTL by CDKs in a mitotic context, nothing is known about the putative contribution of other kinases to MASTL regulation in other cellular contexts. Due probably to the fact that MASTL is a large kinase, many different phosphorylated sites in MASTL have been detected, event though little is known about their relative contribution to the regulation of MASTL activity or the putative kinases upstream of MASTL regulating these sites (Blake-Hodek et al., 2012).

At least three phosphatases, protein phosphatase 1 (PP1), Fcp1 and PP2A-B55 itself, have been reported to be involved in the inactivation of MASTL during mitotic exit, although the precise mechanism of MASTL inactivation is not understood yet (Vigneron et al., 2016).

1.1.4 Role of the MASTL-PP2A/B55 pathway in physiology and disease

Besides its essential function in the control of mitosis and meiosis, the only additional function attributed to MASTL so far is in the DNA-damage checkpoint recovery (Peng et al., 2010). Probably due to the fact that all these data emerged relatively recently, little is known about the physiologycal relevance of MASTL in mammals or its implications in human disease.

The first association of *MASTL* with disease was the discovery of a missense mutation in the human gene (*MASTL*, FLJ14813) on chromosome 10 that linked *MASTL* to a novel form of autosomal dominant inherited thrombocytopenia (Gandhi et al., 2003). In addition, MASTL has been recently related to cancer as it is overexpressed in specific tumors types, such as oral squamous carcinoma, colon cancer and neuroblastoma (Dahlhaus et al., 2016; Vera et al., 2015; Wang et al., 2014), and MASTL inhibition might have a therapeutic benefit (Anania et al., 2015; Nagel et al., 2015). A recent study also suggested that MASTL might promote cell transformation in an ENSA/ARPP19-PP2A-independent manner by hyperactivating AKT (Vera et al., 2015).

PP2A is considered a major tumor suppressor in multiple malignancies. Aberrant expression, mutations and somatic alterations of the PP2A scaffold and regulatory subunits have been detected in several tumor types (Eichhorn et al., 2009). For instance epigenetic silencing by hypermethylation of B55β subunit, encoded by *PPP2R2B*, occurs in almost all colorectal cancer samples analyzed (Tan et al., 2010). Similarly, deletions of *PPP2R2A*, the gene encoding B55α, have been found in a significant fraction of luminal breast tumors (Curtis et al., 2012). On the contrary, B55α has been shown to be overexpressed in pancreatic ductal adenocarcinoma tissue and required for sustained hyperactivity of the AKT, ERK and WNT oncogenic pathways in pancreatic cancer (Hein et al., 2016). In a different work, PP2A/B55α is required for HIF1α stabilization and promotes survival under hipoxia and glucose starvation in different breast cancer cell lines (Conza et al., 2017; Di Conza et al., 2017).

PP2A/B55 complexes function in many different pathways in the cell and, as such, control other cellular or physiological functions in addition to cell cycle progression. Nevertheless, it is not known to what extent all these PP2A/B55-dependent functions are also mediated by MASTL, and, therefore, MASTL might also be relevant for other biological processes beyond cell cycle regulation.

1.2 Role of Rim15 and Ppk18, the yeast MASTL kinases

1.2.1 Conservation of the MASTL-endosulfine-PP2A/B55 pathway

The MASTL-ENSA/ARPP19-PP2A/B55 pathway is evolutionary conserved from yeast to mammals. Rim15, the budding yeast orthologous of MASTL kinase, phosphorylates the endosulfine proteins Igo1/2, the two orthologous of human ENSA and ARPP19, at the site equivalent of their vertebrate counterparts to promote binding to and directly inhibit the phosphatase PP2A/Cdc55, the yeast orthologous of PP2A/B55 proteins (Bontron et al., 2013; Talarek et al., 2010) (**Figure 3**). The evolutionary conservation of the pathway is further strengthened by the finding that Rim15 phosphorylates *in vitro* human ENSA and ARPP19 endosulfines in their equivalent site, and that human ENSA and ARPP19 are able to partially replace Igo1/2 function in budding yeast (Juanes et al., 2013; Talarek et al., 2010). In addition, yeast endosulfines can be phosphorylated by MASTL/Gwl and promote mitotic entry in *Xenopus* egg extracts (Juanes et al., 2013). The MASTL-endosulfine-PP2A regulatory module appears to be conserved in all organisms analyzed to date, with the notable exception of the nematode *C. elegans* where and obvious MASTL-like kinase seems to be missing (M. Y. Kim et al., 2012) (**Figure 3**).

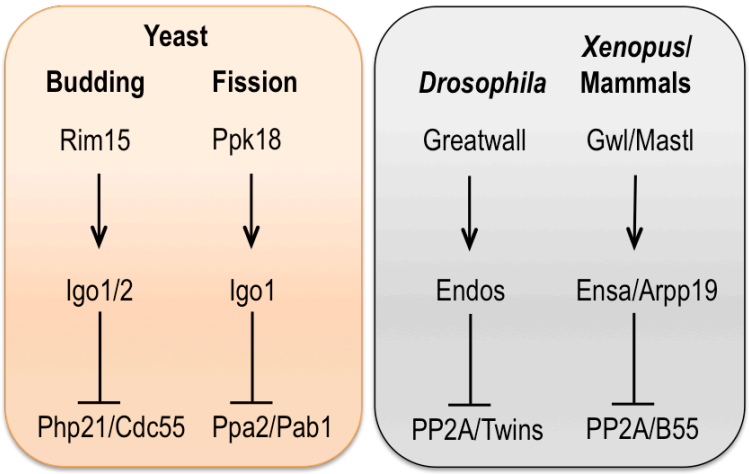

Figure 3. Conservation of the MASTL-ENSA/ARPP19-PP2A/B55 pathway from yeast to mammals. MASTL/Gwl inhibits PP2A/B55 complexes through phosphorylation of Ensa and Arpp19 proteins.

1.2.2 Regulation of Rim15 and Ppk18 by nutrient-regulated pathways

Eukaryotic cell proliferation is controlled by growth factors and essential nutrients, in the absence of which cells cease growing, reversible arrest cell division and enter into a quiescent state (also known as G_0 state) (Malumbres & Barbacid, 2001). In yeast, the decision of cells to initiate, or

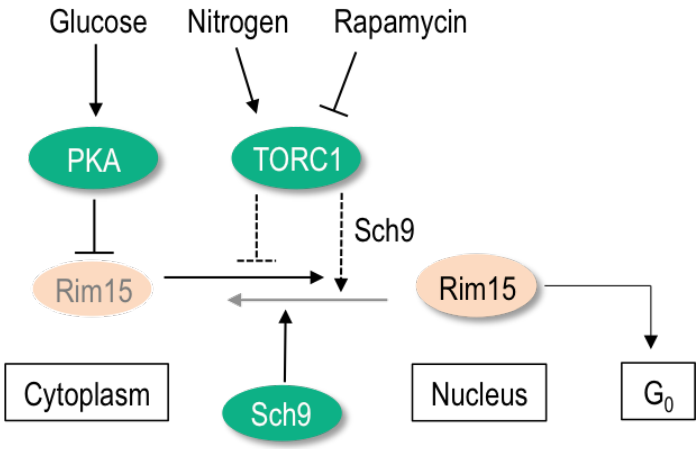

Figure 4. Control of Rim15 activity by PKA, TORC1 and Sch9 pathways in budding yeast. PKA phosphorylates and inhibits Rim15, whereas TORC1 and Sch9 retain Rim15 in the cytoplasm. Dashed lines indicate indirect regulation by a not fully understood mechanism. Adapted from (Pedruzzi et al., 2003)

not, the quiescence program relies on the conserved nutrient signaling pathways of TORC1 and PKA, which are responsive to the abundance in the media of nitrogen and/or carbon, and glucose, respectively. Rim15 integrates signals from these nutrient-dependent protein kinases, and initiates a program to mediate entry into quiescence (de Virgilio, 2012). Rim15 is activated upon nutrient limitation, and its activation requires its nuclear accumulation and Rim15 autophosphorylation (Pedruzzi et al., 2003) (**Figure 4**). Rim15 amino acid sequence has five consensus sites for PKA, and Rim15 kinase activity is under the direct and negative control of Ras2/PKA pathway *in vitro* (Reinders et al., 1998). Rim15 is also inhibited by TORC1, which retains Rim15 in the cytoplasm and impairs its kinase activity (Pedruzzi et al., 2003). However, TORC1-mediated inhibition of Rim15 is indirect through the inhibition of a phosphatase and/or activation of a alternative kinase (Wanke et al., 2005). Sch9, the yeast orthologous of AKT and/or S6K1, signals the combined presence of glucose and nitrogen and negatively regulates Rim15, even though the mechanism is not fully understood (Fabrizio et al., 2001). Sch9, like TOR, is required for the cytoplasmic retention of Rim15. However, unlike rapamycin-induced hyperphosphorylation of Rim15, Rim15 was not hyperphosphorylated in the absence of Sch9, suggesting that TOR and Sch9 are likely to regulate Rim15 function via two different mechanisms (Pedruzzi et al., 2003).

As in budding yeast, the fission yeast MASTL kinase, Ppk18, is also negatively regulated by TORC1 and PKA pathways, and links nutrient status to mitotic size control. Ppk18 protein sequence contains several phosphorylation sites for fission yeast S6K1 kinase, which phosphorylates Ppk18 in nitrogen-rich medium and inhibit its activity (Chica et al., 2016).

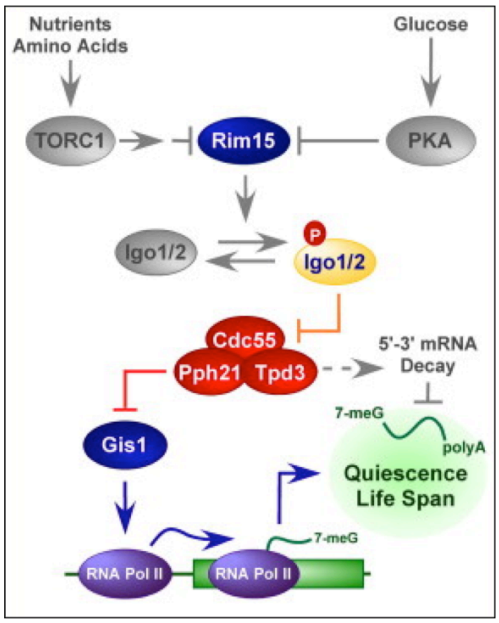

Figure 5. Role of Rim15 in the control of quiescence and stress resistance. In budding yeast nitrogen and carbon limitation causes activation of the Rim15 kinase to promote the transcription of genes required for G_0 program initiation through two mechanisms: i) Rim15 through inhibition of PP2A/Cdc55 promotes Gis1-mediated transcription. ii) Rim15-mediated phosphorylation of Igo1/2 proteins license specific mRNAs to evade de 5'-30 mRNA decay pathway (Bontron et al., 2013).

1.2.3 Role of the Rim15-Igo1/2-PP2A/Cdc55 pathway in the control of quiescence in budding yeast

Rim15 was described for first time in *S. cerevisiae*, as a protein essential to promote initiation of the quiescence program and ensure maximal survival in the stationary phase (e.g. following growth for 5 days), also known as chronological life span (CLS). Cells that lack Rim15 failed to properly enter quiescence after entry into stationary phase and nutrient limitation, had reduced survival, defects in glycogen accumulation and lower capacity to resume proliferation(Fabrizio et al., 2001; Pedruzzi et al., 2003; Reinders et al., 1998). Rim15 ensures this function by controlling the expression of specific stress- and nutrient-regulated genes implicated in G_0 arrest through a dual role of Rim15 (**Figure 5**). The first one involves direct activation of gene transcription through phosphorylation of Igo1/2 and inhibition of the phosphatase PP2A/Cdc55 (Bontron et al., 2013). Inhibition of PP2A/Cdc55 activates the transcription factor Gis1 and induces the expression of specific nutrient-regulated genes. Rim15 also up-regulates expression of genes involved in stress response through the transcription factors Msn2/4 (Cameroni et al., 2004). The second mechanism is mediated by Rim15-dependent phosphorylation of Igo1/2 proteins independently of PP2A/Cdc55 and involves the stabilization of specific mRNAs by preventing its degradation via 5'-3' mRNA decay pathway (Luo et al., 2011; Talarek et al., 2010).

Altogether these data places Rim15 as critical mediator downstream of nutrient regulated pathways, to control entry into quiescence and CLS after nutrient deprivation. Because orthologous of many genes in this network are known to affect aging in higher eukaryotes, these results might point to similar mechanisms in mammalian cells (M. Wei et al., 2008).

1.2.4 Other functions of the MASTL-endosulfine-PP2A/BB5 pathway in yeast

New targets of the Rim15-Igo1/2-PP2A/Cdc55 pathway have been recently described in yeast suggesting the involvement of Rim15 in other aspects of nutrient regulated pathways. Rim15 promotes autophagy under nutrient-limiting conditions and TORC1 inhibition through the inhibition of Rph1, a transcriptional repressor of autophagy-related genes, whose function is also conserved in mammals (Bernard et al., 2015).

The Rim15 pathway also coordinates the phosphorylation status of the CDK inhibitor Sic1, p27Kip1 in mammals, to couple TORC1 signaling with cell cycle progression. Following TORC1 inactivation, Rim15-mediated PP2A/Cdc55 inhibition stabilizes Sic1 and ensures G1 arrest (Moreno-torres et al., 2015).

In budding yeast, Rim15 controls timely mitotic progression through the conserved Igo1/2-PP2A/Cdc55 axis but with some remarkable differences compared to multicellular organisms (Juanes et al., 2013). In mitosis Rim15 activates, rather than inhibits PP2A/Cdc55, which in turn promotes mitotic entry, as PP2A/Cdc55 positively regulates the autocatalytic amplification of CDK1. Rim15 or Igo1/2 deletion had no significant effect in unperturbed mitosis, however under stress conditions delayed mitotic entry and mitotic defects become apparent (Juanes et al., 2013).

The MASTL-endosulfine-PP2A/B55 pathway is equally conserved in fission yeast, where Ppk18 and Pab1 are the fission yeast orthologous of MASTL and B55, respectively, and connect nutritional environment to the cell cycle machinery to control cell size (Chica et al., 2016). Fission yeast is a good model for studying mechanisms coupling cell growth and cell division, as the threshold of cell size necessary for cell division is determined by growth conditions. In the presence of nutrients, inhibition of Ppk18 by TORC1/S6K1 activates PP2A/Pab1 activity to prevent the activation of mitotic Cdk1, and cells increase in size before they divide. By contrast, in nutrient limiting conditions, TORC1 inhibition relieves Ppk18 activity and decreases PP2A/Pab1 activity therefore promoting Cdk1 activation and accelerated entry into mitosis with a smaller cell size (Chica et al., 2016).

1.3 Nutrient- and growth factor- regulated pathways in mammals

1.3.1 The mTOR signaling pathway

The mammalian target of rapamycin (mTOR) is a master regulator of cell growth, proliferation and metabolism and responds to a variety of extracellular and intracellular stimuli, including growth factors, nutrients, and energy. All cells must coordinate their metabolic activity with changes in their nutrient environment to grow and proliferate when nutrients are abundant. In this condition mTOR is activated and stimulates anabolic processes to synthetize essential building blocks such as proteins, lipids and nucleotides. As a central controller of organism growth and homeostasis, aberrant regulation of mTOR signaling has been implicated in cancer, metabolic, neurological, inflammatory and autoimmune diseases (Saxton & Sabatini, 2017).

mTOR belongs to the phosphoinositide 3-kinase (PI3K)-related protein kinases (PIKK) family, and exists in two functionally and structurally distinct complexes, mTORC1 and mTORC2 (Saxton & Sabatini, 2017). mTORC1 is comprised of three essential and evolutionary conserved core subunits: mTOR, RAPTOR (regulatory protein associated with mTOR) and mLST8 (mammalian lethal with Sec13 protein 8). RAPTOR facilitates substrate recruitment to mTORC1 through binding to the TOR signaling (TOS) motif found on several canonical mTORC1 substrates, and is

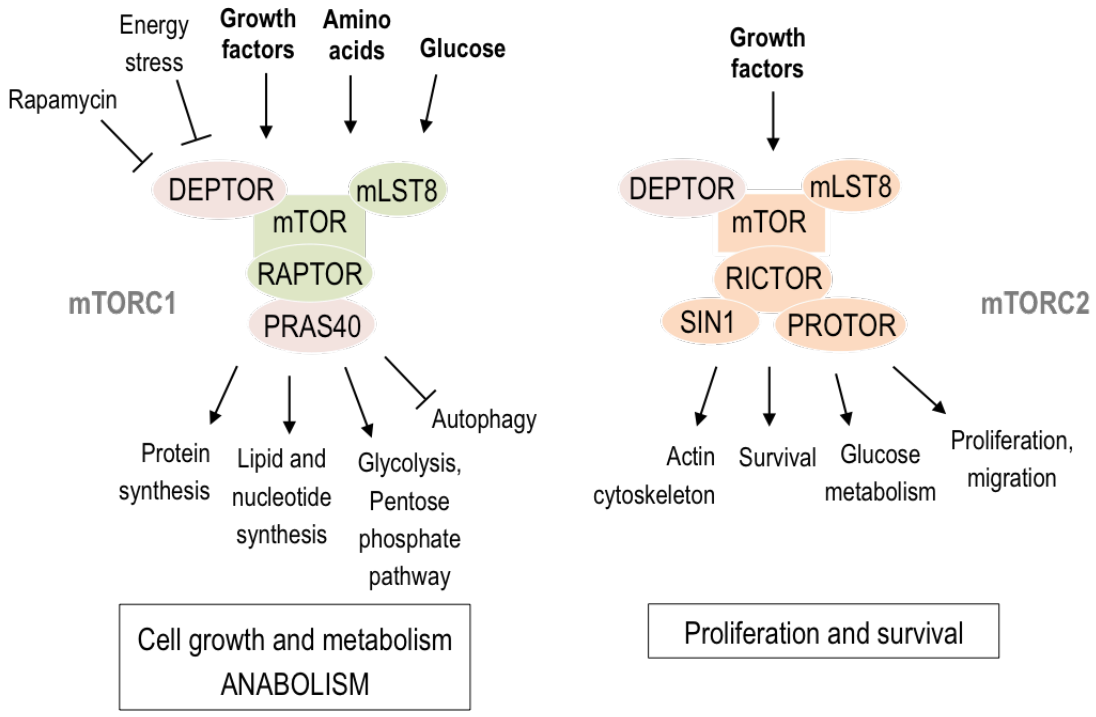

Figure 6. mTORC1 and mTORC2. Subunits of mTOR complexes, upstream regulators and major processes downstream mTOR signaling to help the cell coordinate nutrient input with biosynthetic output.

required for the correct subcellular localization of mTORC1. In addition to these three components, mTORC1 also contains two inhibitory subunits, PRAS40 and DEPTOR (**Figure 6**).

mTORC2 complex is distinguished by having RICTOR (rapamycin insensitive companion of mTOR) instead of RAPTOR, which also function as scaffold for assembling complexes and binding substrates. Additionally mTORC2 contains: mLST8, the regulatory subunits mSin1 and PROTOR1/2, and the inhibitory subunit DEPTOR (**Figure 6**). mTORC1 activity is sensitive to the rapamycin-FKB12 complex, which function as allosteric inhibitor. In contrast, rapamycin-FKB12 complex cannot interact with mTORC2, which is characterized by its insensitivity to acute rapamycin treatment, even though prolonged rapamycin treatment also abrogates mTORC2 signaling (Saxton & Sabatini, 2017).

1.3.2 Processes regulated downstream of mTOR

When activated, mTORC1 phosphorylates a number of substrates, the best characterized of which are S6K1 and 4E-BP1 that promote protein synthesis when phosphorylated at T389 and T36/47-S65, respectively (Saxton & Sabatini, 2017). Through phosphorylation of different substrates, mTORC1 promotes anabolic processes, including *de novo* lipid and nucleotide synthesis, and also inhibits autophagy (**Figure 6**). mTORC1 controls metabolism by enhancing glycolysis and the activity of the pentose phosphate pathway, thereby promoting the production of ATP and NADPH to support anabolic processes. mTORC1 signaling favors glycolysis by increasing the translation of hypoxia-inducible factor 1 (HIF1α), which induces the expression of the glucose transporter GLUT1 and glycolytic enzymes such as phospho-fructo kinase (PFK). In addition, mTORC1 and S6K1 have several substrates, including growth factor receptor-bound protein 10 (GRB10) and insulin receptor substrate proteins (IRS), which restrain insulin pathway activation upstream of mTORC1 forming a negative feedback loop.

mTORC2 instead controls proliferation and survival primarily by phosphorylating several members of the AGC family of protein kinases (Saxton & Sabatini, 2017). The most important function of mTORC2 is likely the phosphorylation and activation of the S/T AKT kinase, a key effector of insulin-PI3K signaling (**Figure 6**). mTORC2 also controls remodeling of the actin cytoskeleton and cell migration through phosphorylation of PKCs.

1.3.3 Signal integration by mTORC1

Systemic changes in the organism are sensed by mTORC1 through pathways activated by secreted growth factors, cytokines and hormones, and nutrients, as activation of mTORC1 is also

dependent on sufficient levels of intracellular amino acids, glucose and oxygen. Nutrients seem to be the more ancient input for mTORC1, as its activation in yeast depends exclusively on nutrient availability. In higher eukaryotes, cell culture experiments suggest that intracellular nutrients only basally activate mTORC1, but are essential for its robust stimulation by extracellular growth factors (Dibble & Manning, 2013).

In comparison to mTORC1, mTORC2 regulation is poorly understood. Growth factors and PI3K signaling stimulate mTORC2 activity, which is in part mediated through PI3K-dependent mTORC2-ribosome association (Zinzalla et al., 2011).

Below there is a description of the signaling pathways upstream of mTORC1 and the mechanisms through which they control mTORC1 activation:

a) Growth factors

Growth factor signaling pathways stimulate an acute and robust increase in mTORC1 activity. mTORC1 is activated by insulin and most other growth factors through either receptor tyrosine kinases (RTKs) or G-protein-coupled receptors (GPCRs) at the cell surface (Dibble & Manning, 2013; Saxton & Sabatini, 2017). Downstream of these receptors, two major signaling pathways are involved in mTORC1 activation: the phosphatidylinositol-3-OH kinase (PI3K)-AKT and RAS-ERK pathways (**Figure 7**), which are differentially activated downstream of specific receptors, with the PI3K/AKT pathway dominating downstream of the insulin and insulin-like growth factor (IGF) receptors. Growth-factor-dependent pathways stimulate mTORC1 signaling by inhibiting the tuberous sclerosis heterotrimeric complex (TSC) composed of TSC2, TSC1 and TBC1D7, whereby TSC1 stabilizes TSC2, and TSC2 acts as GTPase-activating protein (GAP). The TSC complex is a GAP for Rheb (Ras homolog enriched in brain), which is an essential mTORC1 activator present in the lysosomal membrane. Rheb activates mTORC1 when it is in its GTP-bound state, although the precise mechanism of how Rheb activates mTORC1 remains unknown. In response to growth factors, AKT-mediated phosphorylation of TSC2 on T1462 and S939 inhibits the TSC complex by inducing its dissociation from the lysosomal membrane, where Rheb localizes, without altering its GAP activity (Inoki et al., 2002; Manning et al., 2002; Menon et al., 2014). TSC inhibition relieves Rheb activity and allows mTORC1 activation at the lysosomal membrane. Downstream of the growth factor receptors, activation of RSK and ERK can also inhibit TSC2 by inducing its phosphorylation. RSK can phosphorylate TSC on the AKT sites, as well as other sites (Roux et al., 2004). Although, TSC complex is essential to inhibit mTORC1 signaling in the absence of growth factors, parallel mechanisms can also contribute to mTORC1 regulation, such as AKT-mediated phosphorylation and inhibition of PRAS40 on T246 (Vander

Haar et al., 2007). Additional growth factor pathways upstream of TSC include Wnt and the inflammatory cytokine TNFα pathways, both of which activate mTORC1 through the phosphorylation of TSC1 and the inhibition of the TSC complex (Saxton & Sabatini, 2017).

Of note, the TSC complex has also been linked to mTORC2 function. TSC complex interacts with mTORC2 and positively regulates its kinase activity by yet undefined mechanisms (Huang et al., 2008).

b) Amino acids

Amino acids are essential nutrients for mTORC1 activation. The primary amino acid sensing pathway involves the Rag GTPases, which are heterodimeric components that are tethered to the lysosomal membrane through their association to the Ragulator complex (Saxton & Sabatini, 2017). Amino acid stimulation converts the Rags to their active GTP-bound state, allowing them to bind RAPTOR and recruit mTORC1 to the lysosomal surface, where Rheb is located (**Figure 7**). This mechanism allows a very thigh control of mTORC1 activation by nutrients, whereby mTORC1 signaling is only on when both the Rags and Rheb are activated, explaining why both amino acids and growth factors are required for mTORC1 activation.

c) Glucose, oxygen and cellular energy levels

mTORC1 also responds to intracellular and environmental stresses that are incompatible with growth such as low cellular energy levels as a consequence of reduced glucose or oxygen availability (Dibble & Manning, 2013; Saxton & Sabatini, 2017). Cells respond to such changes by tipping the metabolic balance from anabolic to catabolic processes that produce energy, and as a major promoter of anabolic processes, mTORC1 is a key target in this metabolic adaptation.

Glucose controls mTORC1 through different mechanisms and is required for its activation. A reduction in energy levels, such as during glucose deprivation, activates AMPK, which promotes catabolic metabolism and activates autophagy. AMPK inhibits mTORC1 both indirectly, through phosphorylation and activation of TSC2 on T1387, as well as directly through phosphorylation and inhibition of RAPTOR on S792 (**Figure 7**) (Gwinn et al., 2008; Inoki et al., 2003). Interestingly, glucose deprivation still inhibits mTORC1 in cells lacking AMPK, through inhibition of the Rag GTPases and impaired lysosomal localization of mTORC1 (Efeyan et al., 2013; Kalender et al., 2010). MEFs that are homozygous for a constitutively active mutant of RagA are resistant to the inhibitory effects of either amino acid or glucose withdrawal on mTORC1 signaling (Efeyan et al., 2013), although the precise mechanism of glucose sensing upstream Rag GTPases is unknown.

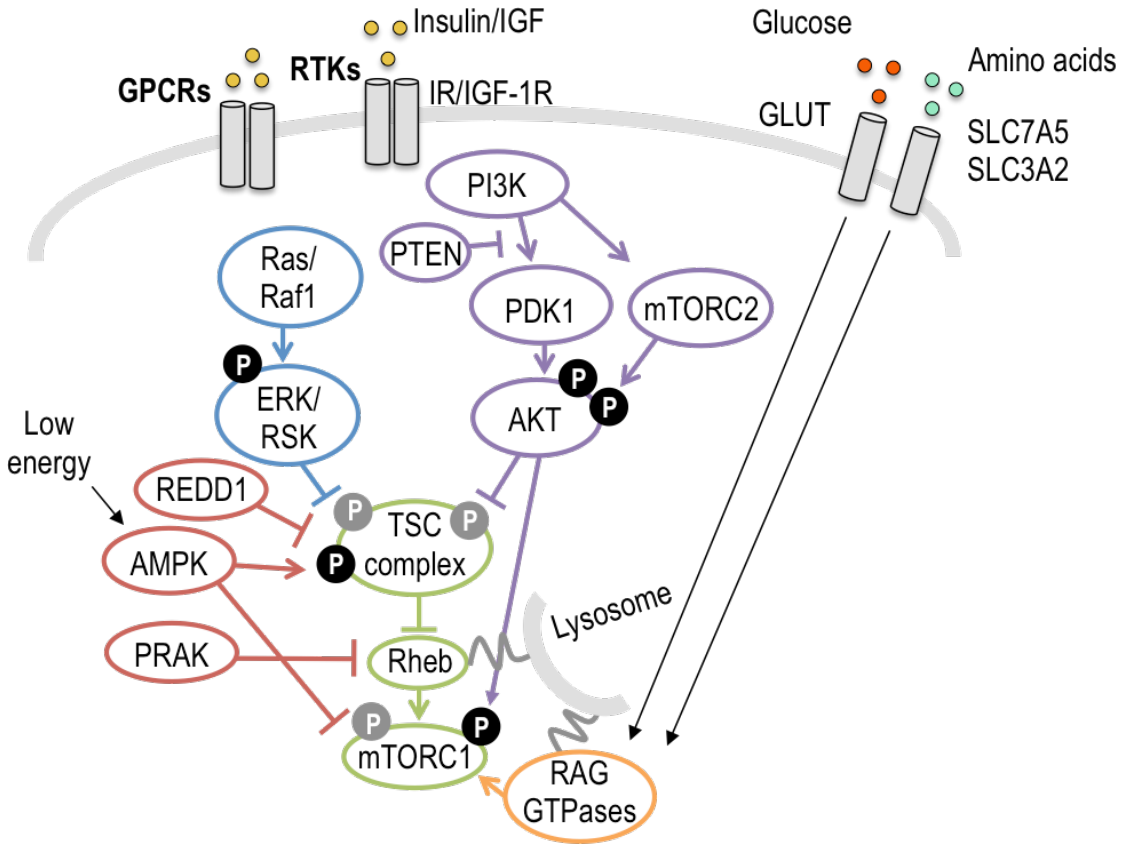

Figure 7. mTORC1 signaling network. Signaling pathways upstream of mTORC1. Growth factors and nutrients (e.g. glucose and amino acids) positively regulate mTORC1 signaling mainly through regulation of TSC complex and Rag GTPases, respectively. Low energy such as in conditions of glucose starvation or hypoxia inhibits mTORC1 signaling through different mechanisms, which are depicted in red. Inhibitory and activating phosphorylations are shown in grey and black, respectively.

Similarly, hypoxia inhibits mTORC1, in part through AMPK activation, but also through the induction of REDD1 mediated by HIF1α, which activates TSC (**Figure 7**) (Brugarolas et al., 2004). REDD1 is also required for the inhibitory effects of glucose starvation on mTORC1 activity (Sofer et al., 2005), but rather this effects result from the deletereous effects of glucose starvation on protein maturation and activation of the unfolded protein response in the endoplasmatic reticulum (ER), and ATF4-mediated transcription of REDD1.

In addition to the mechanisms discussed above, the p38-regulated/activated kinase (PRAK) is activated under energetic stress and is required to supress mTORC1 signaling through inhibition of Rheb (Zheng et al., 2011).

1.3.4 The PI3K-AKT pathway

AKT activation is initiated by growth factors and the stimulation of RTKs and GPCRs on the cell surface (Manning & Toker, 2017). Once activated, RTKs autophosphorylate, creating phosphotyrosine binding sites for the IRS family of scaffolding proteins, among others. IRS1 and IRS2 proteins are subsequently phosphorylated by the insulin and insulin-like growth factor (IGF-I) receptors on several tyrosine residues, which initiate signaling cascades by acting as binding sites for proteins containing src homology 2 domains, including the p85 regulatory subunit of PI3K. IRS-mediated activation of PI3K at the plasma membrane leads to the generation of the lipid second messenger phosphatidylinositol-3,4,5-triphosphate (PIP_3), which recruits a subset of proteins with pleckstrin homology domains, like AKT and PDK1. AKT is then activated upon recruitment to the plasma membrane by subsequent phosphorylation by mTORC2 at S473 in the hydrophobic motif and PDK1 at T308 in the T-loop (**Figure 9**). Phosphorylation of both residues is required for maximal activation of the kinase. Signal termination of PI3K-PIP_3 signaling is achieved by the phosphatase PTEN, which dephosphorylates PIP_3 converting it back to PIP_2. The initial synthesis of PI3K lipid products is observed within minutes after growth factor stimulation, exhibits a peak, and is then down regulated with a timing that depends on the cell type and stimulus. The transient nature of this signal is largely achieved by PTEN combined with other inactivation of PI3K (Manning & Toker, 2017). In addition to PTEN, two other phosphatases have been shown to inhibit AKT by inducing its direct dephosphorylation. PP2A in complex with B55α binds and dephosphorylates the T308 on AKT in murine lymphoid cells (Kuo et al., 2008), whereas the PH domain leucine-rich repeat protein phosphatases (PHLPP1 and PHLPP2) are responsible for S473 dephosphorylation (Gao et al., 2005).

AKT is a central node downstream of growth factors, and contributes to diverse cellular roles, which includes cell survival, growth, proliferation, migration, angiogenesis and metabolism (Manning & Toker, 2017). Aberrant loss or gain of AKT activation underlies the pathophysiological properties of a variety of diseases, including type-2 diabetes and cancer. Given the complexity and diversity of signaling downstream AKT, we will focus on AKT targets involved in this work, mostly related to glucose metabolism.

One of the most important physiological functions of AKT is to acutely stimulate glucose uptake in response to insulin through the induction of GLUT4 translocation to the plasma membrane (Sano et al., 2003) (**Figure 8**). The mechanism by which AKT stimulates GLUT4 translocation involves phosphorylation of the Rab-GAP AS160 (Sano et al., 2003), although other studies have suggested AS160-independent mechanisms and other AKT substrates involved in

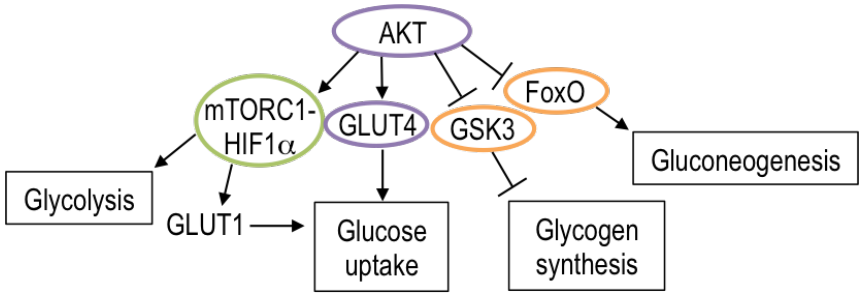

Figure 8. Substrates and functions of AKT involved in glucose uptake and metabolism. Positive and negative regulation of AKT is shown with arrows and flat bars, respectively.

this process (L. Bai et al., 2007). AKT can also positively regulate glucose uptake by upregulating the levels of GLUT1, which is the main glucose transporter in most cell types, and unlike GLUT4, it appears to be regulated through alterations in expression levels. AKT-mediated activation of mTORC1 contributes to HIF1α-dependent transcription of *GLUT1* gene and cap-dependent translation of *GLUT1* mRNA (Zelzer et al., 1998).

Upon entry into the cells glucose can be stored by conversion to glycogen or catabolized to produce energy through glycolysis, and AKT can regulate both processes. AKT increases the rate of glycolysis (Elstrom et al., 2004) due, at least in part, to its ability to promote expression of glycolytic enzymes through mTORC1-dependent induction of HIF1α transcription factor (Lum et al., 2007; Majumder et al., 2004). AKT phosphorylates and inhibits glycogen synthase kinase (GSK3) (Cross et al., 1995), which regulates a large set of targets, among them glycogen synthase activity whose activity is relieved by AKT stimulating glycogen synthesis, a process particularly important in muscle and liver. AKT phosphorylates and inhibits the Forkhead Box O (FoxO) family of transcription factors (Brunet et al., 1999), which are involved in diverse processes including induction of apoptosis, cell-cycle arrest, or gluconeogenesis, a process specially important in hepatocytes (Manning & Toker, 2017).

1.3.5 Feedback regulation of PI3K/AKT signaling by mTORC1/S6K1

The PI3K/AKT axis is subjected to negative feedback regulation after its activation, reflecting the necessity of putting a brake to excessive or chronic activation of the pathway. A very important negative feedback loop involves the inhibition of PI3K/AKT signaling by mTORC1/S6K1, which is also important for mTORC1 regulation itself (Efeyan & Sabatini, 2010). Apart from the inhibition of PI3K/AKT, this feedback loop is also responsible for inhibiting the activity of the Ras-ERK pathway (Carracedo et al., 2008). Feedback regulation occurs at different levels and restrains upstream signaling through insulin/IGF-I receptors as well as other receptor tyrosine kinases

(Rodrik-Outmezguine et al., 2011). Studies done in *TSC*-null MEFs, which show constitutive mTORC1 activation, uncovered a strikingly inability of serum, platelet-derived growth factor (PDGF), and specially insulin and IGF-I, to activate the PI3K/AKT. The insensitivity to PDGFR was due to a loss of expression of both PDGF receptors alpha and beta, and was mediated by S6K1 (Zhang et al., 2007). Two different studies showed that the mechanism of insulin/IGF-I resistance was consequence of constitutive down-regulation of IRS1 and IRS2 proteins due to sustained mTORC1 signaling, as rapamycin treatment of *TSC2*-deficient MEFs completely restored IRS protein levels and the sensitivity to insulin and IGF-I (Harrington et al., 2004; Shah et al., 2004). mTORC1 hyperactivation in *TSC2* null MEFs promotes multisite serine phosphorylation of IRS and triggers its degradation (Harrington et al., 2004; Shah et al., 2004) (**Figure 9**). Knockdown of S6K1 could restore the expression of IRS1 in *TSC2*-null MEFs (Harrington et al., 2004), and a kinase dead version of S6K1 blocked the negative feedback loop and restored the levels of activated AKT (Shah et al., 2004), further suggesting that S6K1 activity downstream of mTORC1 is involved in IRS phosphorylation and inhibition of AKT signaling.

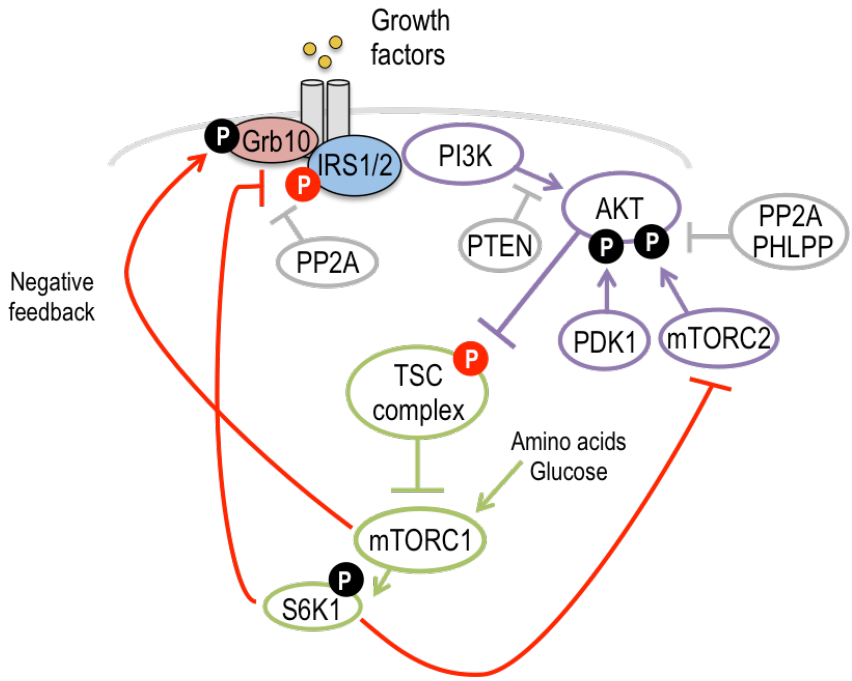

Figure 9. The PI3K/AKT signaling pathway and mTORC1-mediated feedback regulation. Growth factors stimulate activation of the receptors and signal transduction mediated by adaptor proteins containing SH2 domains to the PI3K/AKT signaling. Subsequent mTORC1/S6K1 activation triggers negative feedback loops to inhibit the PI3K pathway after its activation. Phosphatases counteract activating phosphorylations on events of the pathway, and are depicted in gray. Negative feedback loops are shown with red lines. Inhibitory phosphorylations are in red and activating phosphorylations in black.

Activation of mTORC1 by amino acids has been shown to attenuate insulin signaling through mTORC1-dependent effects on IRS1, which imply changes in phosphorylation, localization and/or degradation (Takano et al., 2001; Tremblay & Marette, 2001). Similarly, PI3K/AKT-mediated activation of mTORC1 in response to insulin or PDGF, also leads to multisite serine phosphorylation on IRS which induces its proteosomal degradation in a rapamycin sensitive manner (Carlson et al., 2004; Greene et al., 2003; Haruta et al., 2000) (**Figure 9**).

IRS-independent feedbacks have been also proposed, including mTORC1-dependent phosphorylation of GRB10, a negative adaptor protein of insulin and IGF-I signaling (Hsu et al., 2011a; Y. Yu et al., 2011). mTORC1 phosphorylates GRB10 at multiple sites stabilizing the protein and enhancing its ability to block PI3K/AKT activation. Additionally, a new non-cell autonomous mechanism of mTORC1-dependent feedback inhibition of the IGF-I pathway has been recently described. It involves mTORC1-HIF1α-dependent transcription of IGF binding protein 5 (IGFBP5), which blocks IGFR-I activation in the extracellular space, and synergizes with GRB10 (Ding et al., 2016). Interestingly, GRB10 and IGFBP5 expression is frequently down regulated in various cancers (Ding et al., 2016; Yonghao et al., 2011).

There are also points of cross talk between mTORC1 and mTORC2 that influence full activation of AKT. S6K1-mediated phosphorylation of the mTORC2 components RICTOR and Sin1 decreases mTORC2-dependent phosphorylation of AKT on S473, but curiously not other substrates (Dibble, Asara, & Manning, 2009). These regulatory loops point toward a cellular mechanism that prevents simultaneous activation of mTORC1 and mTORC2 and influence full activation of AKT.

Although the involvement of feedback phosphatases has been far less studied, evidences suggest that the action of mTOR in the phosphorylation and degradation of IRS1 results from inhibition of PP2A. Interestingly, rapamycin treatment increased PP2A activity and IRS1 protein stability was shown to be regulated by PP2A, since treatment of cells with okadaic acid, a PP2A inhibitor, increased the phosphorylation of IRS1 and induced IRS1 degradation (Clark, Molero, & James, 2000; Hartley & Cooper, 2002) (**Figure 9**).

1.3.6 Role of the mTORC1/S6K1-dependent feedback loop in insulin resistance

According to the mTORC1/S6K1-dependent feedback loop described above, high levels of constitutive mTORC1 activity leads to insulin desensitization and attenuated AKT activation in cells. Insulin resistance is a pathological state of obesity and type 2 diabetes that occurs, at least in part, through chronic activation of mTORC1/S6K1 by nutrients and constitutive feedback activity that blocks AKT activation, disrupting the key metabolic actions of insulin (Zoncu et al.,

2011) (**Figure 10**). This state is characterized by high levels of circulating glucose as consequence of reduced glucose uptake and impaired glycogen synthesis in the muscle, adipose tissue and liver, and concomitant increased gluconeogenesis and glucose release by the liver. Insulin is produced and secreted by pancreatic β-cells in response to glucose, and stimulates adaptive signaling events in liver, fat and muscle. β-cells in the pancreas have a specialized role in sensing systemic glucose levels. Glucose is imported by GLUT2 in murine pancreas and through glycolysis increases the ratio ATP/ADP. ATP induces the closure of K_{ATP} channels and causes membrane depolarization that results in a transient rise in intracellular calcium concentration that facilitates insulin release to systemic circulation (Efeyan et al., 2015).

Insulin induces post-prandial glucose uptake and storage specially, in skeletal muscle where it takes place around 75% of glucose uptake, and also in adipose tissue (Leto & Saltiel, 2012; Saltiel & Kahn, 2001). GLUT4 is the predominant glucose transporter expressed in skeletal muscle and adipose tissue, where insulin-stimulated PI3K/AKT activation leads to the rapid

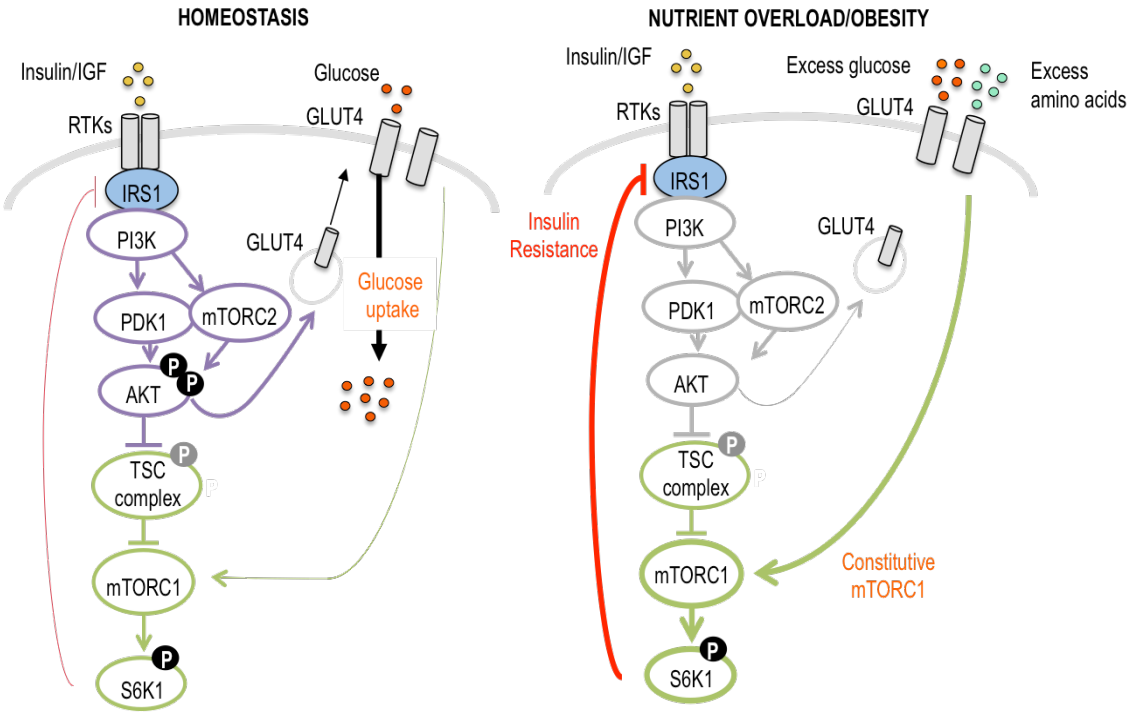

Figure 10. The mTORC1-dependent feedback loop in physiology and disease. a) In conditions of nutrient balance, activation of AKT by insulin triggers the translocation of GLUT4 contained in intracellular vesicles to the plasma membrane, where GLUT4 allows glucose uptake. **b)** Constitutive high activity of mTORC1/S6K1 axis triggers a negative feedback loop that is responsible of the detrimental effects associated to insulin resistance. Under nutrient overload or pathological conditions of obesity, high blood levels of amino acids sustain constitutive mTORC1 hyperactivation, despite of insulin resistance.

translocation of GLUT4 to the plasma membrane allowing glucose uptake. Subsequently, the newly acquired glucose is stored as glycogen in skeletal muscle through the action of glycogen synthase that is activated by AKT through inhibition of GSK3. AKT signaling in skeletal muscle attenuates protein breakdown while enhances protein synthesis through mTORC1 activation, and drives muscle hypertrophy. It has been shown that by promoting an increase in muscle mass, AKT signaling in skeletal muscle can improve systemic metabolism and overcome diet-induced obesity (Izumiya et al., 2008).

Adipose tissue accounts for only a small fraction of insulin-stimulated glucose uptake that is stored as triglycerides. Insulin, through mTORC1 activation, also suppresses lipolysis and fatty acid release. The most important function of the adipose tissues in this context is, however, to sense the energy status and communicate with other tissues by secreting cytokines and chemokines, which in turn regulate metabolism in muscle, liver, and brain (Leto & Saltiel, 2012). In the liver, insulin is essential for suppression of hepatic glucose production, and stimulation of glycogen and lipid synthesis. Inhibition of gluconeogenesis in hepatocytes occurs via AKT-mediated phosphorylation and inhibition of FoxO1, which control expression of the key enzymes controlling this process, phosphoenolpyruvate carboxykinase (PEPCK) and glucose 6-phosphatase (G6PD) (Manning & Toker, 2017). Hepatic insulin resistance and glucose intolerance is associated with the inability of insulin to inhibit glucose production.

Insulin secretion is itself affected by AKT and mTORC1 pathways. Reduced AKT activity in pancreatic β-cells resulted in impaired insulin secretion and impaired glucose tolerance (Bernal-Mizrachi et al., 2004). On the other hand, AKT activation in pancreatic islet cells increased β-cell mass and insulin production likely through mTORC1 activation, as specific activation of mTORC1 in islet cells in a TSC2-/- model, results in a robust expansion of islets, hyperinsulemia and improved glucose tolerance (Rachdi et al., 2008).

Supporting the role of the mTORC1/S6K1 feedback loop in the pathogenesis of type 2 diabetes, S6K1-deficient mice displayed enhanced sensitivity when chronically maintained on high fat diet and were protected from age- and obesity-induced insulin resistance in the presence of reduced IRS-1 phosphorylation (Um et al., 2004). In addition, GRB10-deficient mice also exhibited enhanced glucose tolerance and insulin sensitivity (Lixin Wang et al., 2007), whereas IRS1-deficient mice developed insulin resistance (Saltiel & Kahn, 2001). These evidences suggests that mTORC1 or S6K1 inhibitors could improve glucose tolerance and could be an effective treatment for certain metabolic disorders characterized by insulin resistance, such as type 2 diabetes (Um et al, 2004).

Objectives

MASTL/Greatwall is a kinase responsible for inhibiting the phosphatase PP2A in complex with the B55 family of regulatory subunits. A role for MASTL-PP2A/B55 pathway has been widely described in mitosis, and an additional function for MASTL in recovery from the DNA damage-induced G2 checkpoint has also been suggested. In budding yeast, the role of its orthologous Rim15 in the establishment of the quiescence program after nutrient deprivation has been extensively characterized. Whether the mammalian protein plays similar roles remain unknown, and no additional functions for mammalian MASTL have been described to date. The major aim of the project was therefore to identify new functions of MASTL in mammals. We aim to accomplish the following objectives:

1. Characterize the implications of MASTL-PP2A/B55 pathway in cell cycle regulation.
2. Identify new cell cycle-independent functions of MASTL and characterize the underlying molecular mechanism.
3. Study the physiological relevance of Mastl *in vivo* using a conditional loss-of-function mouse model for Mastl.

2. Material and Methods

2.1 Cell culture and cellular biology

2.1.1 Cell culture, synchronizations and starvation and re-stimulation of cells

Conditional knockout (cKO) mouse embryonic fibroblasts (MEFs) of Mastl, referred to as *Mastl (lox/lox)* MEFs, were obtained at E13.5 following the classical protocol for MEFs extraction. MEFs were immortalized using the first 121 amino acids of the SV40 T large antigen (T121), and have been previously reported (Álvarez-Fernández et al., 2013). MEFs were grown in (DMEM) Dulbecco's modified Eagle's medium supplemented with 10% fetal bovine serum (FBS; Sigma) and gentamycin at 37ºC and 5% CO_2. To stop cell proliferation and synchronize cells in quiescence, or G_0, subconfluent immortal MEFs (iMEFs) or primary MEFs (pMEFs) were arrested in G_0 by serum starvation (0.1% FBS) for 72 or 48 hours, respectively. For quantification of S-phase entry, MEFs synchronized in G_0 were trypsinized and split in complete media containing 10% FBS for the indicated time points, cells were incubated with 10 μM EdU for 30 minutes before harvesting and DNA replication was analyzed by flow cytometry. To analyze entry into quiescence in MEFs, asynchronous cultures were serum starved for the indicated times and cells were incubated with 10 μM EdU for 30 min to monitor the decrease in DNA replication. To assess the maintenance of quiescence, 10,000 MEFs were seeded on μCLEAR bottom 96-well plates (Greiner Bio-One) 24 h before serum starvation for 72h. Loss of staining of the proliferative markers Ki67 and EdU staining was scored using high throughput microscopy (HTM), 10 μM EdU was added 2 h before fixation.

All human cancer cell lines were grown in DMEM supplemented with 10% FBS and gentamycin at 37ºC 5% CO_2. MDA-MB231, BT549, and MCF7 breast cancer cell lines were kindly provided by M.A. Quintela (Breast Cancer Clinical Unit, CNIO). Human embryonic kidney (HEK) 293-T cell line was obtained from American Type Culture Collection (ATCC). The MDA-MB231 cell line has been DNA fingerprinted using the GenePrint 10 System (Promega). All of these cell lines are mycoplasma-free. Single cell clones of the MDA-MB231 cell line stables for the inducible CRISPR-Cas9 system for MASTL ablation, named isgMASTL, and control isgCas9, have been described (Álvarez-Fernández et al., *submitted*). Stable cell lines for the expression of determined genes were generated using constructs described below according to established protocols. Unless otherwise indicated, the MDA-MB231 cell line was used in all the experiments.
For starvation experiments, cells were seeded into 6 well plates at a density of 300,000 cells per well 24 h before. For glucose or amino acid starvation, actively proliferating cells were rinsed twice with Hank's balanced salt solution (HBSS) and incubated in DMEM without glucose or DMEM/Ham's F-12 without amino acids supplemented with 10% dialyzed FBS (dFBS) for 1 h,

unless otherwise indicated. Stimulation with 25 mM glucose was performed for 10 min, unless otherwise noted. For serum withdrawal, cells were rinsed twice with HBSS and incubated in 0.1% FBS DMEM for 6 h and, when specified stimulated with 100 nM insulin, 50 ng/mL human epidermal growth factor (hEGF) or 10% FBS for 30 min, unless otherwise indicated. For oxygen starvation cells were treated with the hypoxic mimetic $CoCl_2$ for 22 h in complete media. Glucose-free media (11966) and dFBS were from Gibco; amino acids free DMEM/Ham's F-12 (D9811-01) was from USBiological, glucose, insulin and hEGF were purchased from Sigma-Aldrich.

2.1.2 Protein knockout and knockdown

The *Mastl* conditional allele was knocked out in MEFs for the mitotic experiments following adenoviral-mediated Cre-recombinase (AdenoCre) delivery, AdenoFlp transduction was used as control. For Mastl ablation in the S-phase entry and quiescence experiments, we used the pLM-CMV-R-Cre plasmid (Addgene #27546) for the lentiviral-mediated delivery of Cre-recombinase, which was tagged in the N-terminal with mCherry, to overcome the adenoviral-associated toxicity in quiescence (O'Shea et al., 2005). Control cells were infected with lentiviral supernatants expressing the mCherry protein. Media was refreshed 16 h after infection. For protein knockdown in MEFs using small interfering RNAs (siRNAs), iMEFs were nucleofected with Amaxa® Nucleofector® Technology (Lonza) following the product specifications.

For *MASTL* and *TSC2* knockdown in human cancer cell lines using short hairpin RNA sequences (shRNA), we used the TRC pLKO.1 lentiviral system obtained from Sigma (Mission Library), references and sequences are listed in **Table 1.** shRNA scramble (Scr) was used as control. For virus production, pLKO plasmids were co-transfected into HEK293-T cells along with packaging pMDL, REV and envelope (VSVG) expression plasmids using Lipofectamine 2000 (Invitrogen) following manufacturer's instructions. Virus-containing supernatants were collected 24 and 48 hours after transfection, filtered to eliminate cells, and target cells were infected in the presence of 4 μg/mL polybrene. Cells were analyzed 64 h later, and knockdown efficiencies were examined by immunoblot analysis using specific antibodies against target proteins.

Table 1. shRNAs used in this work.

Target gene	shRNA sequence	Mission Library	Reference
hMASTL	AGTATAAGCATAACGAAATG	TRCN0000418233	(Álvarez-Fernández et al., submitted)
hTSC2	CGACGAGTCAAACAAGCCAAT	TRCN0000042723	(Llanos et al., 2016)

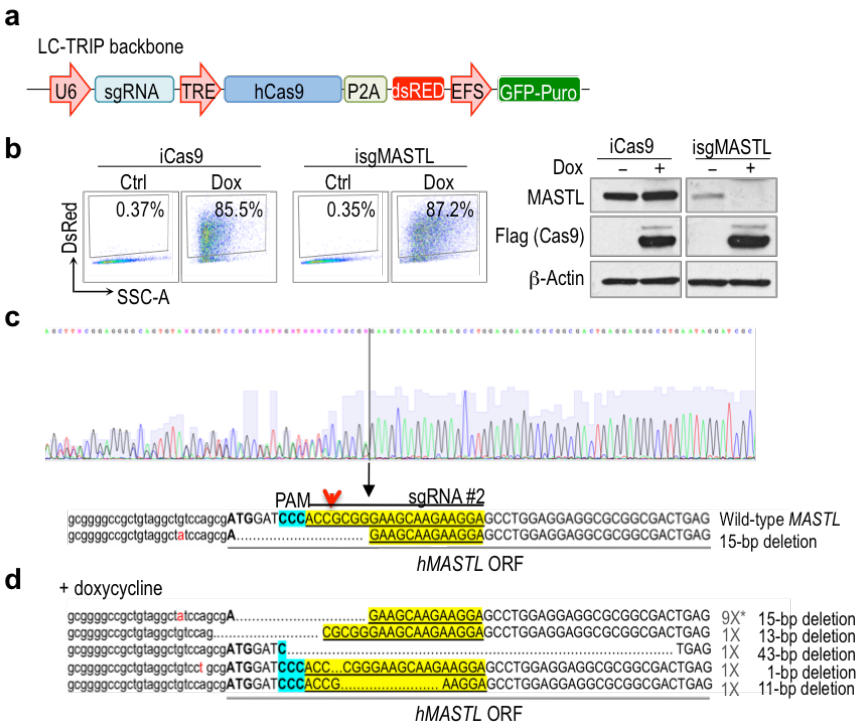

Figure 11. Genetic ablation of MASTL using inducible CRISPR/Cas9 system. a) Schematic representation of the sgRNA/Cas9-inducible lentiviral vector. **b)** Representative flow cytometry plots of dsRed induction in MDA-MB231 clones expressing both Cas9 and sgRNAs against MASTL (isgMASTL) or control cells expressing Cas9 alone (iCas9) upon 4 days of Dox treatment (Left). Numbers indicate the percentage of DsRed-positive cells. Immunoblotting analysis of MASTL depletion in the same conditions (Right). Cas9 induction was monitored with an anti-Flag antibody. **c-d)** Genomic analysis of isgMASTL clone. sgRNA and PAM sequence are highlighted in yellow and blue colors, respectively. Red arrowhead denotes predicted Cas9 cutting site. Note that this clone is already heterozygous for MASTL before treatment due to a 15 bp deletion that leads to a frameshift mutation and a premature stop codon (**c**). Treatment with Dox results in deletion of MASTL in both alleles due to 1-43 bp deletions also causing frameshift mutations as indicated in panel **d)**. Representative sequences are shown.

For conditionally knockout *MASTL* gene in the MDA-MB231 cell line, we generated single cell clones for the inducible CRISPR-Cas9 (isgRNA) system (**Figure 11a**). isgMASTL clones constitutively express the sgRNA targeting the exon 1 of *MASTL* (**Table 2**), and Cas9 expression is induced by doxycycline (Dox) at a concentration of 2 µg/mL. Addition of Dox to the media results in Cas9-mediated and sgRNA-directed specific cutting of the *MASTL* gene generating *MASTL* knockout cells (**Figure 11b-d**). Expression of MASTL protein is already undetectable 60-72 h after Dox addition. Experiments were performed 64-72 h after Dox addition, and starvations and re-stimulations were performed in the absence of Dox following the specifications indicated above.

TSC2 gene was knocked out using the constitutive CRISPR-Cas9 system. The *sgRNA* against human *TSC2* gene (Y. Bai et al., 2015) (**Table 2**) was subcloned into the lentiCRISPR v2 vector (Addgene #52961). MDA-MB231 cells were transduced with supernatants containing lentiviral vectors and selected with 1 µg/mL puromycin for 72 h. TSC2 protein knockout was confirmed by immunoblotting and a *TSC2* knockout cell line was established from the pool of puromycin selected cells and grown as usual.

Table 2. sgRNAs used in this work.

Target gene	sgRNA sequence	Reference
hMASTL	TCCTTCTTGCTTCCCGCGGT	(Álvarez-Fernández et al., submitted)
hTSC2	GTGGCCTCAACAATCGCATC	(Y. Bai et al., 2015)

Knockdown of human ENSA, ARPP19 and B55 alpha and delta proteins was done using specific siRNAs (**Table 3**). Cell lines were transfected with Hiperfect (Qiagen), according to the manufacturer's specifications. siRNA against luciferase (Luci) was used as control.

Table 3. siRNAs used in this work.

Target gene	**siRNA sequence**	**ON-TARGET plus SMART pool (Dharmacon)**	**Reference**
hENSA	GCUAAAGGCCAAAUACCCA AGAGAGCUGAAGAGGCAAA UGAAGAGACUCCAGAAAGG AGGACACGCAGGAGAAAGA	L-011852-00	(Cundell et al., 2013)
hARPP19	CAAGCUGGCUGGCUGAUUA CAACAUGGCUAAAGCAAAA GUUCAGAUUUCUUAAGGAA GCACAAGAGUUCCUACACA	L-015338-00	(Cundell et al., 2013)
		Quiagen	
hPPP2R2A	CTGCAGATGATTTGCGGATTA	SI02225825	(Schmitz et al., 2010)
hPPP2R2D	TTCATCCATATCCGATGTAAA	SI02759148	

2.1.3 Treatments

For cell culture treatment, inhibitors were added either at the same time of the starvation or 10-20 min before re-stimulation for the indicated periods of time in each case. The following drugs were used in cell culture at the indicated concentrations.

Table 4. Inhibitors used in this work and their working concentration.

Inhibitor	Target	Concentration	Supplier
2-DG	Hexokinase	50 mM	Sigma
AKTIV	AKT	500 nM	Calbiochem
Antimycin A	Mitochondrial electron transport	1 µM	Sigma
Erlotinib	EGFR	5 µM	Tarceva; Roche
FCCP	H+ ionophore	0.4-0.8 µM	Santa Cruz
Fostriecin	PP2A	5 µM	Santa Cruz
Linsitinib	IR/IGFR-I	5 µM	Selleckem
PF-4708671	P70S6K1	10 µM	Selleckem
Okadaic acid	PP2A	50 nM	Calbiochem
Oligomycin A	H+-ATP-synthase	10 µM	Sigma
Rapamycin	mTORC1	100 nM	Santa Cruz
Roscovitine	CDK1/2/5	25 µM	Selleckem
Rotenone	Mitochondrial electron transport	1 µM	Sigma
Taxol	Microtubules	1 µM	Sigma
Torin1	mTOR	250 nM	Selleckem

2.1.4 Protein overexpression

For transient protein overexpression of ENSA and ARPP19 and MASTL, respective cDNAs into the pEGFP-C2 or pDEST 3.1-GFP vectors were used. Cells were transfected using Lipofectamine 2000 (Invitrogen) following manufacturer's instructions.

For stable overexpression of proteins, cDNAs were subcloned into the lentiviral pLVX-puro vector in which the cDNA is expressed under the CMV promoter. To generate lentiviral supernatants, pLVX vectors were co-transfected along with pMDL, REV and envelope (VSVG) plasmids in HEK293-T cells using Lipofectamine 2000. Virus-containing supernatants were recovered at 30, 48 and 72 h after transfection, and MDA-MB231 target cells were infected in

presence of 4 µg/mL polybrene. 48 h later, cells stably expressing the cDNA were selected with 1 µg/mL puromycin.

2.1.5 Cell cycle analysis by flow cytometry

Cells were trypsinized and fixed in cold 70% ethanol at 4ºC for at least 12 h. For EdU staining we followed the classical azide-based EdU Click-iT protocol (Invitrogen) plus an additional step for signal amplification using biotin-azide and streptavidin-Alexa fluor. For cell cycle profile analysis, DNA was stained with propidium iodide (PI) (Invitrogen) and samples were incubated in the presence of RNAse at 37ºC for 30 min. To assess the mitotic index, cells were stained using specific antibodies for the mitotic markers S-10-H3 (Millipore; 06-570) and MPM-2 (Millipore; 05-368), which detects mitotic proline-directed Ser/Thr-phosphoepitopes, DNA content was monitored using DAPI (Sigma). Samples were run on a LSR Fortesa flow cytometer (BD, San Jose), and 10,000 single events were acquired. Data were analyzed using the analyzer FlowJo v9.6.4 (Treestar, Oregon)

2.1.6 Videomicroscopy

MEFs expressing stable H2B-mRFP were plated on eight well glass-bottom dishes (Ibidi) at a density of 30,000 cells per well and imaged with a DeltaVision RT imaging system (Applied Precision, LLC; IX70/71; Olympus) equipped with a PI APO 20XI 1.42 NA objective lens and maintained at 37ºC in a humidified CO_2 chamber. Images were acquired every 10 min for mitotic analysis and analyzed using ImageJ software.

2.2 Molecular biology and biochemical analysis

2.2.1 Cloning of cDNA and mutagenesis

Human ENSA (NCBI NM_004436.2 transcript variant 3) and ARPP19 (NCBI NM_006628.5 transcript variant 3) cDNAs in the pOTB7 and pCMV-SPORT6, respectively, were obtained from the CNIO library. Both cDNAs were amplified by PCR (Expand High Fidelity PCR system, Roche) and tagged in the N-terminal with FLAG and HA tags, respectively using specific primers. The PCR product was sub-cloned into the BamHI and XhoI sites of the pLVX-puro lentiviral vector for stable expression, or in the same sites of the pEGFP-C2 vector for transient expression following classical cloning techniques.

Human (NCBI NM_001172303.2 transcript variant 1) and mouse Mastl (NCBI NM_025979.4) cDNAs were sub-cloned into the pENTRY and transferred into the pDESTINY 3.1-GFP using the Gateway system (Invitrogen) for transient protein expression. MASTL proteins were tagged in its N-terminal for not to affect its kinase activity. For stably protein expression, GFP-Mastl cDNA was digested from the pDESTINY 3.1-GFP and sub-cloned into the BamHI and XhoI sites of the pLVX-puro vector.

For rescue experiments in human cell lines, the cDNA of mouse Mastl in the pENTRY was mutagenized using the QuikChange Site-directed mutagenesis kit (Agilent) and specific primers following their specifications. Mutants used in our experiments are numbered according to NCBI and were verified by sequencing. Mutant forms of Mastl were subcloned into pDESTINY 3.1-GFP or pLVX-puro vectors as stated above.

ENSA- and ARPP19-pEGFP-C2 sequences were mutagenized as indicated above for Mastl. Phosphomutant forms for ENSA and ARPP19 (S67A and S62A, respectively) are unable to be phosphorylated by MASTL. Conversely, phosphomimetic forms of ENSA and ARPP19 (S67D and S62D, respectively) mimic constitutive MASTL phosphorylation. After verification by sequencing, ENSA and ARPP19 cDNAs were tagged with FLAG and HA tags in the N-terminal, respectively, by PCR using specific primers. After restriction enzyme digestion, were subcloned into the pLVX-puro vector as specified above.

2.2.2 Immunoblotting

For immunoblot analysis, cells were extracted on ice in cold lysis buffer (50 mM Tris-HCl pH 7.5, 1 mM EDTA, 1 mM EGTA, 0.1% Triton X-100, protease inhibitors, 1 mM sodium orthovanadate, 50 mM sodium fluoride, 20 mM β-glycerophosphate, 0.1% 2-mercaptoethanol). Cell lysates were

cleared by centrifugation at 15,000 xg for 10 min at 4ºC, and protein was quantified using the Bradford method. Protein extracts were mixed with sample buffer (350 mM Tris-HCl pH 6.8, 30% glycerol, 10% SDS, 0.6 M DTT, 0.1% bromophenol blue), boiled for 5 min and subjected to electrophoresis using the standard SDS-method. Proteins were then transferred to a nitrocellulose membrane, blocked in PBS 0.1% Tween-20 buffer containing 3% non-fat dried milk, and probed overnight with primary antibodies (1:1000 dilution) at 4 ºC and for 1 h at room temperature with peroxidase-conjugated secondary antibodies. Blots were developed using enhanced chemiluminiscence reagent (Western Lightning Plus-ECL; Perkin Elmer), exposed to an autoradiograph film and developed using standard methods. Films were scanned and quantifications were performed using ImageJ.

Reagents for western blot (WB) were obtained from the following sources: anti phospho-T308 AKT (9275), phospho-S473 AKT (9271), phospho-T1462 TSC2 (3611), phospho-S939 TSC2 (3615), phospho-T389 S6K1 (9234), phospho-S235/236 S6 (2211), phospho-S612 IRS1 (3203), phospho-S307 IRS1 (2381), phospho-S476 GRB10 (11817), phospho-Y1068 EGFR (3777), phospho-Y1135/1136 IR/IGFR (3024), phospho-T202/Y204 ERK (9101), phospho-S79 ACC (11818), phospho-S792 Raptor (2083), phospho-T246 PRAS40 (2640), phospho-S9 GSK-3β (9336), phospho-T24/32 FoxO1/3 (9464), phospho-S67/S62 Ensa/Arpp19 (5240), total AKT (9272), ERK (9102) TSC (4308), S6K1 (9202), S6 (2217), IRS1 (3407), GRB10 (3702), EGFR (4267), IR (3025), ACC (3676), Raptor (2280), PTEN (9188) were from Cell Signaling technology. Anti human and mouse MASTL (MABT372), phospho-S291 PDHE (AP1062), phospho-S10 H3 (06-570) and MPM-2 (05-368) were from Millipore. Anti mouse Mastl (AP14289c) was from Abgent. Anti pan-B55 (sc-81606) was from Santa Cruz. Anti phospho-T194 MASTL was a gift from Heldfrich. Anti HIF1α (610959) antibody was purchased from BD Biosciences. Anti PDK2 was from Cusabio (CSB-PA618976ESR2HU). Anti ENSA/ARPP19 (180513), and HA (1424) were from Abcam. Anti β-Actin (5441), FLAG (F7425) and Vinculin were from Sigma. Anti GFP was from Roche (11814460001). Unless otherwise indicated β-actin was used as loading control.

2.2.3 Immunofluorescence

MEFs were cultured in 96-well plates for HTM and fixed in 4% buffered paraformaldehyde (PFA) for 10 min at room temperature (RT). EdU staining was performed following de Click-iT EdU specifications (Invitrogen; C10086), and was followed by immunofluorescence (IF) against Ki67 (Master Diagnostica; 0003110QD). Briefly, after EdU detection, cells were permeabilized with 0.5% Triton X-100 for 10 min and blocked with 10% FBS for 1 h at RT, Ki67 antibody was

incubated overnight at 4ºC and nuclei were stained with DAPI. Images were automatically acquired from each well by an Opera High-Content Screening system (Perkin Elmer). A 20x magnification lens was used and pictures were taken at non-saturating conditions. Images were segmented using the DAPI staining to generate masks matching cell nuclei from which mean EdU and Ki67 signals were calculated.

MDA-MB231 cells cultured on glass coverslips were fixed in 4% buffered PFA for 10 min at RT. For GLUT4 immunodetection, PFA was first quenched with 100 mM glycine for 10 min followed by permeabilization using 0.2 % Triton X-100 for 10 min and blocking with 10% goat serum plus 1% BSA for 1 h at RT. Incubation with a specific antibody against GLUT4 (ab654) (Bradley et al., 2014) was done at a 1:200 dilution for 1 h at 37ºC. To have a reference of the plasma membrane delimitation we combined GLUT4 staining with 1 µM HCS cell mask (Invitrogen; H32720) that stains the entire cell, and 1 µM TO-PRO-3 Iodide 642/661 (Invitrogen; T3605) to visualize the nuclei. Images were captured using a laser scanning confocal microscope TCS-SP5 (AOBS) Leica. Image analysis was done using ImageJ software.

2.2.4 Immunoprecipitations and proteomic analysis of phosphoresidues in Mastl

Cells were lysed in TNN (50 mM Tris-HCl pH 7.5, 150 mM NaCl, 1% NP-40) or RIPA buffer (50 mM Tris-HCl pH 7.5, 150 mM NaCl, 1% NP-40, 0.5% Sodium-deoxicolate, 0.1% SDS, 5 mM EDTA) in presence of protease inhibitors (Roche), and phosphatase inhibitors (1 mM sodium orthovanadate, 50 mM sodium fluoride, 20 mM β-glycerophosphate). Cell lysates were cleared by centrifugation at 15,000 xg for 10 min at 4ºC and protein was quantified using the bicinchoninic acid assay (BCA; Thermo). Proteins were immunoprecipitated (IP) from total extracts using specific antibodies (2 µg/1 mg protein) crosslinked to Dynabeads Protein A (Invitrogen), and incubated overnight at 4 ºC on a rotatory wheel. The immunoprecipitates were washed once in RIPA buffer, twice in high salt RIPA buffer (500 mM NaCl) followed by an additional wash in RIPA. Immunoprecipitates were then used with different applications as stated below. Eventually, for immunoblot analysis, IP samples were resuspended in 30 µL of sample buffer, boiled 5 min at 95ºC, and subjected to electrophoresis and immunoblot analysis.

To study specific phosphoresidues on Mastl, endogenous mouse Mastl was IP from iMEFs using a polyclonal antibody against Mastl (Abgent; AP14289c) crosslinked to Dynabeads Protein A. Total lysates were extracted in RIPA buffer following the specifications indicated above and samples were subjected to mass spectrometry analysis. For this, protein eluates from the IP samples were doubly digested using the FASP procedure with some modifications. The resulting peptides were analyzed by LC-MS/MS using a LTQ Orbitrap Velos mass spectrometer (Thermo

Scientific). Besides, the samples were subjected to TiO2 enrichment. Raw files were searched against a UniprotKB/TrEMBL *Mus musculus* database (UniProtKB/Swiss-Prot/TrEMBL 43,539 sequences) using Sequest-HT as the search engine through the Proteome Discoverer 1.4 (Thermo Scientific) software. Peptide identifications were filtered by Percolator at 1% FDR using the target-decoy strategy. Label-free quantification was performed with MaxQuant and extracted ion chromatograms for MASTL phosphopeptides were manually validated in Xcalibur 2.2 (Thermo Scientific).

2.2.5 *In vitro* kinase assay

For the *in vitro* kinases assays, cells stably expressing either GFP-hMASTL wild type (WT) or kinase dead (G44S) were lysed in ELB buffer (50 mM Hepes pH 7.4, 150 mM NaCl, 5 mM EDTA, 1% NP-40) in presence of protease and phosphatase inhibitors. GFP-hMASTL proteins were IP using an anti-GFP antibody (Roche; 11814460001) crosslinked to Dynabeads Protein A (Invitrogen) and proceeded as indicated above for routine IP. For kinase assay, IP were washed two times in ELB buffer, twice in high salt (500 mM NaCl) ELB buffer, followed by to additional washes in kinase buffer (20 mM Hepes pH 7.5, 10 mM MgCl2). Equal amounts of beads were re-suspended in kinase buffer and mixed with 500 ng of recombinant ARPP19 purified from HEK293T cells (A. Castro) in a final volume of 20 µL in the presence of radioactive ^{32}P-labeled ATP, and incubated for 20 min at 30ºC. Reactions were stopped by the addition of sample buffer and boiling for 5 min. Samples were analyzed by SDS-PAGE in a gel of 10% acrylamide, transferred to a nitrocellulose membrane, and revealed by exposure to a radiosensitive screen. Images and quantifications were performed using ImageJ. Total MASTL in the reactions was quantified by immunoblot against MASTL on the transferred membrane.

For kinases assays using mTOR and p70S6K1 as kinases, active recombinant proteins were purchased from Sigma (SRP0364, P0066, respectively). Recombinant purified human MASTL protein was used as a substrate and was from Abnova (H00084930). Reaction was performed in a final volume of 30 µL consisting of kinase buffer (supplemented with 50 mM KCl for the mTOR assay), 200 ng of the upstream kinase and 500 ng of MASTL, and incubated for 30 min at 30ºC. Reactions were stopped by the addition of sample buffer and boiling for 5 min, and were analyzed by SDS-PAGE in a gel of 8% acrylamide. Proteins in the gel were stained using Imperial Stain (Invitrogen) following the manufacturer's instructions, dried and revealed by exposure to a radiosensitive screen.

2.2.6 MASTL phosphorylation site mapping

mTORC1 and S6K1 *in vitro* kinase assays were performed as detailed above with the exception that the reaction was in the presence of 500 μM cold ATP. Samples in 5 M urea were doubly digested using the FASP procedure with some modifications. The resulting peptides were analyzed by LC-MS/MS using an Impact mass spectrometer (Bruker Daltonics). Raw files were searched against a Uniprot *Homo sapiens* database (20,187 sequences) using Andromeda as the search engine through the MaxQuant software. Peptide identifications were filtered by Percolator at 1% FDR using the target-decoy strategy. Label-free quantification was performed and extracted ion chromatograms for MASTL phosphopeptides were manually validated.

2.2.7 Reverse-transcription quantitative PCR (RT-qPCR)

Total RNA was extracted from mouse tissues using the Trizol (Sigma) method, according to the manufacturer's instructions. Reverse transcription from 1 μg of total RNA was performed with the M-MLV retrotranscriptase (Promega) followed by quantitative PCR (qPCR) using either SYBR Green PCR Master Mix (Applied Biosystems) with specific primers (**Table 5**), or TaqMan reagents (Applied Biosystems) for analyzing MASTL expression in murine tissues. Data were analyzed using the comparative Ct method and are expressed as the ratio between the expression of each gene and the housekeeping gene. β-2-microglobulin (B2M) was used as housekeeping for human cells. Primers used for the amplification of specific genes are listed below.

Table 5. Primers for RT-qPCR used in this work. Forward and reverse sequences are indicated.

	Primer sequence	
Gene	**Forward**	**Reverse**
hB2M	AGATGAGTATGCCTGCCGTG	TCATCCAATCCAAATGCGGC
hGlut1	AACTCTTCAGCCAGGGTCCAC	CACAGTGAAGATGATGAAGAC

For quantification of *Mastl* mRNA expression in murine tissues, TaqMan probes against *Mastl* (Mm01329243_m1) spanning exon 4 of *Mastl* gene, and the housekeeping genes of B2M (Mm00437762_m1) and hypoxanthine phosphoribosyl transferase 1 (*HPRT*; Mm00446968_m1) were used.

2.3 Metabolic assays in cells

2.3.1 Seahorse metabolic profiling

Glycolysis and mitochondrial respiration were determined as indirect measurements of the extracellular acidification rate (ECAR) and oxygen consumption rate (OCR) of cells, respectively, and were measured with an XF96 Extracellular flux analyzer (Seahorse Bioscience), following manufacturer's instructions for the Glycolytic and Mitochondrial Stress kit. MDA-MB231 cells were plated at a density of 10,000 cells per well, the day after cells were washed and incubated in buffered glucose- and sodium pyruvate-free DMEM (Seahorse Bioscience) supplemented with 2 mM glutamine and 2% dFBS for glycolysis measurement. The same media was supplemented with 5 mM glucose and 1mM sodium pyruvate to assess mitochondrial capacity. Cells were incubated for 1 h in a CO_2-free incubator at 37ºC to allow for temperature and pH equilibration before loading into XF96 apparatus. Assays consisted of sequential mix (3 min) and measurement (3 min) cycles, allowing for determination of OCR/ECAR every 6 min. To obtain the glycolytic-dependent ECAR and the mitochondrial-dependent OCR, only the 2-DG-sensitive media acidification and the antimycin A-sensitive respiration were used, respectively. ECAR and OCR were normalized to the cell number calculated at the end of the experiments. Cell count at the end of the experiment was assessed by fixing cells with paraformaldehyde 4% for 10 min at RT following by DAPI staining and quantification of total number of cells per well using a laser scanning confocal microscope TCS-SP5 (AOBS) Leica. Image analysis was done using ImageJ software. Data was expressed as mean ± sem of 3 independent experiments. Statistical significant differences were determined using paired Student's *t* test.

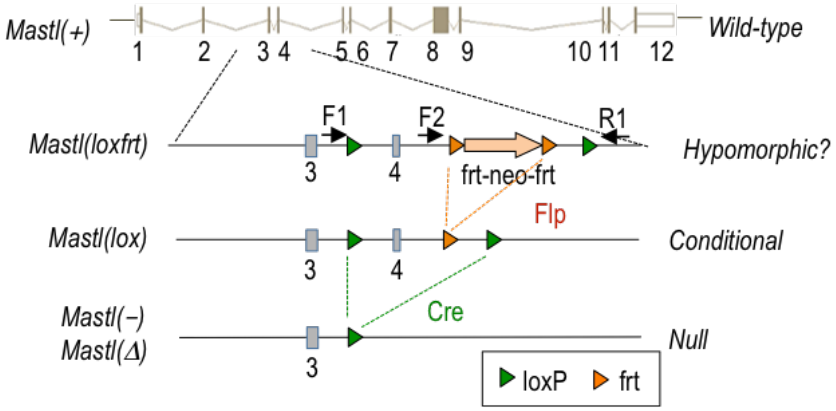

Figure 12. Generation of *Mastl* loss-of-function mutant mice. Schematic representation of the murine *Mastl* gene and the generation of the different *Mastl* alleles. The exon 4 of the *Mastl* gene is flanked by loxP sites (green triangles) and intron 4 contained a neomycin selection cassette (orange arrow) flaked by frt sites (orange triangles) rendering the *Mastl(loxfrt)* allele. Site-specific recombination by Flp results in the conditional *Mastl(lox)* allele, which expresses normal levels of Mastl protein. Cre-mediated recombination renders the germ-line *Mastl(–)* or conditionally induced *Mastl(Δ)* null alleles. (Álvarez-Fernández et al., 2013)

2.4 Studies *in vivo* in Mastl mutant mice

2.4.1 Generation of a conditional *Mastl* knockout mice and genotyping

To generate a Mastl conditional loss-of-function model, *Mastl(lox/lox),* mouse embryonic stem cells carrying a neomycin resistance gene flanked by frt sites in *MASTL* intron 4 and loxP sites flanking exon 4, which contains the ATP binding site critical for the activity of the kinase, were microinjected into developing blastocysts. The resulting positive chimaeric mice *Mastl(+/loxfrt)* were crossed with C57BL6/J mice. Subsequently, the neo cassette was removed by mating with mice expressing the Flp recombinase (Tg.pCAG-Flp), generating the *Mastl* cKO allele, termed *Mastl(lox)* (**Figure 12**). To obtain a ubiquitous and constitutive depletion of *Mastl, Mastl(+/lox)* mice were crossed with animals expressing DNA recombinase Cre (Cre) under control of a human cytomegalovirus minimal promoter (CMV). Excision of exon 4 of the *Mastl* gene leads to a frame shift in the mRNA generating several new premature stop codons that results in loss of Mastl protein, and renders the *Mastl(Δ)* allele. *Mastl* cKO animals were obtained by crossing *Mastl(lox)* mice with mice expressing a knock in of the CRE-ERT2 recombinase inducible by tamoxifen (TAM) in the locus of the ubiquitous RNA polymerase promoter (*RNAP2_CreERT2*). These mouse models have been previously described (Álvarez-Fernández et al., 2013). Liver-specific *Mastl* cKO mice referred as *Mastl_L(lox/lox),* were obtained by crossing *Mastl(lox/lox)* mice with the serum albumin-Cre knockin mice (Schuler, Dierich, Chambon, & Metzger, 2004).

All animals were maintained in a C57BL6/J-129S mixed background. Mice were housed in the pathogen-free animal facility of the CNIO (Madrid) and maintained under a standard 12-h light-dark cycle, at 23ºC with free access to food and water. All animal work and procedures were approved by the ISCIII committee for animal care and research, and were performed in accordance with the CNIO Animal Care program. To induce insulin resistance, mice were fed for 8 weeks with 60% high fat diet (HFD) (60% fat, 20% protein, 20% carbohydrate; Research Diets; D12492). Only males between 2 and 3 months of age were used for HFD experiments.

Routine genotyping of the *Mastl(lox) and Mastl(–)* allele was done by PCR using DNA from the tail of the mice. Both PCRs were done using a standard Taq Polymerase (Promega), and the following protocol with specific primers in each case (**Table 6**): i) 5 minutes at 95ºC to denaturalize the DNA; ii) 40 cycles of denaturing 30 s at 95ºC, annealing 30 s at 58ºC, and elongation 60 s at 72ºC; and iii) final elongation step 10 min 72ºC.

Table 6. Primers used for genotyping *MASTL* mutant alleles.

Primers	***Mastl(–)***	Forward	TCTTTCCACTCCCATACCACA
		Reverse	GGCTGGCAGTTCCATTTTTA
	Mastl(lox)	Forward	GCCCTTTTAAAAACCCAACA
		Reverse	GGCTGGCAGTTCCATTTTTA

PCR products were run in 2% agarose gels and interpreted as follows: *Mastl(–)* PCR gave a band of 783 bp for *Mastl(+)* allele and 289 bp for *Mastl(–).* PCR products for *Mastl(lox*) were 402 bp for *Mastl(lox)* and 296 bp for *Mastl(+)* allele.

2.4.2 Deletion of Mastl in young and adult mice

To excise the *Mastl* gene and generate the *Mastl* knockout mice, mice were treated with tamoxifen (TAM) to induce the nuclear translocation and activation of Cre-ERT2 recombinase. Young mice of 3 weeks (after weaning) or adult mice of between 45- and 52-weeks-old were treated with TAM in the diet (Envigo; TD.55125) for the whole time that the experiment lasted. Alternatively, mice that were under the HFD were treated with TAM by intraperitoneal injection of TAM (Sigma; T5648) at a dose of 200 mg/kg. Mice were injected twice each other day one week before each experiment.

2.4.3 Glucose- and insulin-tolerance tests

For glucose tolerance test assay (GTT) mice were fasted for 16 h and then administered an intraperitoneal glucose injection (2 g/kg body weight). Glycaemia was measured by tail vein blood sampling using a glucometer and glucose strips (Bio Medical) in fasting and 15, 30, 45, 60, 90 and 120 min after glucose injection. For insulin tolerance test (ITT) same mice were fasted for 6 h and intraperitoneally injected with rapid acting insulin (0.75 U/kg body weight) (Actrapid, Novo Nordisk) following by tail vein blood glucose sampling to measure the glycaemia at 0, 15, 30, 45 and 60 min after insulin injection.

2.4.4 Glucose stimulated insulin secretion

To measure glucose-stimulated insulin secretion (GSIS), mice were fasted for 16 h and injected with glucose (2 g/kg body weight). Plasma insulin levels were measured at 0 and 30 min after glucose injection. Blood from the cheek was collected in EDTA tubes, centrifuged at 8,000 xg for 10 min at 4ºC, and the plasma was separated and stored at -80ºC. Insulin was measured in 25 μL of plasma using an ultrasensitive mouse insulin ELISA kit (Mercodia).

2.4.5 Treatment of mice with a CNIO-PI3K inhibitor

The PI3K inhibitor developed at CNIO ETP-44692 (Martínez González et al., 2012) was administered to the 16 h fasted mice by oral gavage in a unique dose of 20 mg/kg 1 h before starting the GTT. ETP-44692 was dissolved in 90% PEG-300 and 10% N-methyl-2-pyrrolidone (NMP). Sham-treated mice, which received only vehicle, were included in the study to discard any effect indirect to the inhibitor.

2.4.6 Immunohistochemistry

For histological analysis tissues were fixed in 10%-buffered formalin (Sigma) and embedded in paraffin wax. Sections of 3- or 5-μm thickness were stained with haematoxylin and eosin (HE) or Periodic Acid Schiff (PAS) staining. Additional immunohistochemical (IHC) examination was performed using specific antibodies against MASTL (Millipore; MABT372), Ki67 (Master Diagnostica), cleaved caspase-3 (Asp175) (Cell signaling; 9661), insulin (Dako; A 0564), and glucagon (Sigma; G2654).

2.5 Statistics

Statistical analysis was carried out using Prism 5 (GraphPad). Statistical tests were performed using either two-sided, unpaired Student's *t*-test, paired Student's *t*-test, 1- or 2-way ANOVA (Bonferroni's multiple test) according to specifications in the figures. Data with $p>0.05$ were considered not statistically significant (ns); *, $p<0.05$; **, $p<0.01$; ***, $p<0.001$.

3. Results

3.1 Role of MASTL kinase in cell cycle regulation in mammals

3.1.1 Mastl is essential for mitotic progression in mammalian cells

The role of MASTL in the maintenance of the mitotic state through inhibition of PP2A has also been reported in mammalian cells using siRNAs against *MASTL* (Burgess et al., 2010). To further understand the role of mammalian Gwl in cell cycle progression and mitosis, our lab generated a *Mastl* conditional knock-out (cKO) mouse model, in which LoxP sites flank the exon 4 of the *Mastl* gene that contains the ATP binding site critical for the activity of the kinase (see section **2.4.1** and **Figure 12**) (Álvarez-Fernández et al., 2013). Expression of Cre under an ubiquitous and constitutive promoter, excises exon 4 of *Mastl* and induces the loss of Mastl protein, rendering the germ-line null *Mastl(–)* allele (**Figure 13a**). *Mastl(+/–)* heterozygous mice developed normally and are fertile. By crossing heterozygous mice it was found that germ line null mutation in *Mastl* leads to embryonic lethality at periimplantational stages comprised between E5.5 and E10.5,

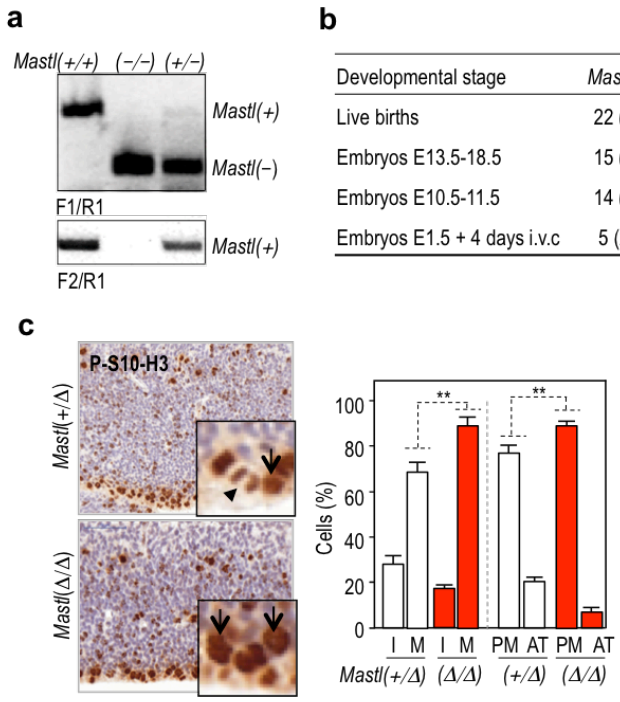

Developmental stage	*Mastl(+/+)*	*Mastl(+/−)*	*Mastl(−/−)*	Total
Live births	22 (27%)	60 (73%)	0 (0%)	82
Embryos E13.5-18.5	15 (37%)	23 (56%)	0 (0%)	38
Embryos E10.5-11.5	14 (21%)	35 (51%)	0 (0%)	49
Embryos E1.5 + 4 days i.v.c	5 (25%)	8 (40%)	7 (35%)	20

Figure 13. *Mastl* is essential for mouse embryonic development. **a)** Representative PCR products showing the *Mastl(–)* and *WT* alleles. **b)** The number and percentage of mice or embryos with the indicated genotype is shown indicating that *Mastl(–/–)* embryos develop normally until blastocyst stage. **c)** Immunohistochemical analysis of E14.5 embryos after injection of the pregnant mother with TAM. S-10-H3 staining shows an increase in M figures versus interphasic (I) cells in the subventricular zone in *Mastl(Δ/Δ)* respect *Mastl(+/Δ)* embryos. PM figures and AT are indicated by arrows and arrowheads, respectively. i.v.c, *in vitro* culture. **p<0.01.

indicating that *Mastl* gene is essential for mouse embryonic proliferation (**Figure 13b**).

To overcome this lethality, we generated a TAM-inducible cKO mouse model for *Mastl*, which expresses Cre fused to the estrogen receptor (Cre_ERT2) in the ubiquitous *RNA polymerase II* locus (*Polr2a*). To analyze the consequences of *Mastl* ablation *in vivo* in a highly proliferative stage, we treated pregnant females at E12.5 with TAM to conditionally knockout *Mastl* in the embryos, which were analyzed at E14.5 (**Figure 13c**). We found increased mitotic (M) figures in the neuroepithelium of *Mastl(Δ/Δ)* embryos compared to *Mastl(+/Δ)* littermates with an enrichment in prometaphases/metaphases (P/M) compared with the more abundant anaphases/telophases (A/T) in control sections. This result suggested that Mastl is essential for proper mitotic progression in mammals *in vivo* (Álvarez-Fernández et al., 2013).

To further explore the role of Mastl in mitosis *in vitro* we took advantage of MEFs derived from the Mastl cKO mouse model. AdenoCre transduction of pMEFs generated *Mastl(Δ/Δ)* cells and resulted in reduced proliferation accompanied by mitotic aberrations in prometaphase, including defective chromosome condensation and abnormal spindle (**Figure 14a,b**).

To study the kinetics of mitotic entry and progression, *Mastl(lox/lox)* immortal MEFs stably expressing histone H2B fused to mRFP were followed by time-lapse videomicroscopy for 48 h. To record the first division after Mastl ablation, MEFs were arrested in quiescence, or G_0, by serum starvation at the same time they were transduced with adenoCre, or adenoFlp viruses as control. Quiescent cells were split and serum stimulated following the protocol depicted in **Figure**

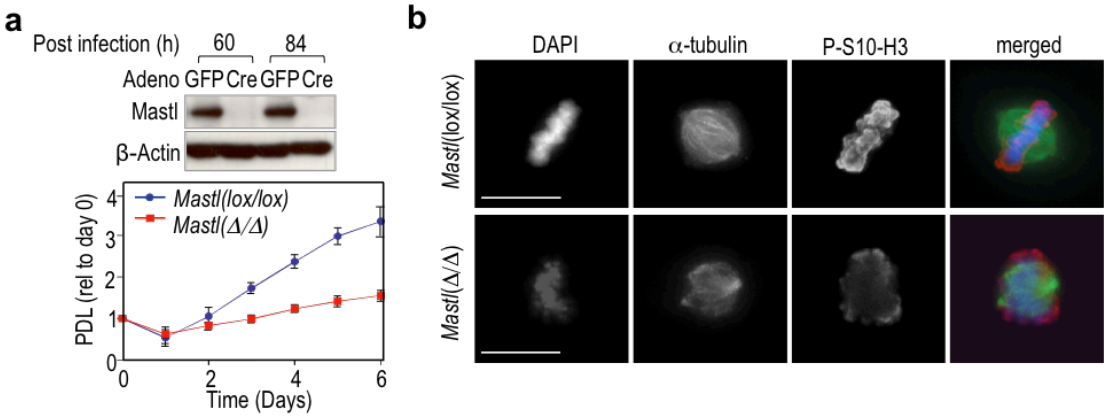

Figure 14. Mastl is required for proliferation *in vitro* in MEFs. **a)** WB showing the depletion of Mastl protein in *Mastl(lox/lox)* pMEFs after transduction with adenovirus expressing Cre. AdenoGFP was used as control. Bottom plot represents a cell growth curve over 6 days in the same cells. Mean ± SD for each time point is shown in the plot. PDL, population doubling levels. **b)** Representative immunofluorescence images of mitotic cells stained with DAPI (blue), a-tubulin (green), and S-10-H3 (red).

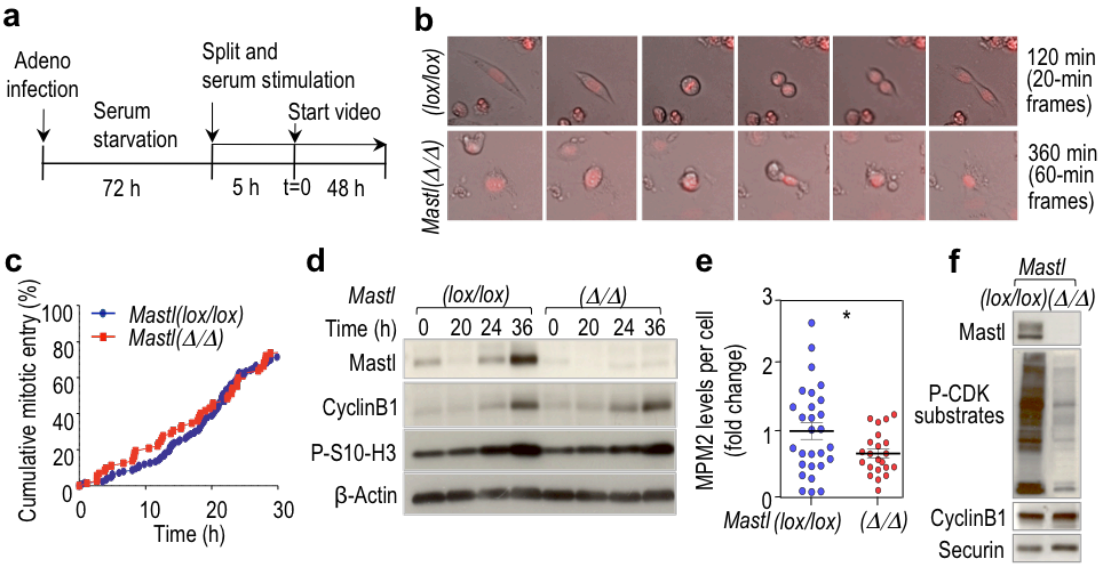

Figure 15. *Mastl* is not essential for mitotic entry in MEFs. **a)** Schematic representation of the protocol used in *MASTL(lox/lox)* iMEFs for synchronization in G_0 and serum stimulation to monitor mitotic entry. Genetic ablation of Mastl was done using adenoCre or adenoFlp as control. **b)** Representative time-lapse images of *Mastl(lox/lox)* and *Mastl(Δ/Δ)* MEFs. H2B-mRFP is shown in red. **c)** Quantification of mitotic entry after analysis of time-lapse images. **d)** Immunodetection of the indicated proteins by WB in a time course after serum stimulation. **e)** Levels of MPM2 per cell scored by IF. **e)** Levels of the indicated proteins in a mitotic shake off extract after treatment with taxol. Error bars indicate SD. ns, not significant; p>0.05 (Fisher's exact test); *p<0.05 (Student *t* test).

15a. No differences were observed in the kinetics of mitotic entry between *Mastl(lox/lox) and Mastl(Δ/Δ)* MEFs, as determined by cell rounding and chromosome condensation (**Figure 15b,c**). In addition, no differences were detected neither in a time course of mitotic entry nor in the accumulation of mitotic markers, such as cyclinB1 or phospho-histone H3 proteins by WB (**Figure 15d**). However, *Mastl(Δ/Δ)* mitotic MEFs showed reduced levels of phosphorylated mitotic proteins scored by IF using an MPM-2 antibody, which mainly detects phosphorylated proline-directed Ser/Thr epitopes abundant in mitotic cells (**Figure 15e**), and also displayed a dramatic reduction in the levels of phosphorylation of CDK substrates by WB after a shake-off of taxol arrested pMEFs (**Figure 15f**).

Video analysis also allowed us to calculate the duration of mitosis (DOM), which was 2.5 times longer for *Mastl(Δ/Δ)* MEFs. Whereas control cultures spent approximately 73 ± 5 min in mitosis, most *Mastl(Δ/Δ)* MEFs arrested in prometaphase and reached DOM of 182 ± 16 min (**Figure 16a**). This delay was due to the activation of the Spindle Assembly Checkpoint (SAC), since knockdown of the essential SAC protein Mad2 significantly reduced DOM in *Mastl(Δ/Δ)* cells. Cell fate analysis showed that approximately 75% of *Mastl(Δ/Δ)* cells lack chromosome

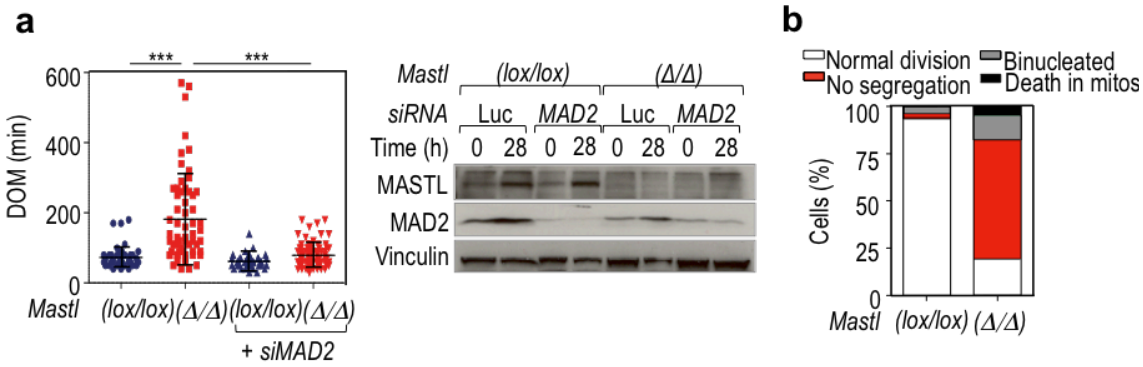

Figure 16. *Mastl* depletion leads to prolonged mitosis and chromosome segregation defects. **a)** Duration of mitosis was considered from NEB until mitotic exit and was scored based on DNA condensation and loss of rounded morphology, respectively. *Mastl(lox/lox)* and *Mastl(Δ/Δ)* iMEFs nucleofected with siRNAs against Mad2 or Luciferase (Luc) as control. WB shows the depletion of Mastl and Mad2. Vinculin was used as loading control. **b)** Quantification of mitotic aberrations in the same cells as in **a)**. ***p<0.001 (Student's *t*-test).

segregation whereas 5% of the cells died during mitosis (**Figure 16b**). In summary, we have shown that ablation of *Mastl* does not impair mitotic entry but triggers a SAC-dependent arrest in prometaphase, and eventually leads to lack of chromosome segregation.

It is known that Mastl inhibits PP2A-B55 complexes to avoid early dephosphorylation of CDK substrates in mitosis (Vigneron et al., 2009), and we have also shown that lack of Mastl results in decreased phosphorylated CDK substrates (**Figure 15f**). Importantly, knockdown of B55 alpha and delta isoforms rescued the defective phosphorylation of these substrates in mitotic entry extracts by WB (**Figure 17a-c**). *Mastl(Δ/Δ)* cells also presented defective chromosome condensation, as observed in metaphase spreads, a phenotype that was also rescued by co-depletion of B55 subunits (**Figure 17d**). PP2A/B55 inhibition also restored the reduced phosphorylation of CyclinB1 on S126, a phosphorylation event that is required for the stable association of CyclinB1 with mitotic chromosomes (**Figure 17e**). These results are in agreement with a requirement for Mastl to maintain the mitotic state after NEB through the inhibition of PP2A/B55 complexes.

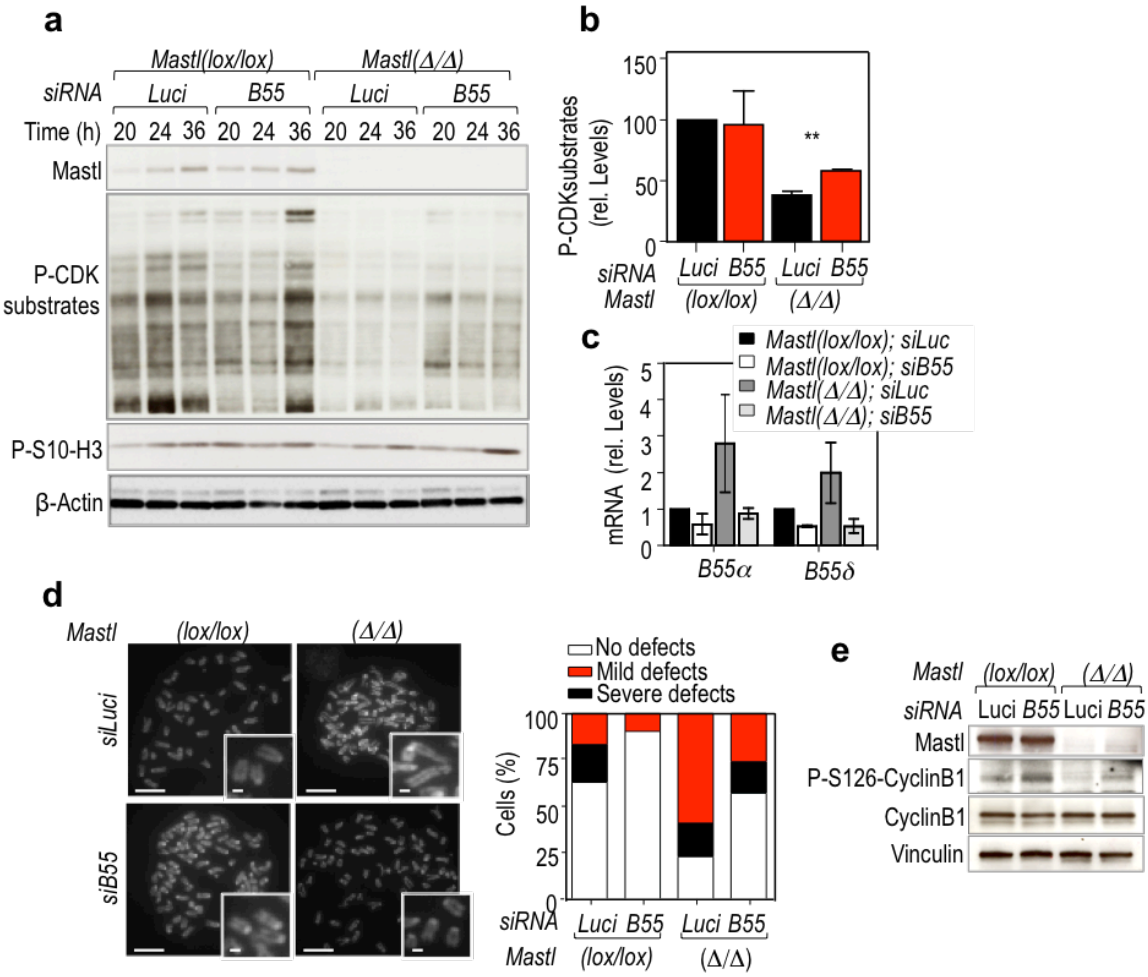

Figure 17. Mastl-mediated inhibition of PP2A/B55 prevents dephosphorylation of mitotic substrates and condensation defects in mitosis. **a)** WB of the indicated proteins in *Mastl(lox/lox)* and *Mastl(Δ/Δ)* iMEFS at the indicated time points after serum stimulation following the scheme represented in Figure 15a for culture synchronization and Mastl depletion. Cells were nucleofected with siRNAs against B55 alpha and delta subunits, or Luci as control. **b)** Quantification of the relative levels of phosphorylated CDK substrates at 24 h from a), values were normalized respect *Mastl(lox/lox)*. **c)** Quantification of the depletion of B55 alpha and delta by RT-qPCR in cells from a. **d)** Representative images of the metaphase spreads from the indicated cultures. Quantification of the percentage of cells per condition (Right). Condensation defects were determined based on the abnormal length of mitotic chromosomes and classified based on the number of affected chromosomes per metaphase as mild (5-10 chromosomes affected) or severe (more than 10). At least 50 metaphases were counted per condition. (Scale bars: 10 µm; Insets, 1 µm). **e)** WB for the indicated antibodies. Depletion of B55 subunits was analyzed by RT-qPCR.

3.1.2 Mastl depletion does not affect S-phase entry

Apart from the above-described role of Mastl in mitosis, and in the recovery from the G2 checkpoint (Peng et al., 2010), no other implications of Mastl in the control of cell cycle have

been described to date. Progression of cells into S phase is controlled by retinoblastoma protein (pRB) and relies on the functional inactivation of this tumor suppressor in late G1 via protein phosphorylation. Interestingly, it has been reported that PP2A/B55α counteracts CDK-mediated phosphorylation of pRB and the pocket proteins, p130 and 107, and restrains cell cycle progression at the G1/S transition (Kurimchak & Graña, 2012). Whether the control of PP2A/B55 activity in this context depends on Mastl has not been addressed. For this purpose, we explored the role of Mastl in S-phase entry using the *Mastl(lox/lox)* iMEFs. To generate *Mastl(Δ/Δ)* cells, MEFs were infected with lentiviral supernatants that expressed the recombinase Cre tagged in the N-terminal with mCherry (LentiCre). Control cells were infected with lentiviral supernatants expressing mCherry alone. As expression of Cre has shown some DNA damage-associated toxicity in MEFs, a *Mastl(+/+)* clone was also included as a control. To analyze entry into S-phase from G_0, cells were synchronized by serum starvation for 48 h and then split and stimulated with 10% serum in a time course experiment (**Figure 18a**). Cells were incubated with the thymidine analogous, EdU, for 30 min before harvesting to monitor DNA replication. EdU incorporation was quantified by flow cytometry. There were no differences in the percentage of cells entering S-phase from G_0 between *Mastl(lox/lox)* and *Mastl(Δ/Δ)* cells as shown by the percentage of EdU positive cells at the different time points (**Figure 18b**). The *Mastl(+/+)* clone had no differences

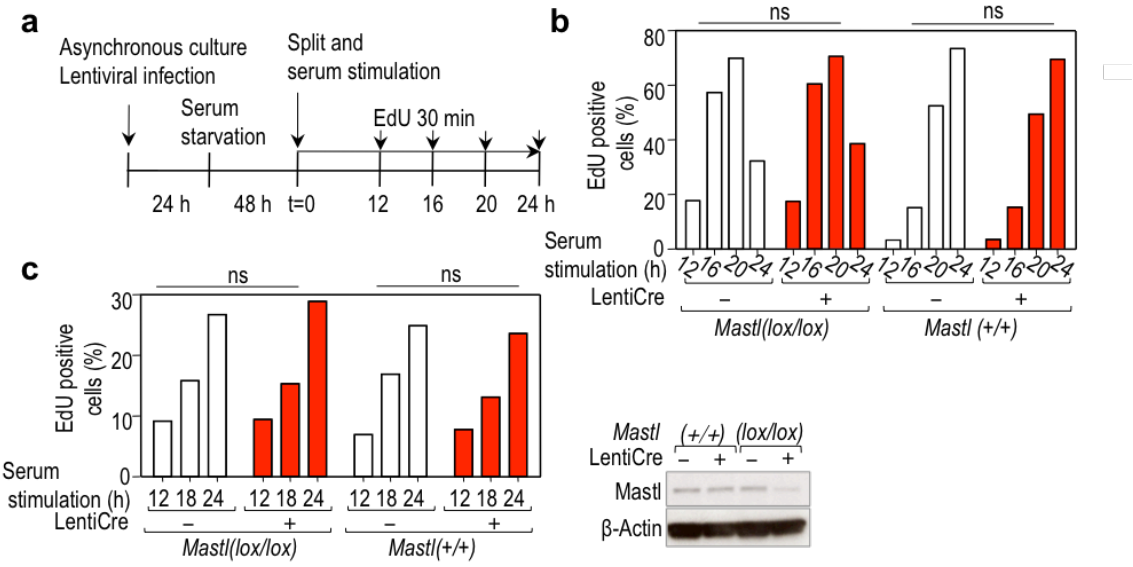

Figure 18. Mastl is not required for S-phase entry. **a)** Schematic representation of the protocol used for synchronization in G_0 and serum stimulation to monitor S-phase entry in *Mastl(lox/lox)* and *Mastl(+/+)* MEFs. Asynchronous MEFs were infected with Lentiviral supernatants to generate *Mastl(Δ/Δ)* and control MEFs. **b,c)** Quantification of EdU positive cells by flow cytometry at the indicated time points in iMEFs **b)** and pMEFs **c)** WB at 12 h after serum stimulation shows the depletion of MASTL protein upon LentiCre infection of pMEFs (Right). ns, not significant p>0.05.

after LentiCre infection neither, indicating that expression of Cre does not alter S-phase entry in this setting (**Figure 18b**). Similar kinetic in S-phase entry was obtained in pMEFs (**Figure 18c**) confirming that Mastl is not required for S-phase entry in MEFs.

3.1.3 Mastl is not essential for quiescence in mammals

The budding yeast Mastl protein, Rim15, is required for entry into quiescence in conditions of nutrient scarcity (Pedruzzi et al., 2003). Following nitrogen and/or carbon limitation Rim15 orchestrates the initiation of a reversible cellular quiescence program. Based on the role of

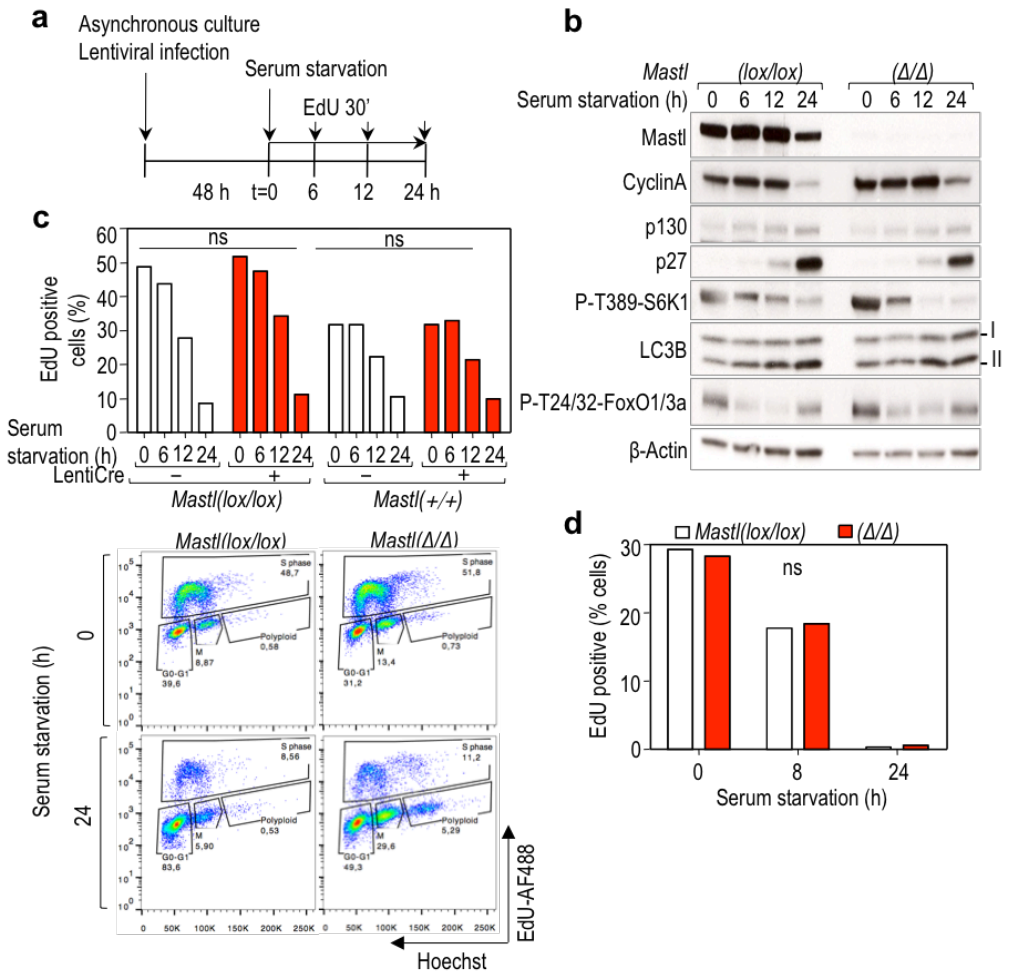

Figure 19. Entry into quiescence is not altered by Mastl deletion in MEFs. **a)** Schematic representation of the protocol used for depletion of Mastl and monitor entry into quiescence in MEFs. Asynchronous MEFs were infected with LentiCre supernatants and 48 h later cultures were serum starved for the indicated points. **b)** Immunoblot analysis for the indicated proteins from total extracts of iMEFs at different time points after serum starvation. **c)** Quantification of EdU positive cells by flow cytometry in iMEFs. Representative plots of the flow cytometry profiles for EdU staining (Bottom). **d)** Quantification of EdU positive cells after serum starvation in pMEFs. ns, not significant p>0.05.

Rim15, we explored the potential role of Mastl in quiescence in mammals. We made use of *Mastl(lox/lox)* MEFs, which were infected with LentiCre supernatants to generate *Mastl(Δ/Δ)* MEFs. Control cells were infected with lentiviral supernatants expressing the mCherry protein alone. Entry into quiescence was analyzed in a time course following serum starvation (**Figure 19a**). 24 h after serum starvation control cells had already decreased the levels of proliferative proteins like cyclinA and signaling through the mTORC1 pathway (scored by P-T389 S6K1), likewise they had increased the levels of the antiproliferative proteins p130 and p27, and had increased autophagy signals such as the appearance of the LC3B-II lipidated band. *Mastl(Δ/Δ)* MEFs, however, did not show any differences in any of these proteins compared to control MEFs (**Figure 19b**). Quiescence state is also characterized by the loss of proliferative markers, such as Ki67 or EdU staining. There were no differences either in the proportion of cells exiting the cell cycle across the different time points analyzed, as shown by loss of EdU staining (**Figure 19c**). We further validated these results in pMEFs, which are more sensitive to the loss of mitogenic signals and become fully quiescent 24 h after serum starvation. Similarly to iMEFs, *Mastl(Δ/Δ)* pMEFs efficiently entered quiescence, following same kinetics as controls cells (**Figure 19d**).

To evaluate if Mastl, rather than for entry into quiescence, was instead required for maintenance of the quiescence state, we starved cells 24 h after LentiCre infection to ensure that Mastl deletion occurs in already quiescent cells, and analyzed the ability of these cells to re-enter the cell cycle after a prolonged serum starvation (**Figure 20a**). 72 h after serum starvation MEFs were efficiently arrested into quiescence, as shown by loss of EdU and Ki67 staining quantified by HTM (**Figure 20c**). However, *Mastl(Δ/Δ)* cells showed no defects in the maintenance of

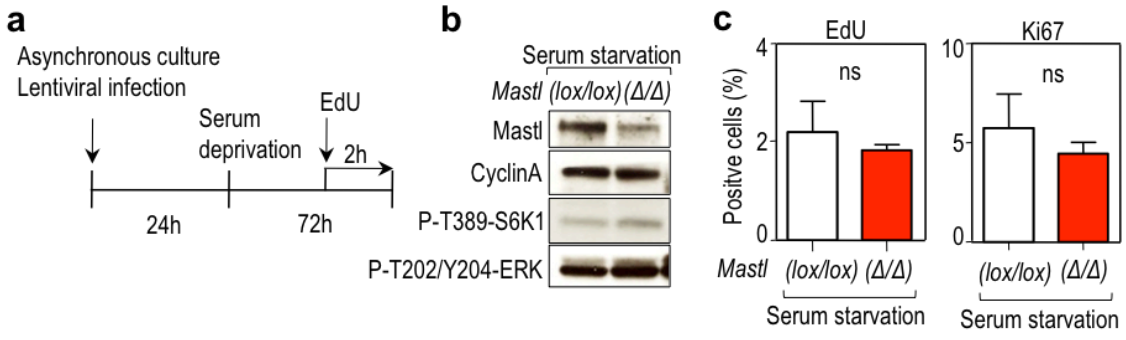

Figure 20. Mastl is not required for maintenance of quiescence in MEFs. **a)** Schematic representation of the protocol used for depletion of Mastl and monitor entry into quiescence in iMEFs. Asynchronous iMEFs were infected with LentiCre supernatants and 24 h later cultures were serum starved for 72 h. 2 h before recovery cells were incubated with EdU. **b)** Immunoblot analysis from 72 h serum starved iMEFs. **c)** EdU (Left) and Ki67 (Right) quantification using HTM after 72 h of serum starvation. ns, not significant p>0.05 (Student's *t* test).

quiescence nor differences in the expression of proliferative markers by WB (**Figure 20b**). These data suggests that, in contrast to budding yeast, Mastl is not essential for either entry into or maintenance of the quiescence state in mammals.

3.2 Mitotic-independent function of MASTL-PP2A/B55 pathway

3.2.1 Role of MASTL in nutrient-modulated pathways in mammals

In line with the observations done in yeast where Rim15 is controlled downstream the master nutrient regulated pathways of TORC1 and PKA (Pedruzzi et al., 2003), we aimed to analyze whether MASTL may also have some relevance downstream nutrient sensing pathways in mammals. For this purpose, we studied the effect of MASTL depletion in human cells in the signaling through the mTORC1 and PI3K/AKT pathways, which are the main routes involved in nutrient and growth factor sensing across organisms (Manning & Toker, 2017; Saxton & Sabatini, 2017). We chose the breast cancer cell line MDA-MB231 as a cellular model, since it expresses high levels of MASTL protein and it responds fast and in a very accurate and consistent manner to changes in concentrations of specific nutrients in the media. We knocked down MASTL expression by interference RNA using a specific shRNA against *MASTL* subcloned in the pLKO.1 lentiviral system (*shMASTL*). As we have shown in the first part of the results, and in agreement with previous work (Burgess et al, 2010), *MASTL* ablation results in reduced proliferation as consequence of defective chromosome condensation and segregation problems in mammalian cells. To avoid any interference with mitotic aberrations in our results, experiments were performed at early time points after *MASTL* depletion, before segregation problems occur. Cell cycle analysis by flow cytometry 72 h after shRNA lentiviral infection, showed no differences in the percentage of cells in the different phases of the cell cycle despite strong reduction in MASTL protein levels (**Figure 21**). All experiments were performed not later than 72 h after induction of

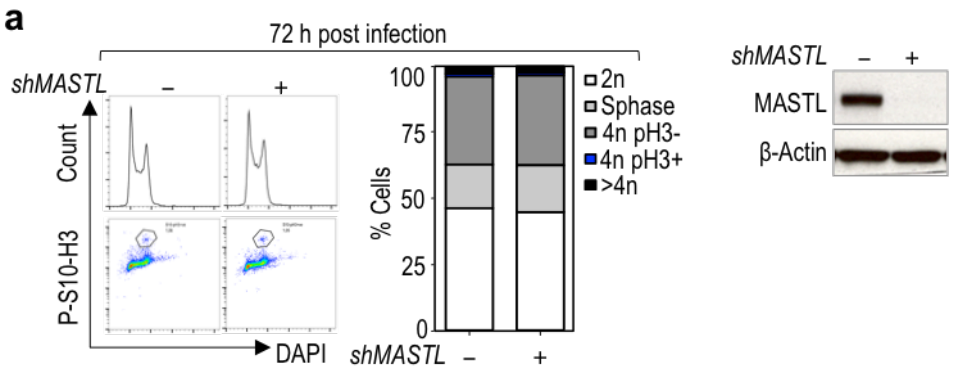

Figure 21. Cell cycle analysis after knockdown of *MASTL*. Quantification of the different phases of the cell cycle in control and MASTL null cells. MDA-MB231 cells were infected with shRNA specific for *MASTL* or Scr as control, and cell cycle was analyzed 72 h later. Mitotic cells were scored using Immunodetection of P-S10-H3 (pH3) and total DNA was stained with DAPI followed by flow cytometry analysis. Left pictures show representative cell cycle profiles and P-S10-H3 staining. WB showing the depletion of MASTL 72 h after *shMASTL* infection (Right).

MASTL ablation.

To study the effect of the MASTL-ENSA/ARPP19-PP2A/B55 pathway in nutrient signaling in cells, MDA-MB231 cells were subjected to different nutritional starvations known to inhibit the mTORC1 pathway following the protocol depicted in **Figure 22a**. mTORC1 pathway signaling was analyzed by WB using specific antibodies for its upstream regulators and downstream targets. In control cells infected with a scramble sequence (shScr), starvation for specific nutrients efficiently inhibited mTORC1 activity, as shown by decreased levels of phosphorylation of S6K1 and 4E-BP1 on their mTORC1 target sites T389 and S65, respectively (**Figure 22b**). *MASTL*-depleted cells showed, however, a significant increased in the phosphorylation of the mTORC1 targets S6K1, accompanied by increased phosphorylation of its substrate S6 (on S235/236), and 4E-BP1, in the absence of glucose, indicating lack of mTORC1 inhibition under these conditions. These signals were concomitant with a significant increase in the inhibitory phosphorylation of TSC2 on T1462, which was also higher in *MASTL*-depleted cells upon amino acid starvation. During glucose starvation, a reduction in cellular energy activates the

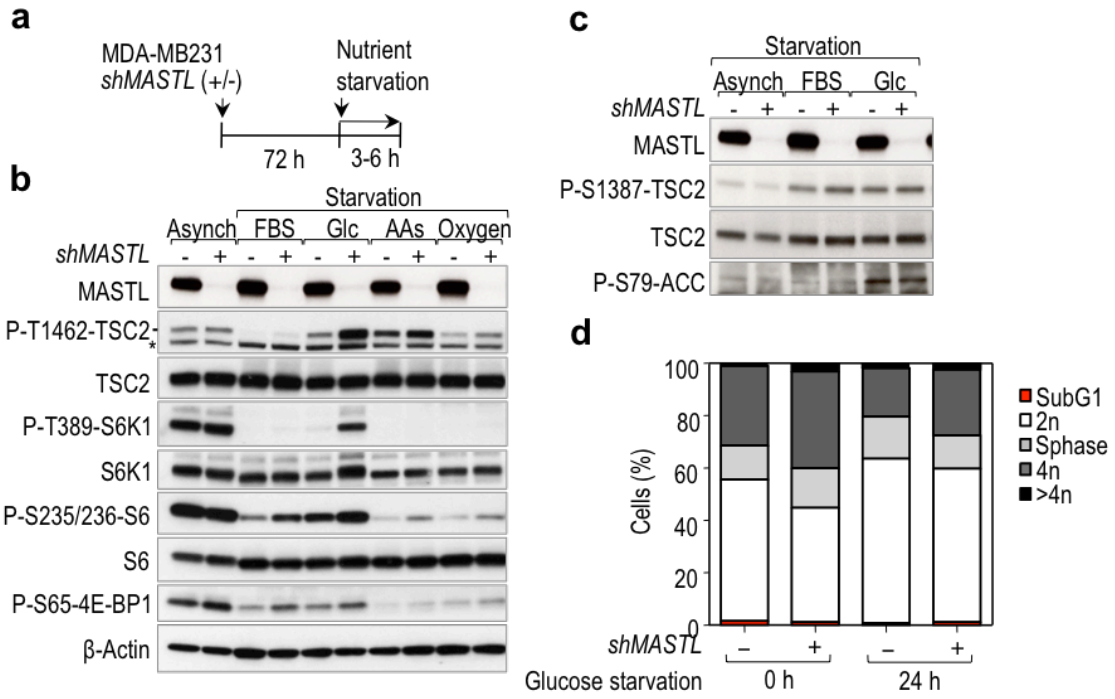

Figure 22. Glucose starvation fails to inhibit mTORC1 in the absence of MASTL. a) Schematic representation of the protocol followed for depletion of MASTL in human cell lines and different nutrient starvations. Asynchronous cells were infected with lentiviral supernatants containing shRNAs against *MASTL* or Scr as control, 72 h later cells were submitted for the different nutrient starvations. **b,c)** Immunoblot analysis of the same extracts using the indicated antibodies. **d)** Quantification of the percentage of cells in the different phases of the cell cycle 24 h after glucose starvation. Cell cycle analysis was done by flow cytometry. DNA content was stained with PI.

stress responsive metabolic regulator AMPK, which inhibits mTORC1 both indirectly, through phosphorylation and activation of TSC2, as well as directly, through the phosphorylation of Raptor (Gwinn et al., 2008; Inoki et al., 2003; Shaw et al., 2004). However, no differences were found in the activity of AMPK toward its substrates in *MASTL*-depleted cells using specific antibodies against TSC2 P-S1387 and ACC P-S79 (**Figure 22c**), suggesting that impaired AMPK activity is not responsible of the lack of inhibition of mTORC1 upon glucose starvation in *MASTL*-depleted cells. AMPK also regulates a cell-cycle checkpoint that monitors glucose availability in proliferating MEFs (Jones et al., 2005). This glucose-dependent checkpoint is at the G_1/S boundary and occurs despite continued amino acid availability and active mTOR. We next checked whether depletion of MASTL might alter the glucose-regulated checkpoint in our cells. For this purpose we analyzed the cell cycle profile of *MASTL*-depleted cells by flow cytometry 24 h after glucose starvation. Glucose starvation induced a mild arrest of control cells in G1, but more importantly, there were no differences upon *MASTL* ablation (**Figure 22d**). In summary, we have found that glucose starvation was able to inhibit mTORC1 only in the presence of MASTL, and that *MASTL* ablation resulted in increased mTORC1 activity that was concomitant with a strong inhibition of TSC2 in *MASTL*-null cells.

As a complementary approach to analyze the consequences of *MASTL* ablation, we have also developed a strategy for conditionally knockout *MASTL* gene using a Dox-inducible form of the CRISPR-Cas9 technology in the MDA-MB231 cell line (isgMASTL) (see section **2.1.2**). *MASTL* was efficiently ablated upon Dox treatment, and resulted in increased S6K1 and TSC2 phosphorylation in a glucose-sensitive fashion (**Figure 23a**). A key player in the regulation of TSC-mTORC1 axis is the Ser/Thr kinase AKT. AKT is activated downstream of growth factor-stimulated PI3K activity, full activation of AKT requires its phosphorylation on two sites: the T308 in the activation loop by PDK1 and the S473 in the hydrophobic motif by mTORC2 (Manning & Toker, 2017). AKT was strongly phosphorylated on T308, and also showed increased phosphorylation on the S473 in *MASTL*-null cells (**Figure 23a**). AKT regulates mTORC1 activity by phosphorylation of TSC2 directly on multiple sites (Ser939, Ser981, Ser1130, Ser1132 and Thr1462) that relieve the inhibitory effects of the TSC complex on Rheb and mTORC1, and thereby activating mTORC1. In consequence, TSC2 was more phosphorylated on S939 and especially on T1462, in *MASTL*-depleted cells. Other AKT substrates, like the mTORC1 inhibitor PRAS40, or GSK3 were likewise more phosphorylated on their AKT sites, T246 and S9, respectively, upon *MASTL* ablation, further suggesting enhanced AKT activity in the absence of MASTL. Slight differences were observed in the phosphorylation of ERK1/2, another positive regulator of the mTORC1 pathway upstream of TSC2, and no differences were observed in the

activity of AMPK towards its substrates Raptor S792 and ACC S79. The effect of *MASTL* ablation on the AKT-TSC2-mTORC1/S6K1 axis was specific for *MASTL* ablation since Dox-mediated induction of Cas9 in the presence of scrambled sgRNAs in a different clone of the MDA-MB231 cells did not modify the phosphorylation status of the components of this pathway (**Figure 23b**).

A similar effect of *MASTL* knockdown in the phosphorylation of AKT in a glucose-sensitive manner was also reproduced and validated in two other breast cancer cell lines, BT549 and MCF7, using shRNAs to knockdown *MASTL* expression (**Figure 23c,d**). The BT549 cell line is null for PTEN, the major phosphatase that counteracts PI3K activity. Ablation of *MASTL* still impaired the effect of glucose on mediating AKT inhibition in this cell line, suggesting that the effect of *MASTL* ablation is independent on PTEN (**Figure 23c**). In addition, total PTEN levels

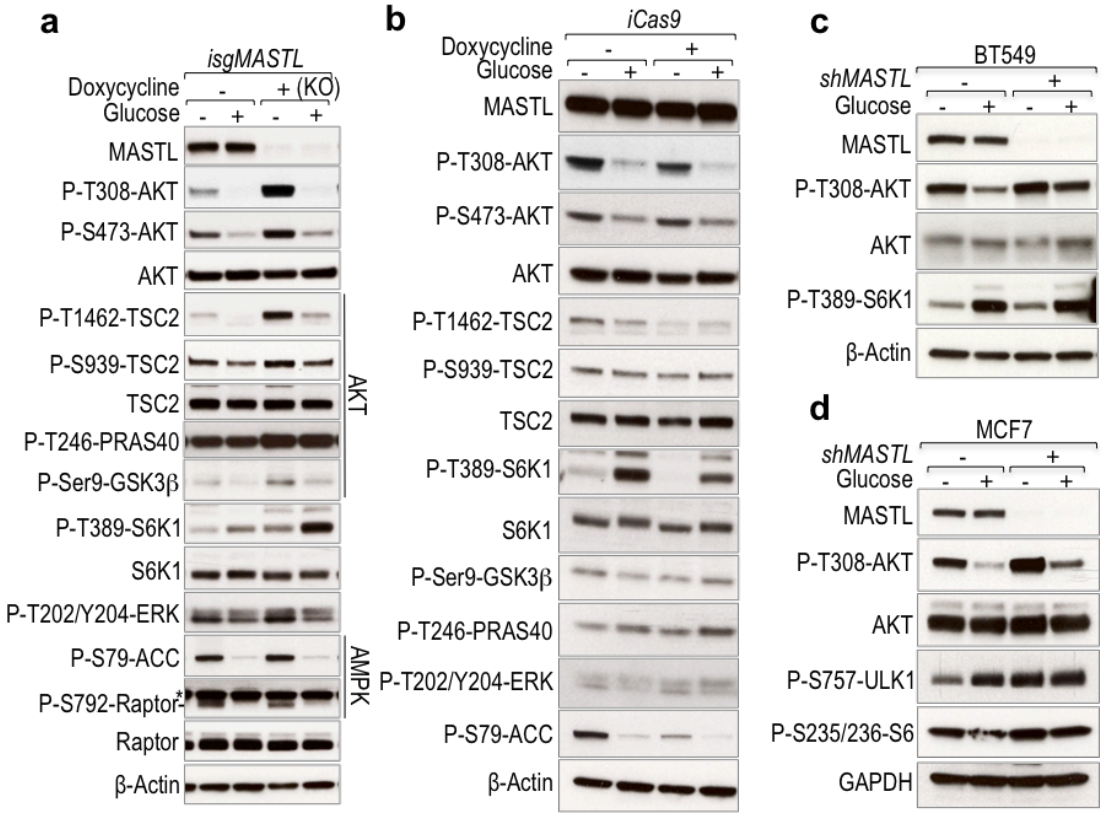

Figure 23. Modulation of the AKT-mTORC1 pathway in a glucose-sensitive fashion in *MASTL*-null cells. Immunoblot analysis for the indicated proteins of the AKT-mTORC1, ERK and AMPK pathways. **a)** MASTL expression was ablated by the isgRNA system upon Dox addition in the MDA-MB231 cell line. 72 h later, cells were starved of glucose in the media in presence of 10% dFBS for 1 h and then re-stimulated with 25 mM of glucose for 10 min before recovery. **b)** Control of the Dox and Cas9 expression in the isgRNA system using a control clone of the MDA-MB231 that expresses Scr sgRNAs. Same protocol as in **a)** was followed. **c,d)** Immunoblot analysis with the indicated antibodies in the BT549 and MCF7 cell lines, respectively. *MASTL* knockdown was done upon infection with shRNAs for *MASTL* or Scr as control. Glucose starvation and re-stimulation experiments were done 72 h after infection with shRNAs following the same protocol as in **a)**. β-Actin, or GAPDH when specified, were used as loading controls.

were unaltered in *MASTL* null cells (**Figure 24b**). Altogether these results suggested that the up-regulation of the mTORC1 pathway upon *MASTL* ablation is consequence of increased AKT activity and subsequent inhibition of mTORC1 inhibitors by AKT.

3.2.2 MASTL regulates AKT through mTORC1/S6K1-dependent feedback mechanisms

The PI3K-AKT-mTORC1 pathway is a highly dynamic network that is balanced and stabilized by a number of negative feedback inhibition loops. AKT both regulates and is regulated by the TSC complex (Huang & Manning, 2009). Through negative-feedback mechanisms, mTORC1/S6K1 activity inhibits growth factor stimulation of PI3K/AKT at the level of the RTKs, and this also has an important role in the regulation of mTORC1 (Shimobayashi & Hall, 2014). In addition, the mTORC1/S6K-dependent feedback loop is as well responsible for inhibiting the activity of the ERK/MAPK pathway (Carracedo et al., 2008). To date there is no evidence of glucose regulating directly the PI3K/AKT pathway. Instead, glucose has been shown to positively regulate mTORC1 activity through the Rag GTPases (Efeyan et al., 2013). Interestingly, amino acids have been shown to modulate insulin signaling through mTORC1-dependent effects in the insulin receptor

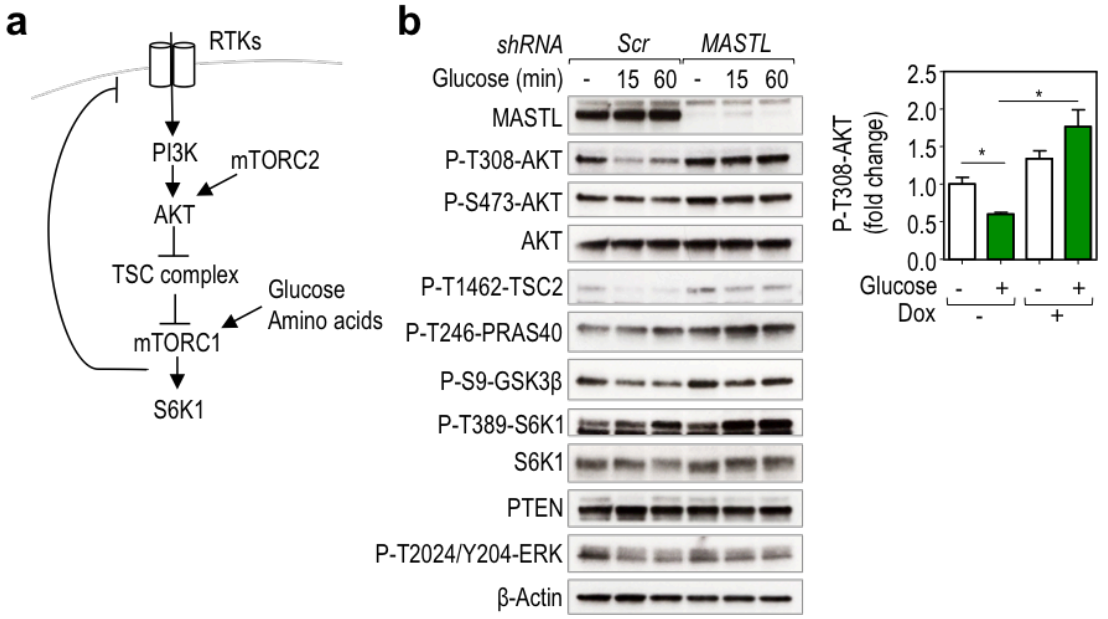

Figure 24. Glucose modulates PI3K/AKT signaling through an mTORC1/S6K1-dependent feedback loop. **a)** Schematic showing the mTORC1/S6K1-dependent negative feedback loop over PI3K signaling and AKT regulation. **b)** *MASTL* was depleted using shRNAs against *MASTL* or Scr as control. Cells were starved from glucose for 2 h and re-stimulated with 5 mM glucose in a time course for 15 min and 1 h. Total extracts were recovered and tested for the indicated antibodies. Quantification of the immunoblots of AKT T308 upon glucose starvation and re-stimulation for 15 min. N=2 independent experiments. Error bars indicate sem. *p<0.05 (Student's *t*-test).

substrate protein IRS1, as excess amino acids attenuate and amino acid starvation stimulates AKT activation via mTORC1 regulation (Takano et al., 2001; Tremblay & Marette, 2001). Given these observations, we hypothesized that glucose availability could control mTORC1-dependent feedback loops to regulate the PI3K/AKT pathway, similarly as amino acids do. If this were true, glucose starvation would inhibit mTORC1 and relieve the negative feedback loop over PI3K pathway, resulting in increased AKT activity. On the other hand, glucose re-addition would induce mTORC1 re-activation and trigger the feedback loop-mediated AKT inhibition (**Figure 24a**). Whereas control cells responded to the glucose-mediated feedback loop, *MASTL*-null cells failed to inhibit AKT in response to glucose stimulation, despite having enhanced mTORC1 activity as shown by S6K1 T389 (**Figure 24b**). This data suggested a defective mTORC1/S6K1-dependent negative feedback loop and AKT inhibition in the absence of MASTL.

The primary pathway by which most growth factors activate mTORC1 appears to be the PI3K/AKT pathway. As with amino acids, several research groups have found that PI3K/AKT mediated activation of mTORC1 also leads to attenuation of insulin signaling in a negative feedback loop. Their studies have demonstrated that activation of the PI3K/AKT-mTORC1 pathway by insulin itself leads to IRS1 serine phosphorylation and downregulation in a rapamycin-sensitive manner (Carlson et al., 2004; Greene et al., 2003; Haruta et al., 2000). To understand the role of MASTL in the regulation of AKT activity following mTORC1/S6K1 activation by insulin, we performed a time course of insulin stimulation after 6 h of serum starvation. Insulin induces a rapid and gradual activation of the AKT-mTORC1/S6K1 axis with a maximal activation 15 min after stimulation in our cells (**Figure 25a**). Following this peak of mTORC1/S6K1 activity and triggering of the feedback loop, there was a strong inhibition of AKT at the point of 30 min in control cells. *MASTL*-null cells despite having comparable levels of AKT-mTORC1/S6K1 activity at 15 min, by contrast, failed to inhibit AKT at 30 min, resulting in sustained TSC2 T1462 and S6K1 T389 phosphorylation (**Figure 25a**). Loss of TSC2 disengages mTORC1 from the upstream inputs, resulting in mTORC1 constitutive activation (Henry, 2003; Kwiatkowski et al., 2002). As consequence, *TSC2*-null cells have potent mTORC1-dependent feedback loops and AKT is less responsive to activation by insulin or IGF-I, exposure to rapamycin can restore AKT activation in these cells (H. H. Zhang, Lipovsky, Dibble, Sahin, & Manning, 2006). Therefore knockdown of *TSC2* is a good model for study mTORC1 feedback regulation of AKT signaling. Interestingly, knockdown of *TSC2* in MDA-MB231 cells using shRNAs triggered AKT inhibition, and co-depletion of *MASTL* in these cells partially restored AKT activity, although did not rescue AKT signaling to the same extent as in wild-type cells (**Figure 25b**). In agreement with that, rapamycin treatment boosted AKT phosphorylation in control cells

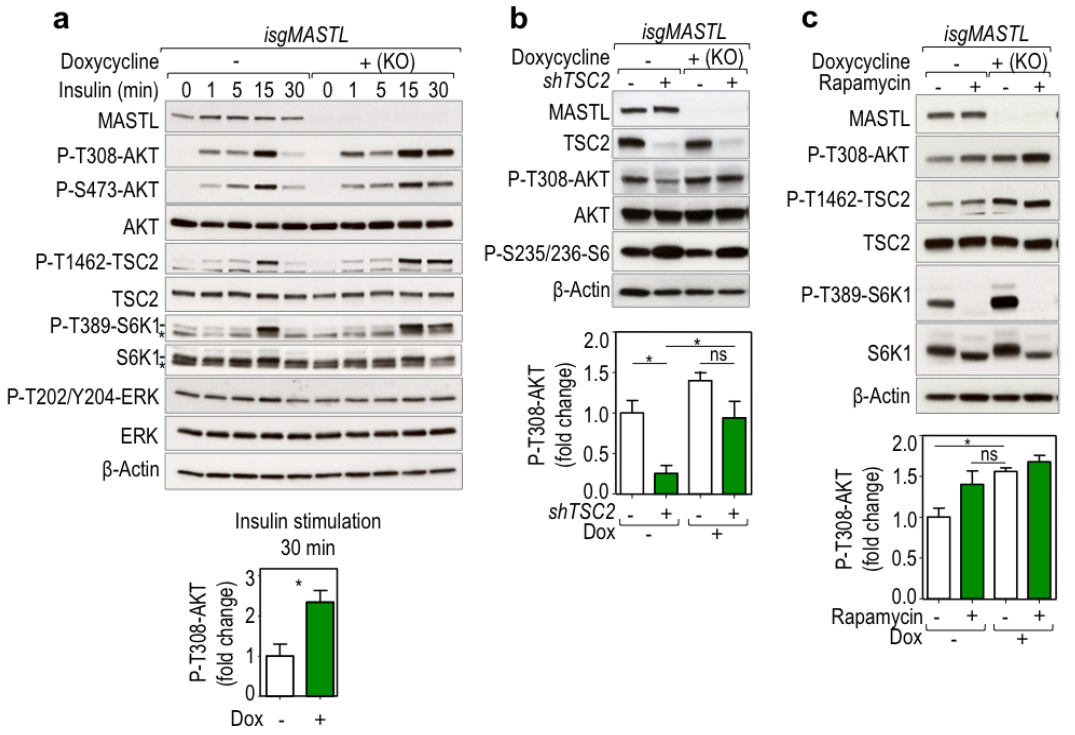

Figure 25. MASTL promotes AKT inhibition by mTORC1/S6K1-dependent feedback mechanisms. **a)** Time course experiment at the indicated time points after 100 nM insulin stimulation in 6 h serum-starved control and *MASTL* knockout cells. MASTL depletion was induced upon addition of Dox and cells were recovered 72 h later. immunoblot for the indicated antibodies is shown in each case. Quantification of AKT T308 at 30 min after insulin stimulation. N=5 independent experiments (Bottom). **b)** TSC2 expression was knocked down in control or *MASTL*-null cells using specific shRNAs for TSC2 or Scr as control. Cells were starved and re-stimulated with insulin for 30 min. WB for the indicated antibodies. Quantification of AKT T308. N=3 independent experiments. **c)** Control or *MASTL* null cells were treated with 100 nM rapamycin or vehicle as control. Cells were starved for glucose for 1 h and re-stimulated with glucose for 15 min; rapamycin was added 15 min before glucose stimulation. Immunoblot of the indicated antibodies. Quantification of AKT T308 (Bottom). N=3 independent experiments. Error bars indicate sem. ns, not significant. *p<0.05 (2-way ANOVA; Student's *t*-test).

to the same extent as *MASTL* depletion did, reinforcing the idea of MASTL having a role in the mTORC1-mediated feedback loop **(Figure 25c**). The effect of *MASTL* knockdown was further increased upon rapamycin treatment, suggesting that MASTL is important for the feedback loop, but that other MASTL-independent mechanisms are also at play.

3.2.3 MASTL activity is modulated in conditions of feedback regulation

To address the question of how MASTL is regulated in a mitotic-independent context, we have analyzed MASTL activity in the experimental conditions of glucose starvation and re-stimulation

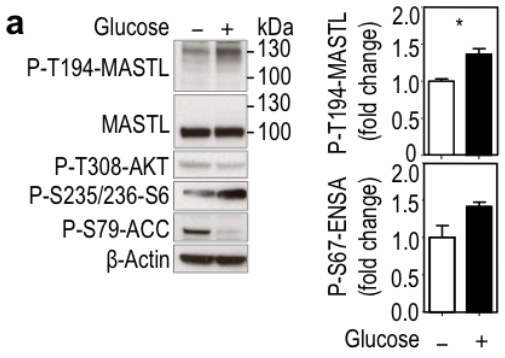

Figure 26. MASTL activity is regulated in a glucose-sensitive manner. **a)** WB for the indicated antibodies. MDA-MB231 WT cells were starved for 1 h and re-stimulated with glucose for 15 min. Immunoblot quantification of phosphorylated MASTL T194 and ENSA/ARPP19 S67/S62 (Right). N=2 independent experiments. Error bars indicate sem. *p<0.05 (Student's *t*-test).

reported above for modulation of feedback activity. As readouts of MASTL activity we have used phosphospecific antibodies generated against the T194 of MASTL, an essential site for MASTL kinase activity (Blake-Hodek et al., 2012), and for its substrates ENSA/ARPP19 S67/S62. Glucose re-addition following glucose starvation triggers mTORC1-dependent AKT inhibition at the same time it increases phosphorylation of MASTL at T194 and of its substrates ENSA and ARPP19 (**Figure 26a**), suggesting that MASTL activity might be positively regulated in response to glucose stimulation.

As shown above, hyperactivation of mTORC1 by means of *TSC2* ablation attenuates AKT activity in a rapamycin-sensitive manner. In our model MASTL activity favors the mTORC1-dependent feedback loop and this raises the possibility of MASTL being positively regulated in conditions of feedback activity. Phosphorylation of MASTL at T194 was increased upon *TSC2* knockout in a rapamycin- and torin1-sensitive manner (**Figure 27a**). MASTL activity was also modulated in these conditions as shown in an *in vitro* kinase assay over GST-ARPP19 using GFP-MASTL immunocomplexes. In this assay MASTL activity increased upon *TSC2* knockout and was partially prevented upon rapamycin and more efficiently upon torin1 treatment (**Figure 27b**). MASTL activity was similarly partially sensitive to mTORC1 inhibitors in cells using as a readout phosphorylation of ENSA and ARPP19 at their MASTL sites by WB (**Figure 27c**). These data further suggest that MASTL activity may correlate with feedback activity and open the question of MASTL as being regulated downstream the mTORC1/S6K1 axis.

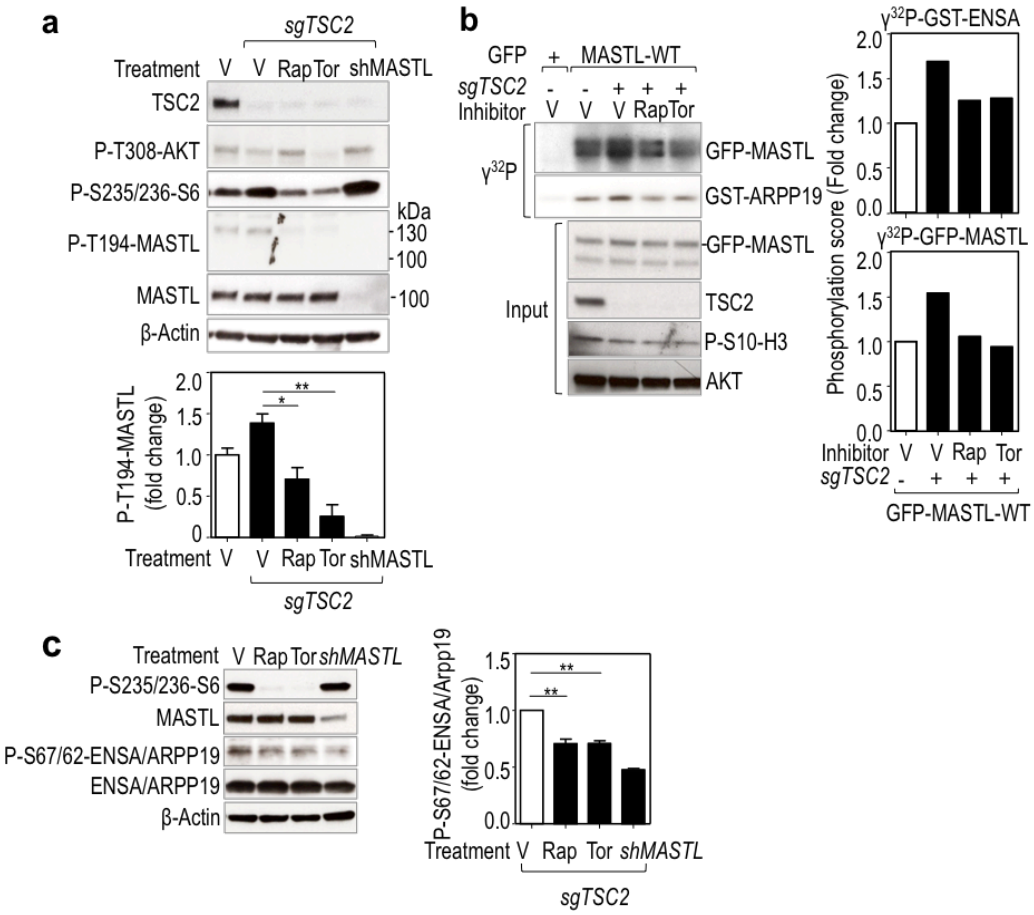

Figure 27. MASTL activity is modulated by mTOR under conditions of feedback regulation. **a)** MDA-MB231 cells stables for the knock out of TSC2 protein or control cells expressing only Cas9 were treated with rapamycin (Rap), Torin1 (Tor), or vehicle as control (V). sgTSC2 cells were depleted for MASTL using shRNA as control of the specificity of the antibody. Inhibitors were added 15 min before glucose re-stimulation for 15 min and total cell lysates were harvested for immunoblot. Bottom plots represent the quantification of MASTL T194. **b)** *In vitro* kinase assay using GFP-hMASTL WT immunocomplexes from asynchronous sgTSC2 or control cells treated with the indicated inhibitors for 1 h. IP of GFP alone was used as control. Phosphorylation over its substrate GST-ARPP19 and autophosphorylation of MASTL were used as readouts of MASTL activity. Left panel shows the radiographs of MASTL activity in the different conditions accompanied by the immunoblots of the whole cell extracts. Quantification of MASTL activity is shown in the plots on the right. **c)** Immunoblot showing MASTL activity over its substrates ENSA/ARPP19 in cells using a specific S67/S62 phosphoantibody. Cells stably overexpressing FLAG- and HA-tagged versions of ENSA and ARPP19, respectively were treated with the indicated inhibitors as in **a)**. Right plot represents the quantification of phosphorylated S67/S62 signal. N=2 independent experiments. Error bars indicate sem. *p<0.05; **p<0.005 (one-way ANOVA).

3.2.4 MASTL controls AKT activity in a ENSA/ARPP19-PP2A/B55 dependent-manner

The role of MASTL in PP2A/B55 inactivation is indirectly mediated through phosphorylation of the endosulfine proteins ENSA and ARPP19, which are the two only known MASTL substrates to date (Vigneron et al., 2009; Gharbi-Ayachi et al., 2010; Mochida et al., 2010). As shown above, treatment with mTORC1 inhibitors partially reduced the activity of MASTL over ENSA/ARPP19 (**Figure 27b,c**), reinforcing the possibility that the participation of MASTL in the mTORC1/S6K1-dependent feedback loop is mediated by the ENSA/ARPP19-PP2A/B55 axis.

To further understand if the effect of MASTL on AKT was mediated through the conserved ENSA/ARPP19-PP2A/B55 pathway, we evaluated whether knockdown of *ENSA* and *ARRPP19*

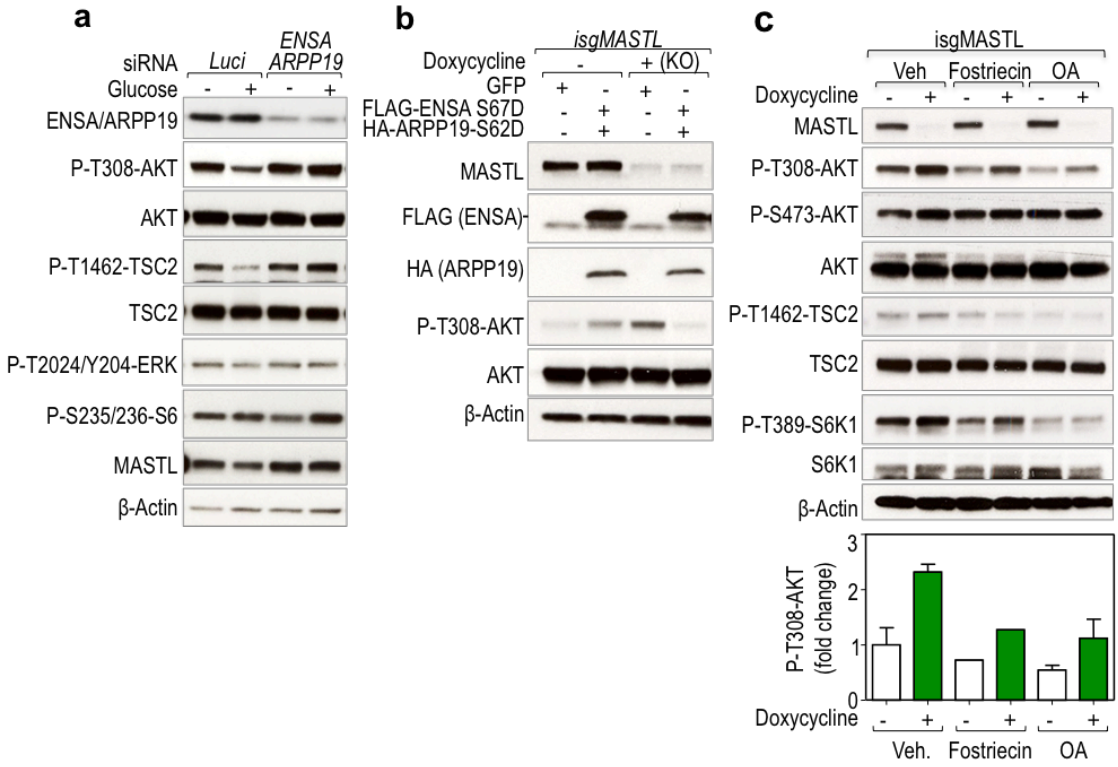

Figure 28. MASTL controls AKT activity through the ENSA/ARPP19-PP2A/B55 pathway. a) Co-depletion of ENSA and ARPP19 proteins in the MDA-MB231 cell line using specific siRNAs or against luciferase (Luci) as control. 72 h after transfection cells were starved for glucose for 1 h and re-stimulated with glucose for 15 min. Total cell extracts were recovered and analyzed for the indicated antibodies. **b)** MDA-MB231 cells stably co-expressed FLAG- and HA-tagged versions of ENSA and ARPP19 phosphomimetic mutants (S67D and S62D). Cells were treated with Dox to induce *MASTL* knockdown, and 72 h later cells were treated as specified in **a)**. **c)** Control and *MASTL* knockout cells were treated with 5 μM fostriecin, 50 nM OA or vehicle (Veh) 10 min before insulin stimulation for 30 min. Total lysates were analyzed for the indicated antibodies. Plot representing the quantification of AKT T308 (Bottom). N=2 independent experiments. Error bars indicate sem.

expression in MDA-MB231 cells using siRNAs could mimic *MASTL* ablation. Similar to *MASTL* depletion, knockdown of ENSA and ARPP19 proteins resulted in increased AKT phosphorylation and prevented the effect of glucose re-addition in the mTORC1-mediated feedback inhibition of AKT (**Figure 28a**). Enhanced AKT phosphorylation led to increased TSC2 T1462 and S6 S235/236 phosphorylations upon glucose re-addition as readout of S6K1/mTORC1 activity. In addition, expression of phosphomimetic mutant cDNAs of ENSA and ARPP19, which mimic MASTL-dependent phosphorylation (S67D and S62D for ENSA and ARPP19, respectively) restored the levels of phosphorylated AKT in *MASTL* depleted cells upon glucose re-addition, suggesting that MASTL activity is dispensable in the presence of these phosphomimetic mutants (**Figure 28b**). To test the involvement of the PP2A/B55 phosphatase, similar assays were done using chemical PP2A phosphatase inhibitors. Treatment of cells, at low doses, with specific PP2A inhibitors, fostriecin, or okadaic acid (OA), led to decreased levels of phosphorylated AKT on T308 and partially rescued AKT phosphorylation in *MASTL*-depleted cells (**Figure 28c**). Altogether, these results further suggested that the role of MASTL in the feedback is through the conserved pathway of MASTL function, and involves inhibition of the phosphatase PP2A/B55 through phosphorylation of the endosulfine proteins, ENSA and ARPP19.

3.2.5 The MASTL-PP2A/B55 axis modulates the phosphorylation status of the mTORC1/S6K1-dependent feedback targets, IRS1 and GRB10

Feedback inhibition of the PI3K/AKT pathway by mTORC1 is an important signaling event that plays a critical role in maintaining the stability of the entire PI3K/AKT-mTORC1 network, but the molecular connections are poorly understood (Hsu et al., 2011a). It involves mTORC1/S6K1-depedent phosphorylation and destabilization of the insulin receptor substrates, IRS1 and IRS2 (Shah et al., 2004; Harrington et al., 2004; Shah & Hunter, 2006), and simultaneous phosphorylation and stabilization of GRB10 (Hsu et al., 2011a). IRS and GRB10 are adaptor proteins of the insulin and IGF-I receptors that couple transduction to the PI3K pathway in a positive and negative manner, respectively. Turnover of the IRS proteins is a physiological mechanism to attenuate insulin signaling during prolonged exposure to insulin and this process is mTORC1/S6K1-dependent, as rapamycin prevents IRS turnover in multiple cell lines chronically exposed to insulin (Shah et al., 2004). IRS proteins are phosphorylated at multiples Ser/Thr sites, which controls protein stability by targeting it to the ubiquitin proteosomal pathway (Rui et al., 2001; Sun et al., 1999). GRB10 is also phosphorylated by mTORC1 at multiple sites (S104, S150, S428 and S476), but in contrast to IRS proteins, GRB10 phosphorylation stabilizes it and prevents it from proteasomal degradation mediated by NEDD4 (Hsu et al., 2011a). Whereas

much is known about the target kinases, little is known about the phosphatases involved. IRS1 protein stability has been shown to be regulated by the proline-directed S/T phosphatase PP2A (Hartley & Cooper, 2002), although the precise mechanism and the regulatory subunits of PP2A involved remain unknown.

We have tested whether the PP2A/B55 phosphatase complexes could control the phosphorylation of the feedback targets IRS1 and GRB10. For this purpose, we knocked down the B55 alpha and delta subunits in cells using siRNAs and analyzed by WB the phosphorylation status of the adaptor proteins using commercial available specific phospho-antibodies against proline-directed S/T sites. Depletion of B55 alpha and delta caused hyperphosphorylation of both IRS1 and GRB10 as shown by lower mobility of the total proteins in WB, and specifically altered the phosphorylation status of IRS1 on S616 and GRB10 on S476. Hyperphosphorylation of IRS1 led to reduced IRS1 total protein levels. No differences were observed in the phosphorylation S312 of IRS1 upon B55 depletion (**Figure 29a**). As expected, growth factor pathways dependent

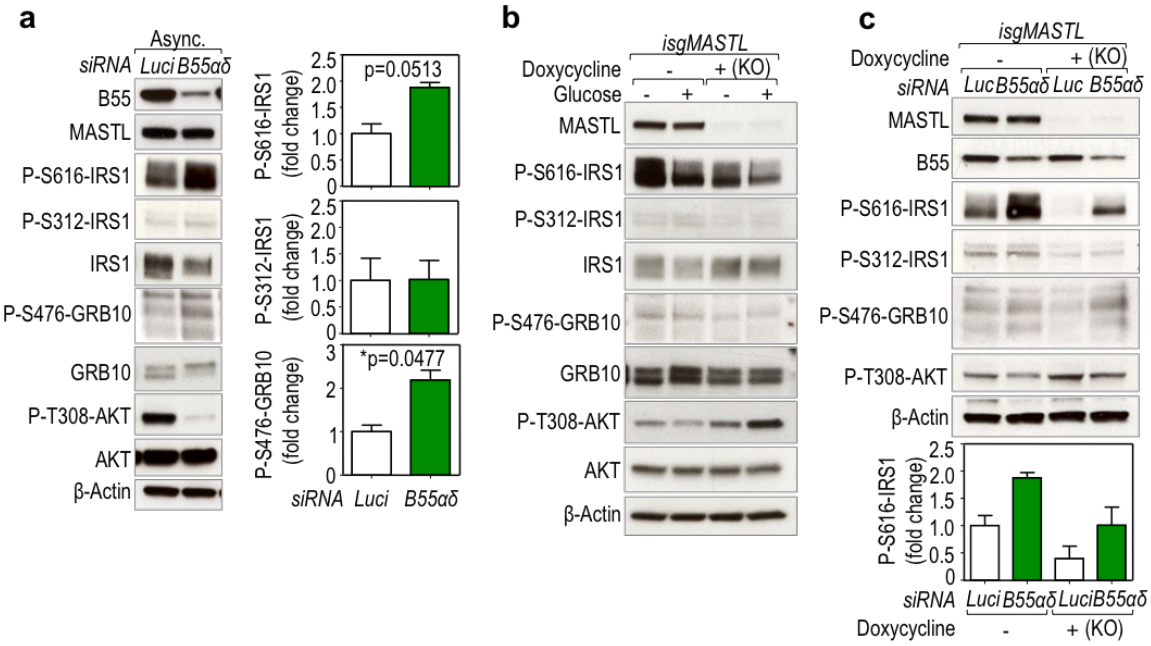

Figure 29. The MASTL-PP2A/B55 axis modulates the phosphorylation status of IRS1 and GRB10. a) B55 alpha and delta proteins were co-depleted using specific siRNAs. Asynchronous cells were recovered and blotted for the indicated antibodies. Plots represent the quantifications of the specified phospho-residues (Right). N=3 independent experiments. **b)** Control and *MASTL* knockout cells were starved from glucose and re-stimulated with glucose for 15 min. Phosphorylation status of the adaptor proteins with the indicated antibodies in conditions of active mTORC1/S6K1-dependent feedback loop. **c)** Genetic depletion of B55 alpha and delta subunits using siRNAs in control and *MASTL* null cells. The phosphorylation status of the different proteins was scored in conditions of glucose re-addition. Error bars indicate sem. *p<0.05 (Student's *t*-test).

on IRS1 and GRB10, like AKT, displayed attenuated phosphorylation in B55 depleted cells. To test the involvement of MASTL in the control of PP2A/B55 complexes in this context, we analyzed the phosphorylation status of the adaptor proteins IRS1 and GRB10 in *MASTL* depleted cells in response to glucose. Ablation of *MASTL* reduced the phosphorylation of both IRS1 and GRB10 on S616 and S476, respectively, and resulted in increased IRS1 and decreased GRB10 total protein levels (**Figure 29b**). This is in agreement with enhanced transduction to the PI3K/AKT pathway in *MASTL*-depleted cells as reflected by increased phosphorylation of AKT on T308. Concomitant depletion of B55 alpha and delta with siRNAs in *MASTL*-null cells partially rescued the phosphorylation status of IRS1 and GRB10 proteins (**Figure 29c**). These results suggested that B55 alpha and delta proteins might be the regulatory subunits of the PP2A phosphatase responsible to control the phosphorylation status of the feedback target proteins, IRS1 and GRB10, and promote growth factor signaling. In addition, MASTL-ENSA/ARPP19 axis would participate in the feedback by inhibiting PP2A/B55 complexes to prevent the dephosphorylation of the adaptor proteins, and attenuate growth factor signaling to PI3K/AKT.

If IRS and GRB10 are the main targets that mediate the role of MASTL-PP2A/B55 in the mTORC1/S6K1-dependent feedback, and underlie the increased AKT activation in *MASTL*-depleted cells, then growth factor pathways dependent on both adaptor proteins should be sensitive to *MASTL* depletion and display enhanced AKT activation, whereas IRS- and GRB10-independent pathways should remain relatively unaffected. Indeed, AKT activation in response to insulin stimulation, a pathway where IRS and GRB10 are obligatory, is significantly enhanced in *MASTL*-null cells (**Figure 30a**). In contrast, FBS treatment, which mainly contains mitogens that activate GPCR independently of IRS1 and GRB10, did not show enhanced AKT activation in *MASTL*-null cells. GRB10, but no IRS1, can also interact with the epidermal growth factor receptor (EGFR), although with less avidity than IR/IGFR-I (He et al., 1998). In agreement with that, *MASTL*-null cells present increased tyrosine phosphorylation of the EGFR and mild enhanced sensitivity to hEGF (**Figure 30b**). MASTL depletion had no effect on insulin receptor tyrosine autophosphorylation on Y1135/1136, suggesting that MASTL elicits a selective inhibitory effect on AKT activation at a point downstream of the insulin receptor. Importantly, treatment with specific inhibitors of IR/IGFR-I or EGFR, completely or partially rescued, respectively, the increase in AKT T308 in *MASTL* null cells (**Figure 30b**). All this data reinforce the idea that MASTL attenuates insulin-induced AKT phosphorylation through the participation in the feedback at the level of the IRS1- and GRB10-coupled receptors, and modulates insulin and IGF-1 pathways, and, to a lesser extent to EGFR.

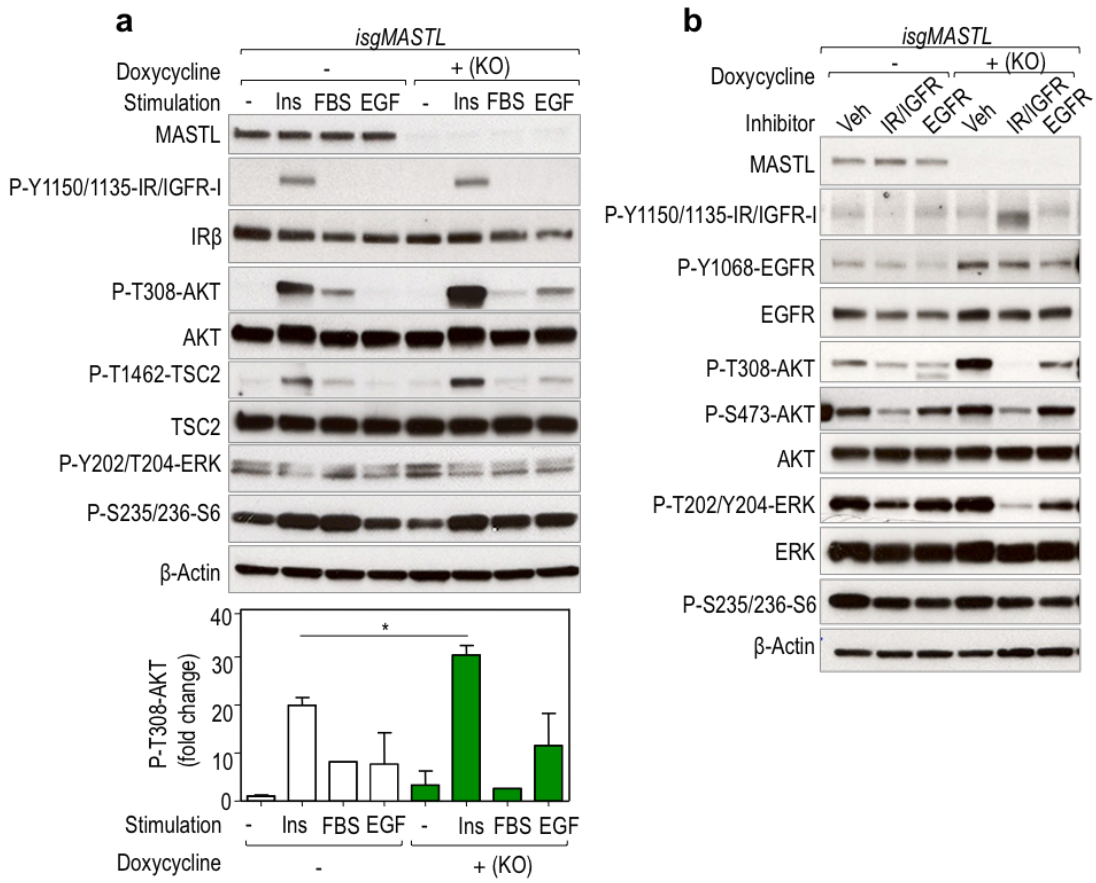

Figure 30. *MASTL*-null cells show increased sensitivity to insulin-regulated pathways. **a)** Control and *MASTL*-null cells were serum starved from serum for 4 h before perform stimulations with the indicated mitogens for 30 min. Immunoblot for the indicated proteins. Quantification of AKT T308 signal from immunoblots (Bottom). **b)** Control and *MASTL*-null cells were treated for 30 min before recovery with 5 μM linsitinib and 5 μM erlotinib, inhibitors of IR/IGFR-I and EGFR, respectively. Cell lysates were analyzed for the indicated antibodies. Error bars indicate sem. N=3 independent experiments for Ins and hEGF. *p<0.05 (Student's *t*-test).

3.2.6 Characterization of mTORC1/S6K1-dependent regulation of MASTL

Our previous data suggested that MASTL may be activated downstream of the mTORC1/S6K1 axis (**Figure 27**). The increased activity of MASTL shown in the absence of TSC2, together with its sensitivity to the specific mTORC1 inhibitor rapamycin, pointed to mTORC1, but not mTORC2 (Huang et al., 2008), as the main regulator of MASTL.

As the mTOR-regulated sites may be phosphorylated by mTOR or by downstream kinases, we sought to distinguish if MASTL may be directly phosphorylated by mTORC1 or by any direct effector of the mTORC1 pathway like S6K1. mTOR phosphorylates hydrophobic motifs (HMs) of the AGC kinases as well as distinct proline-directed sites of proteins such as 4E-BP1 and has unique preference for proline, hydrophobic and aromatic residues at the +1 position (Hsu et al.,

2011). Interestingly, MASTL sequence contains several candidate mTOR sites. Moreover, a S6K1 consensus phospho-acceptor site (R/K)X(R/K)XX(S*/T*) is also present within MASTL sequence. We performed *in vitro* kinase assays using commercial purified mTOR/Raptor/mLST8 (mTORC1 complex) and S6K1 kinases and GST-hMASTL as a substrate. To reduce any interference with the autophosphorylation activity of MASTL on its own, we first incubated MASTL alone with non-radioactive ATP and, then, we added the exogenous kinases mTORC1 and S6K1 together with radiolabelled ATP. Both kinases, mTORC1 and S6K1, were able to phosphorylate MASTL (**Figure 31a**). We next performed mass-spectrometry analysis to identify candidate mTORC1- and/or S6K-regulated phosphorylation sites in MASTL *in vitro*. To discard those phosphorylations present in the purified MASTL or resulting from MASTL autophosphorylation, we selected only those phosphopeptides enriched in the presence of the candidate upstream kinase. We identified 4 specific phosphorylation sites (T710, T716/717, T722 and S878) from 23 detected phosphosites. Phosphorylation at T722 was increased 3-fold relative to MASTL alone by both mTORC1 and S6K1, and phosphorylation at T710 and T716/718 was enriched 8- and 7-fold, respectively, in presence of mTORC1, and around 2.5-fold increase by S6K1. Phosphorylation at S878 was dramatically increased by mTORC1 more than 150-fold, suggesting that this phosphosite is a *bona fide* candidate for being a direct mTORC1- site, at least *in vitro* (**Figure 31b**). Interestingly, the four sites were mapped in the C-terminal tail of MASTL and presented high conservation among species (**Figure 31c**). Moreover, sequence analysis revealed that the 4 residues contained proline or hydrophobic residues at the +1 position, a requirement for mTOR phosphorylation motifs, and further suggested that these sites might be mTOR-phosphorylated sites. We cannot rule out whether these residues are direct mTORC1- or S6K-sites *in vitro*, or instead these kinases may promote MASTL activity that in turn triggers autophosphorylation at these sites.

Data in human cells and *Xenopus*, as well as in other independent proteomic screens, indicate that S878 is also phosphorylated *in vivo* in mitosis (Blake-Hodek et al., 2012; Vigneron, Gharbi-Ayachi, et al., 2011). To check if this and the other sites identified on MASTL, were sensitive to growth factors in cells and further identify other serum-responsive sites of MASTL, we also analyzed the phosphorylation of MASTL *in vivo* in immunoprecipitates of endogenous MASTL from MEFs, arrested in quiescence by serum starvation (G0), and re-stimulated for 6 h FBS (G1). We identified 3 out the 4 potential mTORC1/S6K1-dependent sites identified *in vitro* to be also phosphorylated *in vivo*. Interestingly, phosphorylation at S878 was responsive to growth factors and it was increased 3-fold in G1 compared to G0 arrested cells (**Figure 32a**). Previous research had shown that mutation of the equivalent site to S878 to alanine in *Xenopus* MASTL

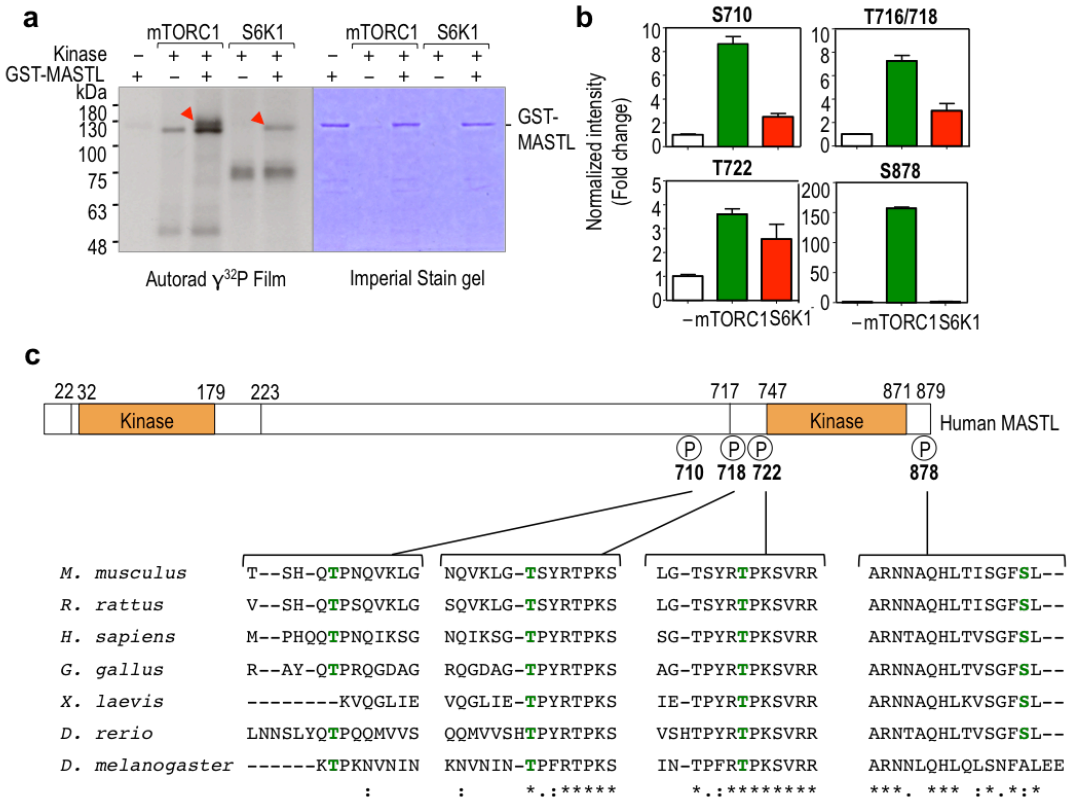

Figure 31. Characterization of mTORC1/S6K1-dependent phosphorylation sites on MASTL *in vitro*. a) *In vitro* kinase assay using purified GST-hMASTL as a substrate and purified mTORC1 and S6K1 kinases. A condition of MASTL without kinase was included as control of autophosphorylation. Autoradiograph showing the phosphorylation of MASTL by mTORC1 and S6K1. Red arrowheads show a phosphorylated band at the high of MASTL. mTORC1-mediated phosphorylation of MASTL induces a band shift of the protein (Right). Imperial staining shows the dried gel and the GST-MASTL protein. **b)** Mass spectrometry analysis of samples treated as **a)**. Plots represent mTORC1- S6K1-regulated sites on human MASTL. Intensities of the phosphopeptides were normalized to the total levels of MASTL and plotted as relative values to the condition of MASTL alone. **c)** Schematic representation of human MASTL protein structure with the phosphorylation sites from vertebrate orthologous aligned below. Nd, not detected (when the peptide containing this phosphosite was not detected on the proteomic analysis).

protein results in a partial inactivation of MASTL in mitosis (about 60% kinase activity on its substrates), whereas mutation to A of the other sites (T710, T716/T718 and T722) did not affect MASTL activity (Blake 2012). Considering all this data together, S878 appears to be the most promising site on MASTL for being mTOR-regulated (**Figure 32b**). Functional analysis of this site and its relevance in the role of MASTL regulating the mTORC1/S6K1-AKT feedback is currently ongoing.

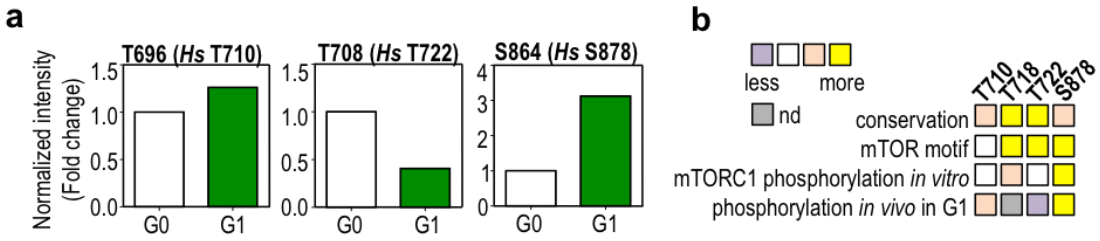

Figure 32. Characterization of growth factor-stimulated phosphosites on MASTL *in vivo*. a) Plots represent sites on mouse MASTL regulated upon serum stimulation for 6 h (G1) compared to G0 cells that had been serum starved for 24 h. Endogenous MASTL was immunoprecipitated from MEFs in the indicated conditions and phosphosites on MASTL were identified by mass spectrometry analysis. Intensities of the phosphopeptides were normalized to the total levels of MASTL and plotted as relative values to the condition of MASTL alone. *Hs* indicate the corresponding phosphorylation site on human MASTL. **b)** A summary of **Figure 31 b,c)** and **Figure 32 a)** for each MASTL phosphorylation site. Nd, not detected.

3.2.7 MASTL depletion alters GLUT4 translocation and glucose metabolism in cells

The PI3K/AKT pathway is a central signaling node within all cells of higher eukaryotes and plays critical roles in insulin-mediated glucose uptake and metabolism (Manning & Cantley, 2007; Manning & Toker, 2017). In both 3T3-L1 adipocytes and myocytes it has been demonstrated that, via mTORC1-dependent feedback loop regulation, amino acid starvation stimulate AKT activation and subsequent glucose uptake in response to insulin (Takano et al., 2001; Tremblay & Marette, 2001). The stimulation of glucose uptake by insulin requires translocation of GLUT4 transporter protein from intracellular storage sites to the cell surface (Leto & Saltiel, 2012), and IRS adaptor proteins and AKT are necessary for this process (Clarke, Young, Yonezawa, Kasuga, & Holman, 1994; Quon et al., 1994) (**Figure 33a**). Given the participation of MASTL in the mTORC1-mediated feedback control of AKT, we have tested whether MASTL depletion could affect glucose homeostasis in cells. We first analyzed whether MASTL depletion and concomitant AKT activation in MDA-MB231 cells had an effect in GLUT4 translocation following insulin stimulation. We quantified by IF the percentage of cells positive for GLUT4 localization at the plasma membrane (PM). As expected, insulin stimulation increased the percentage of cells positive for GLUT4 translocation compared to serum-starved cells, and *MASTL* knockdown further increased the percentage of cells positive for GLUT4 at the PM after insulin stimulation **(Figure 33b,c**). Same analysis was done upon glucose starvation and re-stimulation. Similarly, we found increased percentage of cells positive for GLUT4 in the PM upon *MASTL* depletion, further supporting a role for MASTL in the regulation of AKT-mediated GLUT4 translocation (**Figure 33d**).

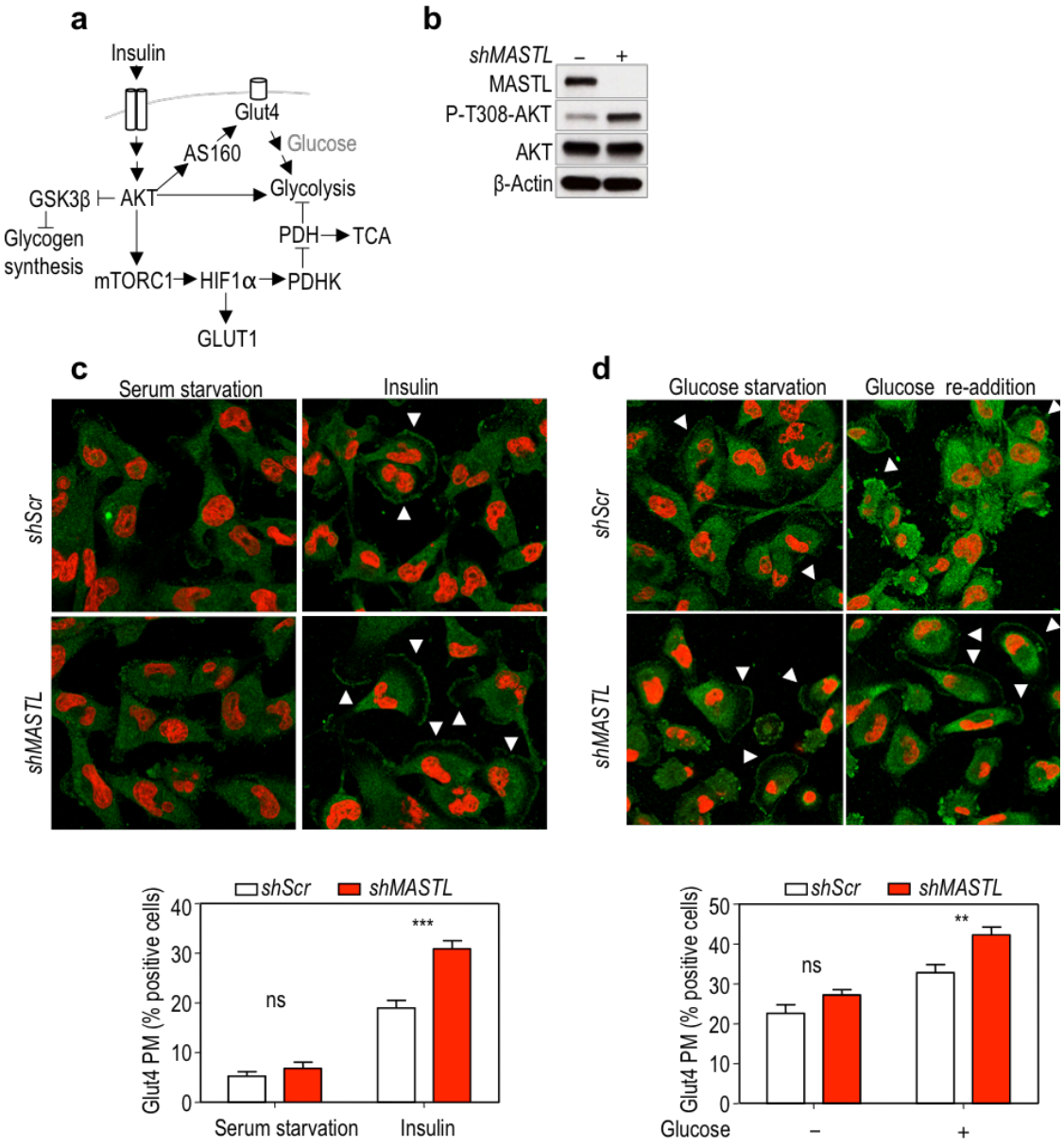

Figure 33. Depletion of *MASTL* alters GLUT4 translocation in cultured cells. a) Scheme of the AKT-mediated regulation of glucose uptake and metabolism. **b)** Immunodetection confirming *MASTL* depletion and activation of the AKT pathway in MASTL null cells in the conditions of the assay. MASTL was knocked down using shRNAs for MASTL and Scr as control. **c,d)** Immunofluorescence for GLUT4 in MDA-MB231 cells in conditions of serum starvation and insulin stimulation **c),** and glucose starvation and re-addition **d)**. Representative micrographs of GLUT4 (green) and nucleus (red) (Upper panels). Arrowheads indicate positive cells for GLUT4 translocation to the PM. Plots represent quantification of the percentage of cells positive for GLUT4 translocation to the PM (Bottom right). Around 800 cells were counted per condition. Error bars indicate SD. Ns, not significant; **p<0.005; ***p<0.001 (2-way ANOVA).

Apart from the regulation of glucose uptake, AKT activation can also affect glucose metabolism by stimulating glucose conversion to glycogen through phosphorylation and inhibition of GSK3β, thus relieving glycogen synthase activity (Cross et al., 1994) . AKT can also increase the rate of glycolysis (Elstrom et al., 2004) due, at least in part, to its ability to promote expression of glycolytic enzymes through mTORC1-dependent induction of Hypoxia Inducible Factor 1α (HIF1α) transcription factor (Lum et al., 2007; Majumder et al., 2004). The mTORC1-HIF1α axis also mediates transcription of *GLUT1* gene and cap-dependent translation of GLUT1 mRNA (Taha et al., 1999; Zelzer et al., 1998). Therefore the AKT-mTORC1 pathway promotes a switch from mitochondrial oxidative metabolism to glycolysis (**Figure 33a**). We next analyzed whether the increased AKT-mTORC1 signaling observed upon *MASTL* depletion in conditions of feedback regulation had any impact on the metabolic status of these cells. We detected increased levels of HIF1α upon glucose re-addition in *MASTL* null cells, which were accompanied by increased expression of its target pyruvate dehydrogenase kinase 2 (PDHK2) and increased phosphorylation of the pyruvate dehydrogenase E1 (PDHE1) protein at S293 (**Figure 34a**). PDHK2-mediated phosphorylation of PDHE1 inactivates the PDH complex, which is the gatekeeping enzyme that converts pyruvate to acetyl-CoA, thus linking glycolysis to TCA cycle. Increased PDHE1 S293 phosphorylation in *MASTL* null cells upon glucose re-addition suggested increased glycolytic activity in these cells. Importantly, these signals were prevented in *MASTL*-deficient cells treated with AKT inhibitors, further suggesting that ablation of MASTL may lead to increased glycolytic flux in an AKT-dependent manner in conditions of feedback regulation (**Figure 34a**). In addition, we also found a modest increase in the transcription of the HIF1α-target gene *GLUT1* in *MASTL* depleted cells after glucose stimulation (**Figure 34b**).

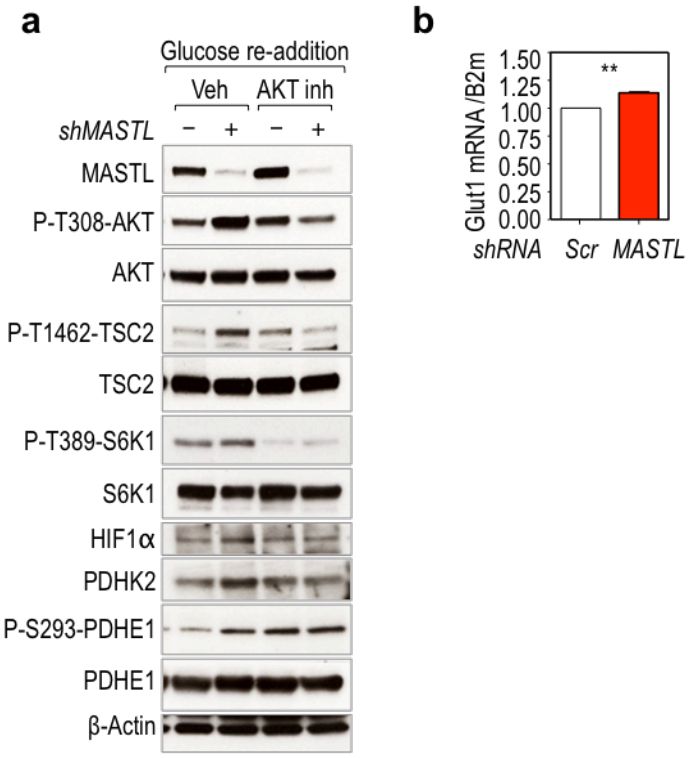

Figure 34. Depletion of *MASTL* upregulates the AKT-mTOR-HIF1α axis. a) Immunoblot for the indicated antibodies of the AKT-mTOR-HIF1α. MASTL was knocked down using shRNAs for *MASTL* and Scr as control. Cells were glucose starved followed by glucose stimulation. AKT inhibitor was added 15 min before glucose re-addition. **b)** Quantitative PCR for GLUT1 in control and MASTL depleted cells upon glucose re-addition for 30 min. N=2 independent experiments. Error bars indicate sem. Ns, not significant; **p<0.005 (Paired Student's *t* test).

To further explore this idea we performed Seahorse analysis that allows the quantification in real time of the extracellular acidification rate (ECAR) and the consumption of oxygen (OCR) in the media, whose values can be correlated to glycolysis and mitochondrial respiration, respectively. To analyze the glycolytic flux, cells are incubated in glucose-free media followed by sequential addition of glucose and oligomycin A to score the glycolytic flux and capacity of the cells, respectively. Ablation of MASTL induced a mild increase in ECAR upon glucose re-addition at two different concentrations reflecting higher glycolytic flux in *MASTL* null cells in these conditions (**Figure 35a**). However, there were no differences in the glycolytic capacity of the cells suggesting that *MASTL* depletion does not induce a general metabolic switch but rather a controlled and well-defined upregulation of glycolysis under conditions of feedback-mediated AKT regulation. We also analyzed the mitochondrial respiratory capacity in conditions of regular complete media, in which cells are challenged with different drugs targeting the machinery of OXPHOS. *MASTL* null cells had a mild reduction in maximal respiration upon treatment with the

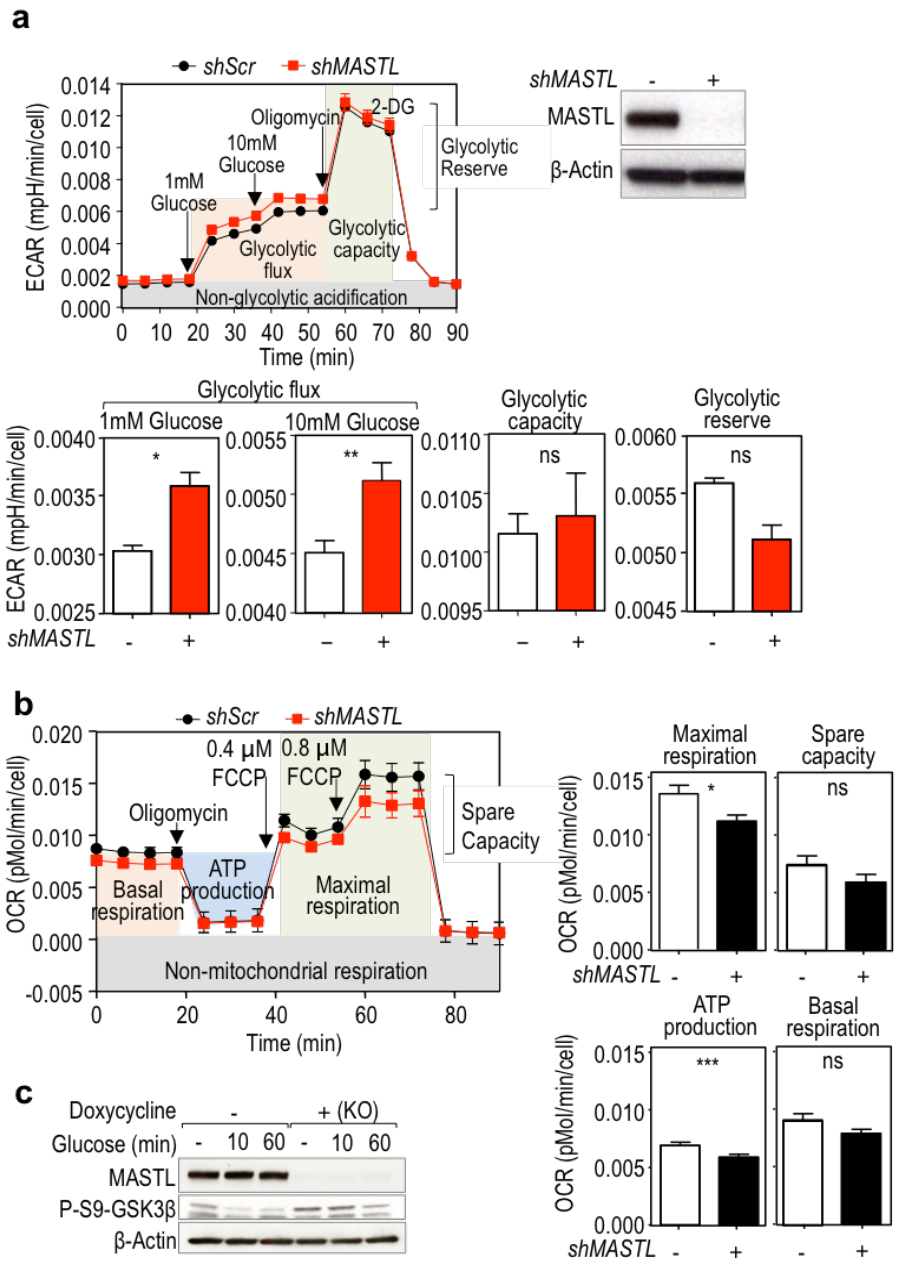

Figure 35. Depletion of *MASTL* promotes glycolysis under glucose re-stimulating conditions. **a)** Seahorse experiment to assay glycolysis in control and *MASTL* depleted cells. Indicated compounds were added over the time and ECAR values were plotted over the time in control and *MASTL*-null cells (Upper left). Data was expressed as mean ± sem of 3 independent experiments. Immunodetection of MASTL confirming *MASTL* depletion (Right). Plots representing quantifications of glycolytic flux, capacity and spare according to manufacturer instructions. Data is represented as mpH/min per cell (Bottom). **b)** Seahorse experiment to determine the mitochondrial respiratory capacity in control and *MASTL*-depleted cells. **c)** Immunoblot showing phosphorylation of GSK3β on S9 in control and *MASTL*-null cells in glucose starvation and re-addition in a time course of 15 min and 1 h. Data was expressed as mean ± sem of 3 independent experiments. Error bars indicate sem. Ns, not significant p>0.05; *p<0.05; **p<0.005; ***p<0.001 (Paired Student's *t*-test).

decoupling agent FCCP that might reflect some mitochondrial alteration (**Figure 35b**).

Together, the above observations suggested that depletion of *MASTL* in conditions of feedback-mediated AKT regulation results in increased AKT-mediated GLUT4 translocation and likely glucose uptake. Moreover, AKT couples glucose metabolism to glycolysis by increasing the expression of glycolytic proteins downstream the mTORC1-HIF1α axis. AKT may as well favor glycogen synthesis through phosphorylation and inhibition of GSK3β, as is suggested by the increased phosphorylation at S9 in *MASTL*-null cells (**Figure 35c**).

3.3 Physiological functions of Mastl *in vivo* in mammals

3.3.1 Control of tissue proliferation by Mastl in young and adult mice

To address the physiological relevance of Mastl *in vivo*, we made use of the ubiquitous and conditional loss-of-function mouse model for Mastl previously generated. TAM treatment induces Cre-mediated recombination of *Mastl* gene and generates a mouse KO for *Mastl* in the whole body. We first analyzed the consequences of *Mastl* depletion in young mice by treating them with TAM in the diet starting at 3 weeks of age. *Mastl(Δ/Δ)* mice died within 3-4 weeks after treatment whereas control littermates survived normally and did not presented any abnormality (**Figure 36a**). Body weight at the human end point (HEP) was dramatically decreased in *Mastl(Δ/Δ)* mice, which had lost around half of their weight (**Figure 36b**). According with the above-described mitotic function of Mastl in cells, histological analysis of tissues revealed the presence of dramatic mitotic defects in highly proliferative tissues, which were severely affected by *Mastl* loss. Among them, the small intestine was one of the most affected tissues. Its architecture was completely

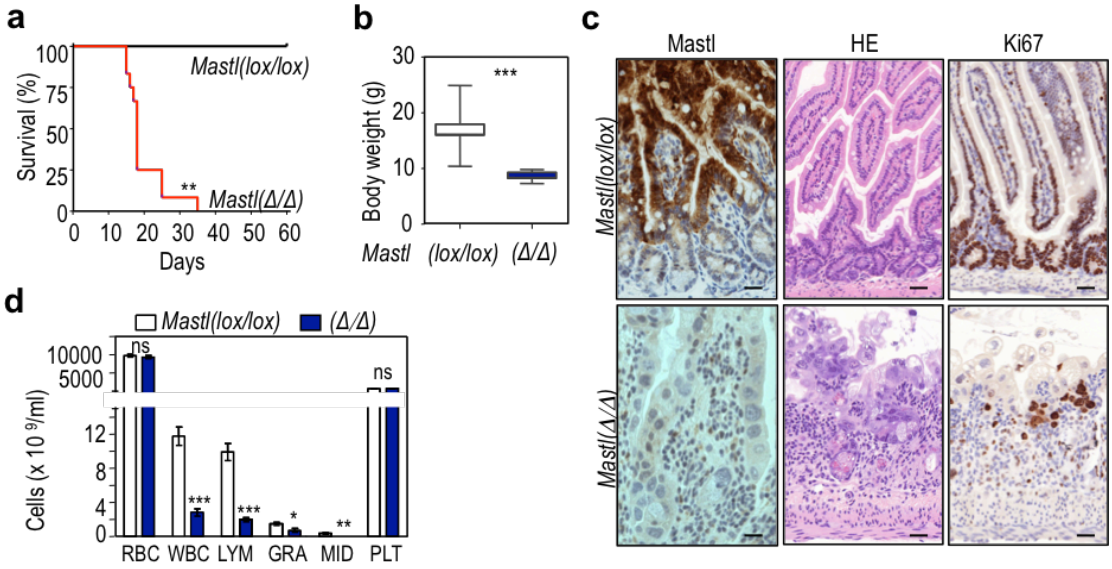

Figure 36. Deletion of *Mastl* in young mice causes severe proliferative defects. a) Survival curves of *Mastl(lox/lox)* and *(Δ/Δ)* mice. 3-week-old mice were fed with TAM diet to induce *Mastl* deletion. Graph show the proportion of mice that survived, HEP was applied according CNIO regulation. Mice were sacrificed for samples at the HEP. **b)** Body weight of the mice as in **a)** at the HEP. **c)** HE staining and Ki67 IHC of small intestine sections of control and Mastl KO mice. **d)** Full blood cell counts at the HEP. Plot representing the quantifications of the different lineages. Red blood cells (RBC), white blood cells (WBC) including lymphocytes (LYM) and granulocytes (GRA), precursor white cells and rare cells (MID), and platelets (PLT). N=8 *Mastl(lox/lox);* N=10 *(Δ/Δ).* Error bars indicate sem. Ns, not significant. *p<0.05; **p<0.005; ***p<0.001 (Student's *t*-test).

disrupted as seen by HE staining and suffered a dramatic reduction in cell proliferation, which was detected by loss of staining for the proliferative marker Ki67 (**Figure 37c**). The efficiency of Mastl deletion was confirmed by IHC for MASTL in the small intestine of *Mastl(Δ/Δ)* mice. The severe damage to the intestine was very likely the main cause of the severe weight loss and consequent death of *Mastl(Δ/Δ)* mice. *Mastl(Δ/Δ)* mice also presented atrophy in the skin and spleen, with reduction of the red pulp; and hypoplasia in the bone marrow. In agreement, blood cell count analysis reflected a dramatic reduction of the whole white blood cell lineage including lymphocytes, and granulocytes (**Figure 36d**).

We next sought to analyze the effect of *Mastl* depletion in adult mice. For this purpose, and following the protocol for Mastl depletion in young mice, 1-year-old mice were treated with TAM in the diet for the whole time the experiment lasted. Surprisingly, *Mastl(Δ/Δ)* mice survived in similar proportions to control mice with no obvious phenotype until 6-months after TAM treatment (**Figure 37a**). At that time we had to apply the HEP since *Mastl(Δ/Δ)* mice experienced some signs reminiscent of aging including kyphosis, difficulties in movement, and in some cases, cataracts in one or both eyes. Only elder *Mastl(Δ/Δ)* females suffered from a mild loss of weight compared to their controls, that in contrast to young *Mastl(Δ/Δ)* mice, did not compromise survival in any case (**Figure 37b**). No differences in body weight were observed in male mice. Histological analysis of tissues extracted after 3 and 6 months on TAM diet, revealed no major abnormalities in *Mastl(Δ/Δ)* mice, and much less severe proliferative problems compared to young *Mastl(Δ/Δ)* mice, even in highly proliferative tissues such as the intestine, and despite having a comparable deletion of Mastl (**Figure 37c**). In addition, *Mastl(Δ/Δ)* mice showed a mild reduction in cell blood counts although there were no significant differences, except for red blood cells (**Figure 37d**). This data suggests that elder mice are more tolerant to *Mastl* depletion than young mice, suggesting that, either proliferative tissues become more independent on the mitotic function of Mastl as they age, or they become more tolerant to mitotic aberrations given probably due to reduced regenerative capacity as organism ages.

However, a detailed histopathology analysis showed that some proliferative tissues from *Mastl(Δ/Δ)* mice still presented some mitotic aberrations, increased apoptosis and reduced regenerative capacity. These alterations were present at 3 months after TAM and were even more pronounced at 6 months after TAM. This was specially clear in the intestine, where quantification of positive cells for Ki67, revealed a strong reduction of Ki67 in the transit amplifying compartment of the villi, together with some signs of atrophy and irregular villi morphology (**Figure 38a**). Even though Ki67 was not significantly decreased in the crypts, there were reduced mitotic figures and increased apoptosis, based on cleaved caspase-3 (CA3)

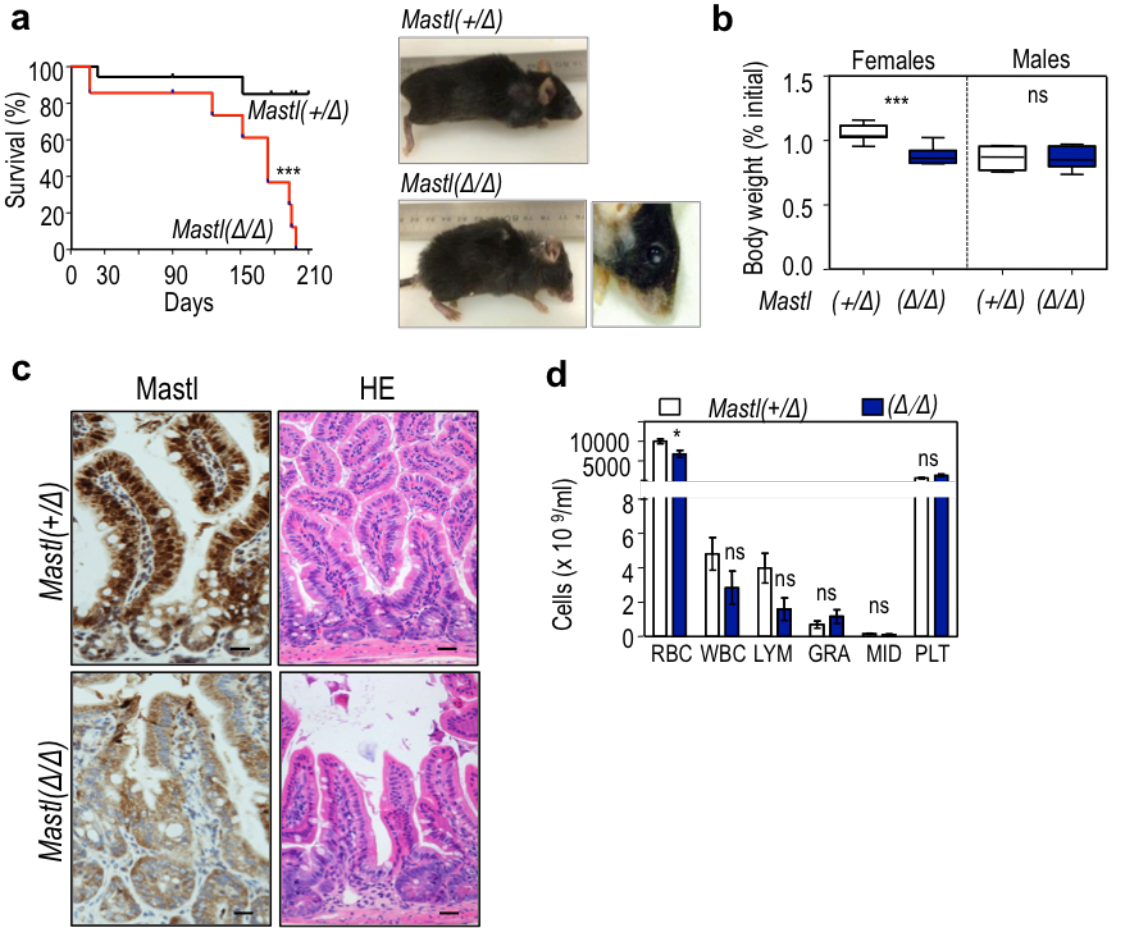

Figure 37. Effect of Mastl deletion in adult mice. a) Survival curves of *Mastl(lox/lox)* and *(Δ/Δ)* mice. 52-week-old mice were fed with TAM diet to induce *Mastl* deletion. Graph show the proportion of mice that survived along the time, humane end point (HEP) was applied according to CNIO care program. Mice were sacrificed for samples at the HEP. Representative pictures of Mastl KO mice at the HEP are shown (Left). **b)** Relative loss of body weight at HEP compared to their initial weight before TAM. **c)** HE staining and Mastl immunohistochemistry of small intestine sections of control and Mastl KO mice at 3 months after TAM. **d)** Full blood cell count at 3 months after TAM diet. Plot representing the quantifications of the different lineages. N=14 *Mastl(+/Δ);* N=12 *(Δ/Δ).* Error bars indicate sem. Ns, not significant. *p<0.05; ***p<0.001 (Student's *t* test).

staining, probably reflecting the loss of regenerative capacity in this tissue (**Figure 38a**). The colon also had a reduction in Ki67 positive cells concomitant with an increase in apoptotic cells (**Figure 38a**).

At the time of 6 months after TAM it was also prominent the presence of rare cells with big, vacuolated nuclei, and less condensed chromatin in liver, kidney, skin and eye from *Mastl(Δ/Δ)* mice. This was accompanied by disorganized tissue structures that had lost tissue homeostasis and that were absent in *Mastl(+/lox)* control mice. Liver was among the most affected tissues with high levels of nuclear pleomorphic nuclei and fragmented chromatin in

hepatocytes, resembling dead and damaged cells. This was accompanied by an increased percentage of Ki67 positive hepatocytes, probably reflecting the attempt to regenerate those damaged hepatocytes (**Figure 38b**).

As a summary of this part, we conclude that deletion of *Mastl* in young mice causes severe proliferative defects, and mice die early after *Mastl* ablation. In contrast, knockout of *Mastl* in adult mice results in less severe proliferative defects and improved survival compared to young

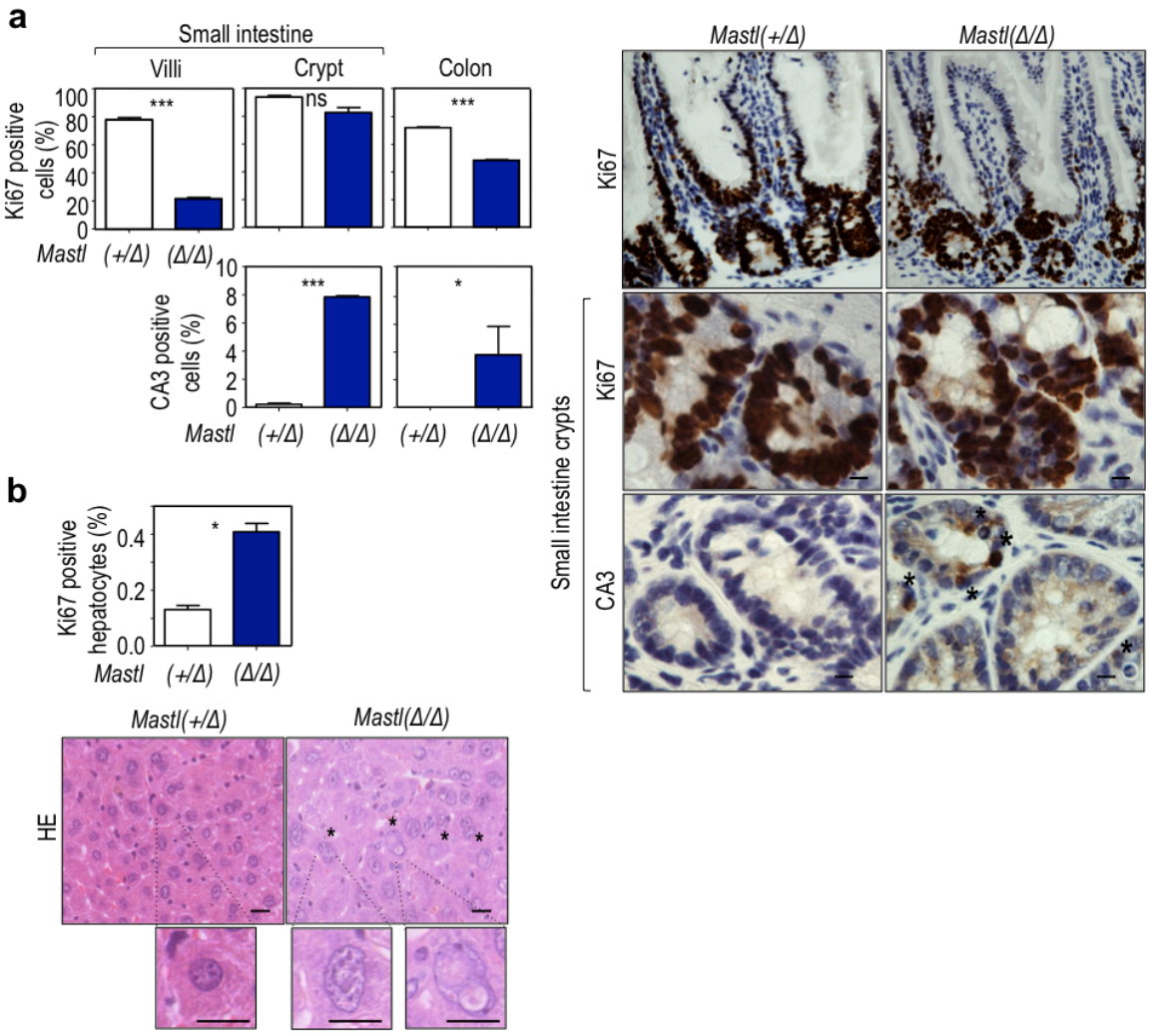

Figure 38. Histological analysis of *Mastl* deletion in adult tissues. a) Plots showing quantifications of immunohistochemical staining for Ki67 and CA3 in small intestine and colon tissue sections of *Mastl(+/Δ) control and Mastl(Δ/Δ)* mice after 3 months of TAM diet. Representative images of IHC for Ki67 and CA3 in the crypts of small intestine sections (Right). Asterisks indicate apoptotic cells. **b)** Quantification for Ki67 positive hepatocytes by IHC. Representative images of HE staining in liver sections of 64-week-old *Mastl(+/Δ) control and Mastl(Δ/Δ)* mice 6 months after TAM diet (Bottom). Asterisks indicate representative images of irregular vacuoles, protein aggregates and damaged hepatocytes. N=2 *Mastl(+/Δ);* N=2 *(Δ/Δ).* Error bars indicate sem. Ns, not significant. ***p<0.001 (Student's *t*-test).

Mastl(Δ/Δ) mice. Accumulation of mitotic defects may eventually lead to impaired regenerative capacity of the tissues and inability to maintain tissue homeostasis, which, in the long term, may contribute to the systemic organ failure and premature death of *Mastl(Δ/Δ)* mice.

3.3.2 Mastl depletion improves glucose tolerance *in vivo*

As discussed above, our results in cells suggested the participation of the MASTL-PP2A/B55 axis in the modulation of the mTORC1/S6K1-feedback inhibition of PI3K/AKT pathway. Through this feedback loop mTORC1 hyperactivation is a critical event in rendering cells unresponsive to insulin/IGF-I, and has physiological relevance in controlling insulin sensitivity of peripheral tissues, such as fat and skeletal muscle, and profound effects in metabolic disorders characterized by insulin resistance, such as obesity or type-2 diabetes (Saxton & Sabatini, 2017). S6K1-deficient mice remain sensitive to insulin despite HFD and constitutive mTORC1 activation (Um et al., 2004). This has led to speculate that mTORC1 or S6K1 inhibitors that relieve AKT-mediated feedback inhibition could improve glucose tolerance and protect against type 2 diabetes. Taking into account the potential role of MASTL in metabolism, beyond its function in proliferation, we analyzed the expression of Mastl by RT-qPCR in several different metabolic tissues, such as the pancreas and the insulin-sensitive tissues including skeletal muscle, white adipose tissue (WAT) and liver. We found expression of Mastl in all analyzed tissues at comparable levels to the expression of Mastl in spleen, as a reference of proliferative tissue, indicating that expression of MASTL is not restricted to proliferative tissues (**Figure 39a**). We also observed that Mastl expression at mRNA level was modulated *in vivo* in response to food intake in muscle and epididimal WAT (eWAT). *Mastl* expression was increased in *ad libitum* fed mice compared to overnight fasted mice in both tissues (**Figure 39b**), further suggesting a non-mitotic role for Mastl in these tissues.

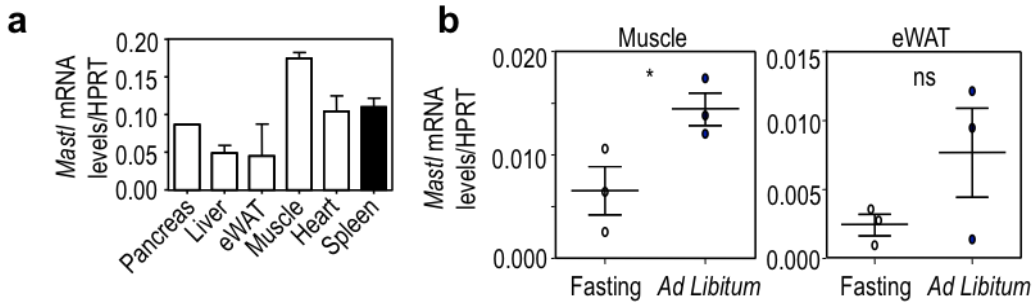

Figure 39. Expression levels of *Mastl* in metabolic tissues. a) RT-qPCR analysis for Mastl in different tissues from *ad libitum* mice. N=3 mice. **b)** RT-qPCR for Mastl in muscle (Left) and eWAT (Right) in fasting and *ad libitum* fed mice. N=3. Error bars indicate sem. *p<0.05 (Student's *t* test).

To address the question of whether MASTL-mediated modulation of mTORC1/S6K1-feedback activity could affect glucose homeostasis *in vivo* we performed a GTT in young mice that had been fed with HFD for 9 weeks. To avoid interference of the mitotic phonotype in *Mastl* KO upon continuous TAM treatment, *Mastl* was acutely ablated by intraperitoneal injection of TAM one week before the GTT (**Figure 40a**). TAM injection and concomitant loss of *Mastl* did not affect the body weight of *Mastl(Δ/Δ)* compared to control *Mastl(+/+)* mice, and there were no differences neither in body weight gain after the HFD or after fasting among groups (**Figure 40b**).

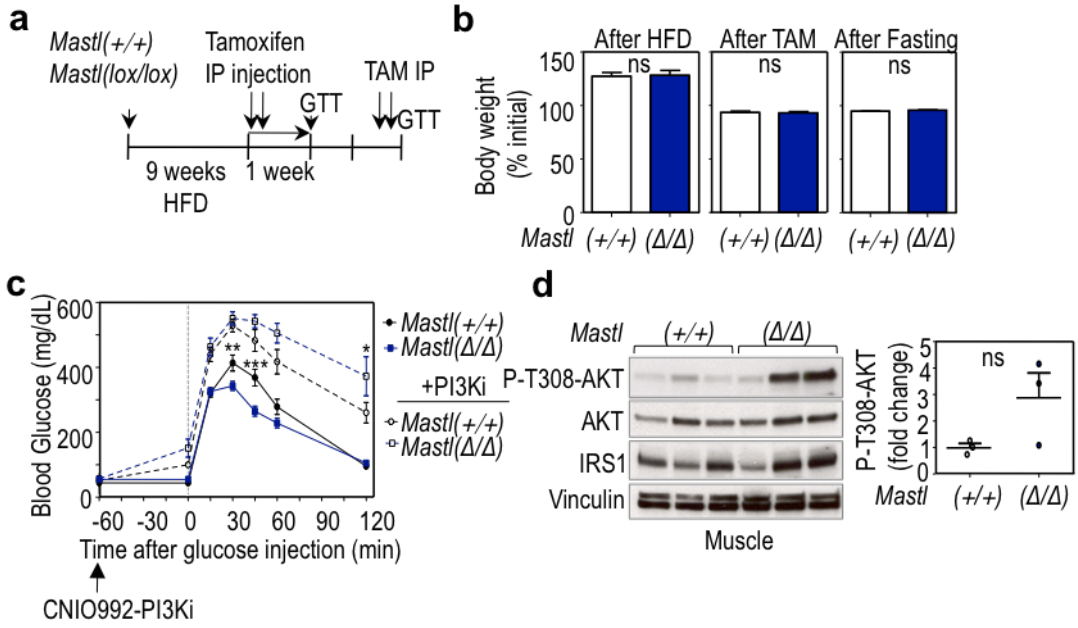

Figure 40. Improved glucose tolerance in *Mastl(Δ/Δ)* mice. a) Schematic of the protocol followed. 8- to 12-week-old mice were fed with HFD 60% for 9 weeks to induce glucose intolerance and insulin resistance. 1 week before every experiment mice were injected twice with TAM every other day to induce *Mastl* deletion; control mice *Mastl(+/+)* were also injected with TAM. Mice were left to rest for 2 weeks in between experiments and fed always with HFD. **b)** Plots representing the relative body weight at the indicated times. Body weight gain after 9 weeks of HFD (Left); Weight loss 1 week after TAM injection (Middle); Weight loss after 16 h fasting (Right). N=6 *Mastl(+/+)* and N=11 *Mastl(Δ/Δ)*. **c)** GTT experiment in *Mastl(+/+)* and *Mastl(Δ/Δ)* mice from **b)**. Dashed lines indicate GTT experiment in the same mice a different day upon treatment with the CNIO-PI3Ki (ETP46992). Inhibitor was administered by oral gavage to 16 h fasted mice at a single dose of 20 mg/kg body 1 h before the GTT. **d)** Immunoblot for the indicated antibodies in muscle extracts. Mice were fasted overnight for 16 h and injected intraperitoneally with glucose (2 g/kg body) and mice were sacrificed 30 min later for samples. Quantification of the signal of AKT P-T308 represented as fold change relative to total AKT. 3 mice were analyzed per genotype. Same mice as in **c)** were used. Error bars indicate sem. Ns, not significant p>0.05; *p<0.05 (Student's *t* test); **p<0.005; ***p<0.001 (2-way ANOVA).

Mastl(Δ/Δ) mice were more glucose tolerant in a GTT experiment, having significantly reduced blood glucose levels 30 and 45 min after glucose injection (**Figure 40c**). This result was indicative of better glucose clearance by peripheral tissues in *Mastl(Δ/Δ)* mice. As a direct mediator of glucose uptake in cells and tissues, we next evaluated PI3K/AKT activation upon a boost of glucose in control and *Mastl(Δ/Δ)* mice. *Mastl(Δ/Δ)* mice exhibited increased glucose-stimulated AKT activation in muscle (**Figure 40d**). No significant differences were found in eWAT or liver (data not shown). In agreement with and increased AKT activation in *Mastl(Δ/Δ)* mice, treatment with a single dose of an orally bioavailable and specific PI3K inhibitor (CNIO992-PI3Ki) (Martínez González et al., 2012) 1 h before the GTT assay completely rescued the differences among groups. As expected, the inhibitor increased the fasted glycaemia and both group of mice become glucose intolerant in the assay (**Figure 40c**). Of note, the effect of the inhibitor was even more pronounced in *Mastl(Δ/Δ)* mice, who reached the highest and most sustained levels of hyperglycemia. Noteworthy, 3 out of the 10 *Mastl(Δ/Δ)* mice died 2 days after the assay due to extreme hyperglycemia, suggesting that *Mastl(Δ/Δ)* mice might be more sensitive to the inhibitor, probably reflecting a higher dependence of *Mastl(Δ/Δ)* mice on the PI3K/AKT pathway. These data also suggest that the enhanced glucose tolerance upon MASTL ablation might be a consequence of increased PI3K/AKT activity in *Mastl(Δ/Δ)* tissues responsible of glucose uptake, such as muscle, even though we cannot discard contribution of other tissues like the WAT or liver.

Better glucose tolerance is consequence of increased glucose uptake by peripheral

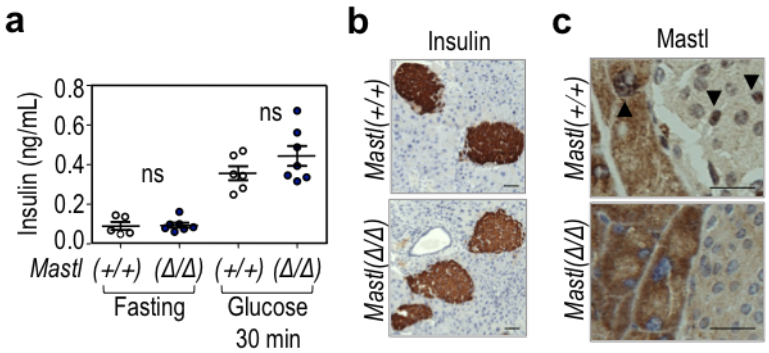

Figure 41. *Mastl* deletion does not affect glucose-stimulated insulin secretion. a) Insulin plasma concentration determination in a time course in 16 h fasted mice and 30 min after glucose injection. Same mice as in **Figure 41 b)** were used. N=6 *Mastl(+/+)* and N=7 *Mastl(Δ/Δ)*. **b)** IHC for insulin in pancreas tissue sections of *Mastl(+/+) and Mastl(Δ/Δ)* mice. **c)** IHC for Mastl in pancreas tissue sections of *Mastl(+/+) and Mastl(Δ/Δ)* mice. Arrows indicate representative positive cells for Mastl. Error bars indicate sem. Ns, not significant p>0.05 (2-way ANOVA).

tissues, which can be modulated by either increased glucose-induced insulin secretion (GSIS) by the pancreas and concomitant enhanced AKT signaling in insulin-responsive tissues, or by the mTORC1-dependent feedback loop, whereby impaired feedback-mediated AKT inhibition improves glucose uptake. GSIS is also affected by the PI3K/AKT (Bernal-Mizrachi et al., 2004), and mTORC1 pathways (Rachdi et al., 2008). To rule out the possibility of *Mastl(Δ/Δ)* mice having increased GSIS, we measured levels of insulin in plasma 30 min after glucose injection. We found no differences in the levels of GSIS in *Mastl(Δ/Δ)* mice compared to controls (**Figure 41a**). There were no differences in plasma insulin concentration in fasting either. Histological examination of pancreas sections showed no gross abnormalities or differences in the number or size of the Langerhans islets (**Figure 41b**). Positive nuclear staining for Mastl by IHC in tissue sections was found in some cells of the exocrine an endocrine pancreas as well, and Mastl was efficiently ablated in *Mastl(Δ/Δ)* mice (**Figure 41c**). This data suggests that the increased glucose tolerance of *Mastl(Δ/Δ)* mice is likely not consequence of increased GSIS.

In order to determine the potential involvement of the liver in the better glucose tolerance of *Mastl(Δ/Δ)* mice, we generated a hepatocyte-specific conditional mouse model for *Mastl*. For this, we crossed our *Mastl(lox)* model with a strain expressing a TAM-inducible Cre-recombinase under the control of the albumin gene promoter, *Mastl_L(lox/lox)*. Mice were also feed with HFD for 9 weeks and injected with TAM (**Figure 42a**). Ablation of *Mastl* specifically in hepatocytes does not recapitulate the glucose tolerance phenotype observed upon ubiquitous ablation of *Mastl* in the whole body (**Figure 42b**). However, the kinetics of the response of *Mastl_L(Δ/Δ)* mice is delayed compared to controls. At 15 min after glucose injection *Mastl_L(Δ/Δ)* mice

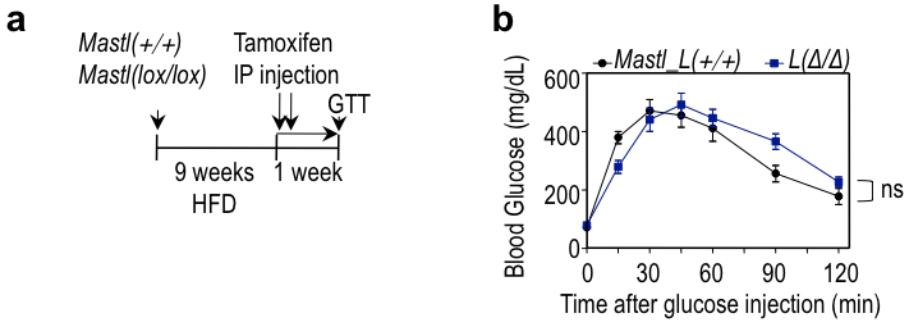

Figure 42. No differences in glucose tolerance upon *Mastl* specific knock out in the liver. a) Schematic of the protocol followed. 8- to 12-week-old mice were fed with HFD 60% for 9 weeks to induce glucose intolerance and insulin resistance. 1 week before every experiment mice were injected twice with TAM every other day to induce *Mastl* deletion. **b)** GTT experiment in mice in *Mastl_L(lox/lox)* mice. Mice were fed with HFD and intraperitoneally injected with TAM to deplete Mastl following the protocol as in **a)**. N=6 *Mastl_L(+/+)*; N=8 *Mastl_L(lox/lox).* Error bars indicate sem. Ns, not significant p>0.05 (2-way ANOVA).

reached significantly lower glucose levels, although we do not have an explanation for this observation, one hypothesis is that glucose-induced inhibition of gluconeogenesis, which depends on AKT activation, is enhanced in *Mastl_L(Δ/Δ)* mice. Even though we can cannot rule out a contribution of the liver to *Mastl* KO phenotype, this results suggests that other tissues rather from the liver are responsible for the better glucose clearance of *Mastl(Δ/Δ)* mice.

In agreement with a better glucose tolerance of young *Mastl(Δ/Δ)* mice fed with HFD, we found that 1-year-old whole-body *Mastl(Δ/Δ)* mice fed with chow diet *ad libitum* had a significantly reduced glycaemia compared to control littermates *Mastl(+/Δ)* mice (**Figure 43a**). Again, there were no differences in insulin plasma concentration evaluated in the same feeding conditions (**Figure 43b**). Despite the lower glucose levels, *Mastl(Δ/Δ)* mice fed with chow TAM diet failed to show better glucose tolerance in a GTT assay (**Figure 43c**). This result suggests that Mastl ablation likely improves glucose tolerance upon a stressful and challenging condition such as HFD and also lowers basal glycaemia in old mice. Altogether, this data place Mastl as a new

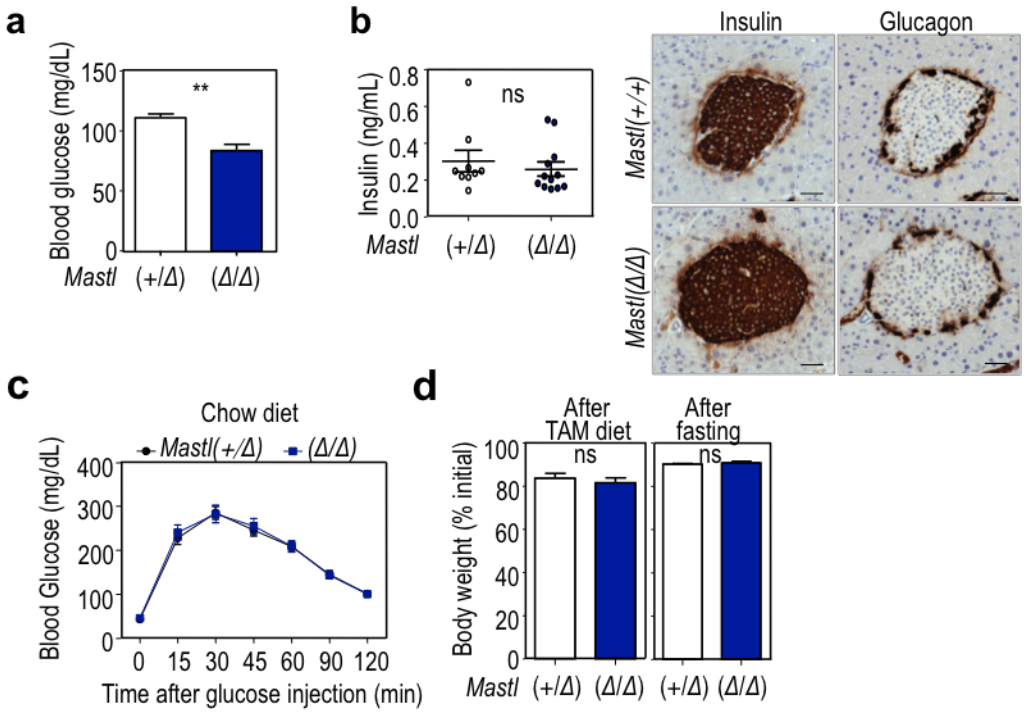

Figure 43. 1-year-old *Mastl(Δ/Δ)* mice present reduced glycaemia. a) Blood glucose levels in *Mastl(Δ/Δ)* and *Mastl(+/Δ)* mice. Mice were treated with TAM chow diet to induce Mastl depletion in the whole body. 1-month later blood glucose concentration was determined in the morning in ad libitum fed mice. N=11 *Mastl(+/Δ)* and N=12 *Mastl(Δ/Δ)*. **b)** Insulin plasma concentration determined in same feeding conditions as in **a)**. N=9 *Mastl(+/Δ)* and N=12 *Mastl(Δ/Δ)*. **c)** GTT in *Mastl (+/Δ)* and *Mastl(Δ/Δ)* treated as in **a)**. N=9 *Mastl(+/Δ)* and N=12 *Mastl(Δ/Δ)*. **d)** Plots representing the relative body weight at the indicated times of the mice in **c)**. Body weight loss upon 1 month in TAM diet (Left); Weight loss after 16 h fasting (Right). N=9 *Mastl(+/Δ)* and N=12 *Mastl(Δ/Δ)*. Error bars indicate sem. Ns, not significant; **p<0.005 (Student's *t* test).

potential target of intervention for metabolic diseases, such as obesity-induced diabetes.

4. Discussion

4.1 Cell cycle-dependent functions of MASTL

4.1.1 Different requirements of MASTL for mitotic entry

Different studies, including ours, have shown that Mastl/Greatwall is an essential mitotic kinase in different organisms. Depletion of Mast/Gwl in *Xenopus* oocytes (Mochida et al., 2010) as well as in HeLa cells using siRNAs impaired mitotic (M) entry (Burgess et al., 2010; Voets & Wolthuis, 2010). These results are in contrast to our findings in mouse embryonic fibroblasts (MEFs) from the conditional knockout (cKO) mouse model of Mastl, in which genetic ablation of Mastl does not impair M entry but, instead, affect mitotic progression upon NEB. Mastl depleted cells enter into M with the same kinetics as control cells, although due to the presence of mitotic defects, such as chromosome condensation, they remain arrested in prometaphase; eventually they abnormally exit mitosis presenting segregation defects. One reasonable explanation for this difference is that, in our experiments, MEFs are synchronized by serum starvation and Mastl is ablated in non-dividing cells, thus allowing us to monitor the first division after Mastl loss. However, experiments in HeLa cells are performed in asynchronous cultures where a first division in the absence of MASTL might have already occurred before M entry analysis. From out data, we known that cell dividing in the absence of MASTL frequently fail to segregate and exit mitosis as tetraploid (4n) cells, a phenotype that interferes with a successful progression through the next cell cycle and timely mitotic entry. In addition, HeLa cells were synchronized at the G1/S transition with an overnight thymidine block before scoring M entry. This treatment may cause a certain level of DNA damage and force cells to recover from the DNA-damage associated checkpoint before resuming the cell cycle. In line with a role for MASTL in the checkpoint recovery (Wong et al., 2016), it is not surprising that MASTL deficient cells experienced defects in the G2/M transition as scored in their experiments. Altogether, the data from our cKO MEFs, along with the accumulation of M figures in Mastl null embryos (**Figure 13c**), suggest that Mastl is largely dispensable for M entry in unperturbed cell cycles in mammals, but essential for a proper progression through M phase.

An intriguing conclusion from our results is that MASTL-mediated inhibition of PP2A/B55 may be dispensable for full activation of Cdk1-cycB during M entry in MEFs, a requirement thought to essential for M entry. A similar observation has been done in starfish oocytes, where depletion of the Mastl orthologous, Gwl, does not impair M entry, but, instead, causes segregation defects upon NEB (Okumura et al., 2014). In this system the absence of Gwl is compensated by Cdk1-mediated phosphorylation of Arpp19, which promotes binding to and inhibition of PP2A/B55 and allow full Cdk1 activation, via its autoregulatory loop, and M entry. However, further reduction of

PP2A/B55 activity by Gwl-mediated phosphorylation of Arpp19 in mitosis is required to ensure proper chromosome segregation. According to these results, Gwl is dispensable, in starfish and MEFs, for the initial PP2A/B55 inhibition and activation of Cdk1-cycB at the cytoplasm, but instead, Gwl-mediated inhibition of PP2A/B55 is essential after NEB to prevent premature dephosphorylation of Cdk1-cycB phosphosubstrates, and allow normal progression through mitosis and proper chromosome segregation. This hypothesis is in agreement with a model in which Mastl/Gwl is almost exclusively nuclear before Cdk1-cycB complexes get activated and enter into the nucleus. Mastl is subsequently phosphorylated by nuclear Cdk1-cycB complexes and shuttles to the cytoplasm just before nuclear envelope breakdown to inhibit PP2A/B55 and prevent the massive dephosphorylation of mitotic proteins (Álvarez-Fernández et al., 2013; Wang et al., 2013).

The above-mentioned different roles of Arpp19 upon either Cdk1 or Mastl phosphorylation suggest different affinity towards PP2A/B55 and different levels of phosphatase activity inhibition. In the same line, PP2A/B55 substrates might also have different sensitivity to the levels of PP2A-B55 phosphatase activity. Interestingly, the homologous site of Cdk1-cycB phosphorylation in starfish Arpp19 is also present in *Xenopus* Ensa and Arpp19 proteins, in human and murine Arpp19, and in *C. elegans* Ensa; but it is absent in Ensa from human or *Drosophila*. In *Drosophila*, the equivalent position to the Cdk1 site is a phosphomimetic aspartic acid, and genetic studies have shown that lack of Mastl does not impair M entry, and mostly leads to delays in M entry accompanied by defective chromosome condensation (Yu et al., 2004). In *C. elegans*, which appears not to have a Mastl homologue, Cdk1 phosphorylation of Ensa appears to compensate for the lack of Mastl. Therefore, it is plausible that Cdk1-dependent phosphorylation, or a phosphomimetic mutation in the equivalent site, of at least one endosulfine family member is sufficient for mitotic progression in almost all metazoans.

The only exception to the above-mentioned hypothesis is *Xenopus*, where depletion of Gwl from cycling extracts in *Xenopus* prevents Cdk1-cycB activation and mitotic entry (Yu et al., 2006), and the concomitant inhibition or depletion of PP2A-B55 rescues defective mitotic entry (Castilho et al., 2009). One plausible explanation is that in *Xenopus,* Cdk1-mediated ENSA phosphorylation only moderately increases its affinity for binding to and inhibiting PP2A-B55 (Mochida, 2014), and in the absence of Mastl this is not sufficient to counteract the phosphatase activity and reach the Cdk1-cycB threshold required for M entry in *Xenopus.* Another possibility is that the threshold of Cdk1-cycB activity for M entry might be higher in *Xenopus,* making Gwl mediated inhibition of PP2A/B55 essential to reduce the amount of Cdk1-cycB required for M entry (Hara et al., 2012), similarly to what happen under stressful conditions such as recovery

from DNA damage (Peng et al., 2010). It is also plausible that *Xenopus* has higher levels of phosphatase activity compared to other species, which need to be reduced for M entry, thus making essential Gwl-mediated phosphorylation of endosulfines. This is just speculation since a comparison of phosphatase activity among species has not been addressed. In summary, these data highlight the different requirements of Cdk1-cycB and PP2A/B55 activity, and, as consequence, of Mastl/Gwl for M entry among species.

Interestingly, in fission yeast, as in *Xenopus*, cells depleted of the Mastl orthologous, Ppk18, are unable to enter into mitosis due to high PP2A/B55 activity (Chica et al., 2016). It is not known, however, whether in *S. pombe*, similar to multicellular organisms, Cdk1-cycB phosphorylates endosulfine, and if this promotes binding to PP2A/B55. In any case, this putative Cdk-mediated phosphorylation of endosulfine, would not be sufficient to reach the threshold of Cdk1 activity required for M entry in *S. pombe*, thus making essential Mastl activity. In budding yeast, the pathway is still conserved but with some conceptual differences. PP2A/B55 activity promotes, rather than prevents, entry into mitosis, and yeast Mastl and endosulfines orthologous, activate rather than inhibit PP2A/B55 at mitotic entry (Juanes et al., 2013). In *S. cerevisiae*, this pathway is dispensable for mitotic entry in unperturbed cell cycles, and, only under stress conditions lack of either Rim15 or endosulfines delay mitotic entry, and mitotic defects become apparent.

4.1.2 Mitotic-independent roles in cell cycle regulation

PP2A is a master phosphatase involved in cell cycle regulation and as such, has mitotic independent roles (Kurimchak & Graña, 2012). PP2A/B55 complexes restrain the G1/S transition in human cell lines by counteracting CDK-mediated phosphorylation and inhibition of the retinoblastoma protein (pRb). PP2A/B55 complexes also dephosphorylate the other pocket family proteins, p107 and p130, which are important for entry into quiescence (Kurimchak & Graña, 2012). Nevertheless, it was not known if these PP2A/B55-dependent roles could be mediated by MASTL. We analyzed S-phase and quiescence entry in our MEFs cKO for Mastl and found no differences (**Figure 18,19**), indicating that Mastl does not control PP2A/B55 function at the G0-G1/S transition in mammals.

In yeast, the Rim15-Igo1/2-PP2A/Cdc55 module regulates entry into quiescence and survival in the stationary phase, also known as chronological life span (CLS). Given the universal role of TORC1 in nutrient sensing and regulation of CLS across species, as well as the remarkable conservation of the Rim15-Igo1/2-PP2A/Cdc55 module, it was interesting to examine whether the MASTL-ENSA/ARPP19-PP2A/B55 pathway also regulates quiescence and CLS in higher eukaryotes via similar mechanisms as described in budding yeast (Bontron et al., 2013).

However, ablation of Mastl in MEFs did not impair either entry into or maintenance of quiescence (**Figure 19,20**), suggesting that the central role of Rim15 in the control of quiescence in yeast is not conserved in mammals. It would be as well interesting to know whether in fission yeast Ppk18 controls entry into quiescence and CLS upon nutrient deprivation.

As a summary, the only essential role of Mastl in the control of the mammalian cell cycle is regulation of mitosis, a function mediated by Ensa/Arpp19 phosphorylation and inhibition of PP2A/B55 phosphatase.

4.1.3 Different requirements of Mastl for cell proliferation *in vivo*

The essential function of Mastl in mitosis has also physiological consequences *in vivo*. TAM-inducible *Mastl* deletion in young mice caused severe proliferative defects, especially in highly proliferative tissues, such as intestine or bone marrow, which led to dramatic loss of weight and rapid death after ablation of *Mastl*. In contrast, depletion of *Mastl* in adult mice resulted in improved survival compared to young *Mastl(Δ/Δ)* mice and less severe proliferative defects, even in highly proliferative tissues like the intestine, whose renewal occurs at approximately the same rate in adult and young organisms. It was very surprising the difference observed in survival among young and adult mice upon *Mastl* ablation in the cKO mouse model, since both groups were continuously treated with TAM in the diet and reached similar efficiencies of Mastl depletion. This is in striking difference to the phenotype observed upon deletion of other essential mitotic regulator, such as the kinase Plk1, in adult mice. Plk1 null mice experience severe loss of body weight, disruption of the architecture of proliferative tissues and rapid death after treatment, a phenotype that was observed in both young and adult mice null for Plk1, and resembled *Mastl(Δ/Δ)* young mice (de Cárcer et al., 2017). Data from Plk1 and Mastl cKO mouse models are comparable, since both express Cre-ERT2 under the ubiquitous promoter of *Polr2a*, and deletion is induced by TAM treatment in the diet in both models. These results led us to speculate that either highly proliferative tissues become more independent on the mitotic function of Mastl as the organism ages, or other pathways might compensate for the loss of Mastl in adult organisms.

According to the mitotic role of Plk1, Plk1 promotes adaptive pancreatic β-cell proliferation in response to insulin, and ablation of an essential mediator of Plk1 function impairs adaptive β-cell growth and chronic glucose intolerance (Shirakawa et al., 2017). Mastl, by contrast, does not seem to be an essential mediator of β-cell proliferation as *Mastl(Δ/Δ)* mice do not present alterations either in the number of β-cells or the morphology of the Langerhans islets in the pancreas, and more importantly, *Mastl(Δ/Δ)* mice have increased glucose tolerance.

4.2 MASTL as a new modulator of the mTORC1/S6K1-dependent feedback loop

4.2.1 Metabolic roles of cell cycle regulators

Additional roles for well-established cell cycle regulators have recently emerged in non-proliferative tissues to control metabolism independently of cell cycle progression. Different works have demonstrated that CDK4-cycD complexes control glucose homeostasis through different mechanisms. In pancreas, the CDK4-pRb-E2F axis activates the expression of *Kir6.2*, a key component of K_{ATP} channels, promotes insulin secretion, and improves glucose tolerance in mice (Annicotte et al., 2009). CDK4 is also important in adipose tissue where it phosphorylates IRS2 and enhances AKT signaling and insulin sensitivity *in vivo* (Lagarrigue et al., 2016). In liver, CDK4 suppresses hepatic glucose production through activation of GCN5, and subsequent inhibition of PGC-1α (Lee et al., 2014). Nevertheless, CDK4-cycD activity is chronically elevated and deregulated in diabetes patients, probably reflecting the relevance *in vivo* of the ability of CDK4 to activate mTORC1 through the phosphorylation of TSC2 and inhibit the PI3K/AKT pathway (Zacharek, Xiong, & Shumway, 2005). CDK4 also affects cell metabolism through the pRb pathway, as CDK4 inhibition increases oxidative metabolism (Franco et al., 2016). Another example of control of metabolism by cell cycle regulators is given by mitotic checkpoint p31-MAD2-BUBR1 module, which has recently emerged as a regulator of insulin receptor internalization and controls insulin signaling and glucose homeostasis in mice (Choi et al., 2016).

In this work we describe a new mitotic-independent role of MASTL-ENSA/ARPP19-PP2A/B55 (**Figure 31**), another cell cycle module with a metabolic function that appears to be relevant in non-proliferative cells as well as in insulin-responsive tissues to maintain glucose homeostasis *in vivo*.

4.1.1 mTORC1/S6K1-dependent feedback modulation in a glucose-dependent manner

mTORC1 activation is a critical event in the mTORC1/S6K1-dependent negative feedback loop that leads to AKT inhibition and renders cells irresponsive to insulin. Full mTORC1 activity requires growth factors and nutrients, and both amino acids and growth factors have been shown to modulate insulin signaling through mTOR-dependent effects (Haruta et al., 2000; Tremblay & Marette, 2001). However, whether glucose levels have the ability to modulate mTORC1-dependent feedback loop has not been directly explored. Chronic activation of mTOR by glucose and IGF-I in pancreatic β-cells decreased AKT phosphorylation in a rapamycin-dependent manner (Briaud et al., 2005), and now it is also known that mTORC1 has the ability to sense

glucose (Efeyan et al., 2013). The increased AKT-TSC2 and S6K1 phosphorylation in a glucose-sensitive manner in *MASTL* null cells, together with the lack of evidence for glucose regulating directly the PI3K/AKT pathway, led us to speculate that glucose may regulate AKT activity through the mTORC1-dependent feedback loop, and that MASTL might participate in this loop to potentiate AKT inhibition. We have explored this idea in our experiments by doing starvations and short re-stimulations with glucose. We have observed that glucose starvation increases and glucose re-stimulation decreases AKT phosphorylation, and this inversely correlates with mTORC1 activity, suggesting that glucose is able to modulate AKT activity downstream of mTORC1 signaling (**Figure 24**). Given that glucose activates mTORC1 through a similar mechanism as amino acids, which involves the Rag GTPases and mTORC1 recruitment to the lysosome (Efeyan et al., 2013), it is not surprising that glucose also modulates insulin signaling through mTORC1.

4.2.2 Downstream targets of MASTL-PP2A/B55

The fact that ENSA/ARPP19 depletion mimicked the absence of MASTL in the feedback-mediated regulation of AKT, together with the rescue of MASTL-depletion phenotype using PP2A inhibitors, suggested that MASTL function in the feedback is mediated by PP2A/B55. From the use of chemical inhibitors of PP2A it is known that PP2A can positively regulate AKT and mTOR signaling through the insulin pathway, as PP2A dephosphorylates and stabilizes the adaptor protein IRS1 (Hartley & Cooper, 2002). A recent work has shown that PP2A/B55α sustains hyperactive signaling of the AKT, ERK and Wnt pathways in pancreatic cancer cells through an unknown mechanism (Hein et al., 2016). Therefore, increased PP2A/B55 phosphatase activity might explain the increased AKT and mTOR activity and sustained insulin signaling observed in absence of MASTL.

mTORC1 and S6K1 activity down-regulates insulin/IGF-I signaling through effects on IRS serine phosphorylation and protein stability, which are the result of a balance between specific kinases and phosphatases. IRS phosphorylation by S6K1 and mTORC1 induce their delocalization and degradation (Haruta et al., 2000). Conversely protein dephosphorylation by PP2A protects IRS1 against excessive serine phosphorylation and degradation (Hartley & Cooper, 2002), and PP2A counterbalances mTOR/S6K1-mediated phosphorylation of IRS by directly dephosphorylating S312 (of human IRS1) (Carlson et al., 2004). Importantly the regulatory subunit that mediates PP2A function, and the effect of PP2A on specific phosphorylated residues of IRS remains elusive. In our work we have characterized the proline-directed S616 on IRS1 as a new phosphosite targeted by the proline-directed S/T PP2A/B55

phosphatase (**Figure 18a**), whose phosphorylation is decreased upon S6K1 inhibition, and contributes to the degradation of IRS1. S312 on IRS1 was not affected by B55 depletion, suggesting that additional B regulatory subunits of PP2A might target this site. Additional residues on IRS1 are phosphorylated by S6K1, such as S307 (of human IRS1) (Harrington et al., 2004), and S527, as both sites matched the S6K1 consensus site (RXRXXS/T) (Shah & Hunter, 2006). The proline-directed S/T sites on IRS1, S312, S616, and S636 (all of human IRS1), were more phosphorylated in *TSC2* –/– MEFs and were sensitive to rapamycin. Although they were not phosphorylated *in vitro* by S6K1, expression of a rapamycin-resistant gain-of-function S6K1 mutant partially rescued phosphorylation at these S/P sites after rapamycin treatment, suggesting that phosphorylation of these sites *in vivo* requires S6K1 activity (Shah & Hunter, 2006). Additional kinases can phosphorylate IRS proteins in response to different stimuli, such is the case of S312 on IRS1 that is targeted by JNK1 upon TNFα stimulation (Rui et al., 2001).

In the last years new targets of the feedback have also emerged. GRB10 is phosphorylated by mTORC1 at multiple serine sites and cooperates with IRS to control insulin signaling (Hsu et al., 2011a). Whether PP2A counteracts mTORC1 activity towards GRB10 is not known. Here we have shown that the proline-directed S476 on GRB10 is dephosphorylated by PP2A/B55 phosphatase, and phosphorylation of this site influence insulin signaling.

As a summary we propose a new function for the MASTL-PP2A/B55 pathway in the regulation of the mTORC1/S6K1-mediated feedback loop. Through inhibition of PP2A/B55, MASTL prevents the dephosphorylation of the feedback-target proteins, IRS1 and GRB10, which are adaptors of the RTKs and mediate signal transduction to the PI3K/AKT pathway. MASTL functions to negatively regulate AKT signaling by promoting feedback activity (**Figure 44**).

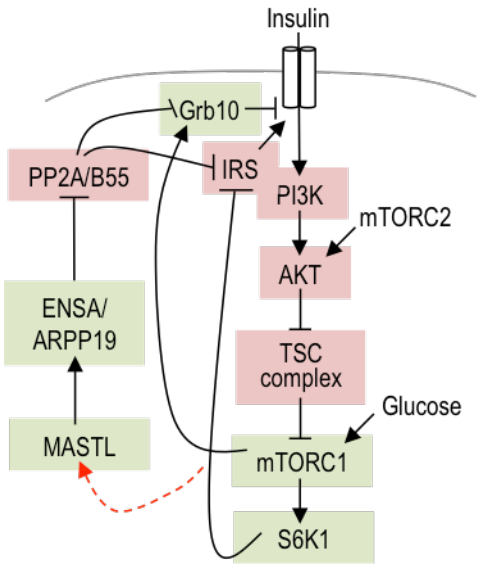

Figure 44. Model for the function of the MASTL-PP2A/B55 pathway in the regulation of the negative feedback loop mediated by mTORC1/S6K1. Schematic of the PI3K-mTOR signaling pathway, depicting feedback regulation and the proposed MASTL-PP2A/B55 participation. Green and red boxes indicate active and inactive protein, respectively. Red arrow over MASTL indicates that MASTL is activated in feedback conditions although its upstream regulators are not known.

PP2A has a dual role, as PP2A not only activates insulin signaling but also inhibits AKT and mTORC1 (Wlodarchak & Xing, 2016). PP2A/B55α dephosphorylates AKT on T308, leading to kinase inactivation in a murine prolymphocytic cell line and NIH3T3 murine fibroblasts (Kuo et al., 2008). PP2A can also revert phosphorylation of S6K1 at T389, although the regulatory subunit involved is not known. In our experiments, we did not found decreased levels of AKT T308 or S6K1 T389 in the absence of MASTL suggesting that either this pathway does not operate in this context or it is not regulated by MASTL. Further, PP2A/B56 counteracts mTORC1 activation by amino acids by targeting through MAP4K3 (Yan et al., 2010), and PP2A/B55α targets mTORC1-dependent phosphorylation in ULK1 on S637 to promote autophagy in pancreatic cell lines (Wong et al., 2015). As MASTL null cells did not presented increased autophagy, it is likely that MASTL is not controlling PP2A/B55α to regulate autophagy in our cellular context. The only evidende of MASTL positively regulating AKT published so far, comes from experiments of MASTL overexpression in cancer cell lines. MASTL induced hyperphosphorylation of AKT on S473, through an ENSA/ARPP19-PP2A/B55-independent mechanism, which seems that involve activation of GSK3 and degradation of the S473-target phosphatase PHLPP (Vera et al., 2015).

This dual role of PP2A may therefore serve to counterbalance the actions of mTOR/S6K1 signaling to promote coordinated signaling output, and demonstrates that protein phosphatase activity must be also regulated to modulate signaling. Analogous to its kinase courterparts, which are subjected to nutrient regulated pathways and multiple layers of regulation, PP2A may also sense nutrient and growth signaling. Multiple reports have shown that mTOR can negatively regulate PP2A activity. Treatment with rapamycin increases PP2A activity (Hartley & Cooper, 2002; Peterson et al., 1999) and most of this negative regulation supports mTOR activation through insulin signaling and PI3K. More recent data has demonstrated that mTORC1 inactivation relieves PP2A/B55 phosphatase activity (Di Conza et al., 2017), although nothing is known about the precise mechanisms involved in mTORC1-dependent regulation of PP2A. In yeast, the PP2A regulatory subunit Tap42 is target of TOR signaling and is another mechanism of TOR-mediated PP2A inhibition (de Virgilio, 2012). However, this function is not conserved in mammals, where the association between PP2Ac and α4, the mammalian homolog of TAP42, is not dependent on mTOR (Wong et al., 2015; Yoo et al., 2008). Interestingly, if the PP2A/B55-inhibitory kinase MASTL is regulated downstream mTORC1 to coordinate the effect of the feedback on insulin signaling, MASTL could emerge as the missing link between mTORC1 and PP2A/B55.

4.2.3 Upstream regulation of MASTL

The mechanism by which MASTL is activated during M phase involves phosphorylation of the T-activation loop by CDK1/cycB at T194 and T207 sites and subsequent MASTL autophosphorylation at the C-terminal tail on S875 (Blake-Hodek et al., 2012). These two sequential phosphorylations are thought to be essential for MASTL activity as mutation to alanine of any of them prevents MASTL activity over its substrate *in vitro*. In the current model phosphorylation of MASTL at the C-tail allows the C-tail to interact with the N-lobe to help stabilizing the active kinase conformation. Whether MASTL is also active in a mitotic-independent context, or whether other kinases can contribute to MASTL regulation by phosphorylating MASTL at different sites, is not known.

Additional CDKs, apart from CDK1/cycB complex might target MASTL's T-loop in other phases of the cell cycle where CDK1 activity is low. As such we have observed that this phosphosite is sensitive to the CDK1/2 inhibitor RO-3306 (data not shown). Phosphorylation of MASTL on T194 was enhanced upon TSC2 knockdown and was prevented by treatment with the CDKs inhibitor, suggesting that mTORC1 hyperactivation indirectly favors MASTL phosphorylation at T194 by CDKs. Interestingly, treatment with the mTORC1 allosteric inhibitor rapamycin, or with the mTOR kinase inhibitor Torin1, also prevented phosphorylation of MASTL on T194, indicating that either mTORC1 can directly phosphorylate MASTL on T194 or that mTORC1 inhibits the phosphatase that targets this residue (**Figure 27a**). Similar observations were done in HeLa cells by phosphoproteomics, where phosphorylation on T194 of MASTL decreases up to 2-fold upon rapamycin treatment (Chen et al., 2009). T194 is a proline-directed site and PP2A/B55α has been proposed to dephosphorylate it, contributing to MASTL inactivation at mitotic exit (Hegarat et al., 2014). One possibility is therefore, that mTORC1 inhibition contributes to MASTL inactivation by relieving MASTL inhibition over PP2A/B55α, but still the direct mechanism of mTORC1-mediated regulation of MASTL activity remains elusive. Based on our preliminary results, mTORC1 can directly phosphorylate MASTL *in vitro*, and the S878 emerge as a clear candidate phosphosite, given that mTORC1 increased its phosphorylation over 150-fold in a kinase assay *in vitro* (**Figure 31b**). Of note, this site is phosphorylated *in vivo* and contributes to MASTL kinase activity in mitotic extracts of *Xenopus* (Blake-Hodek et al., 2012). Further characterization of phosphorylation on MASTL *in vivo,* in interphase and mitotic cells indicated that this site was targeted by a non-mitotic kinase and was not an autophosphorylation site MASTL (unpublished data from our collaborators). S878 is located at the end of the C-tail, just 3 amino acids after S875 and 1 amino acid before the last

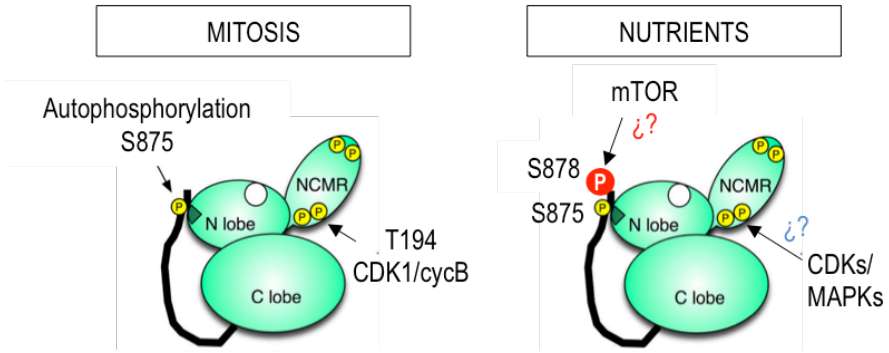

Figure 45. Proposed model of MASTL activation in mitosis and under nutrient-regulated conditions. Phosphorylation of MASTL on the C-tail is a requisite for MASTL activity. In mitosis priming phosphorylation by CDK1 on the T-loop is required for MASTL autophosphorylation and full kinase activity. Under nutrient regulated conditions mTORC1 might phosphorylate MASTL on S878 at the C-tail to fine tune modulate MASTL activity.

one of MASTL sequence, and is highly conserved among species. According to the last refinement of mTORC1 phosphorylation motif, which revealed preferences for non-charged residues surrounding the phosphoacceptor site, in addition to a preference for either proline or a non-proline hydrophobic residue in the +1 position (Kang et al., 2013), S878 on MASTL is a good potential mTORC1 site. Further experiments are required to confirm if phosphorylation of MASTL at S878 is necessary *in vivo* and contributes to MASTL activity in conditions of feedback activity (**Figure 45**).

Interestingly, a TOR signaling motif (TOS) is found in some of the mTORC1 substrates and is essential for substrate recognition mediated by RAPTOR and subsequent phosphorylation (Schalm & Blenis, 2002; Schalm et al., 2003). MASTL sequence might have a putative TOS motif within its N-domain (FDEEMA, 128-133 aa of human MASTL) as the amino acidic sequence resembles the TOS motif of well-known mTORC1 substrates, reinforcing the idea of MASTL being directly regulated by mTORC1. Of note, this putative TOS motif is well conserved across species, suggesting that might play an important role in MASTL regulation.

mTORC1-mediated phosphorylation of MASTL implies that they should co-localize in the same cellular compartment, whereas have not directly addressed this question in our experimental conditions, there are some evidences indicating that this may happen. mTOR and Raptor have been found in abundant levels in the cytoplasm and the nucleus (X. Zhang et al., 2002), and mTORC1 assembly predominantly occurs in the cytoplasm although it also exists in the nucleus in non-transformed human fibroblasts (Rosner & Hengstschläger, 2008). Indeed, mTORC1 phosphorylates some transcription factors and associate with rDNA suggesting that it might have a role in transcription regulation (Betz & Hall, 2013). Data obtained by

videomicroscopy using a GFP-tagged version of MASTL showed that MASTL is a nuclear protein that shuttles to the cytoplasm just before NEB in mitosis (Álvarez-Fernández et al., 2013; Wang et al., 2013). Moreover, in a subfractionation analysis endogenous MASTL is found both in the nucleus and in the cytoplasm (data not shown). Accordingly, MASTL sequence has two nuclear localization signal (NLS) and one nuclear export signal (NES) consensus sequence, which are responsible for the nuclear and cytoplasmic localization of MASTL, respectively. It would be interesting to know where MASTL localizes in response to nutrient stimuli, and where the putative mTORC1-dependent regulation of MASTL might occur. PP2A/B55 complexes are mostly cytoplasmic, and endosulfines are nucleocytoplasmatic proteins providing enough flexibility for MASTL-mediated inhibition of PP2A/B55 in any cellular compartment.

4.2.4 Metabolic implications of MASTL function in the regulation of AKT

Depletion of MASTL renders cells more sensitive to insulin stimulation and AKT activation in conditions of feedback activity. Markedly, AKT targets involved in glucose metabolism are upregulated in MASTL null cells, including GLUT4 translocation to the plasma membrane and the expression of glycolytic enzymes through the mTORC1-HIF1α axis, which mediates glucose uptake and allocates intracellular glucose towards the glycolytic pathway, respectively (**Figure 34,35**). Eventually AKT can also potentiate the conversion of glucose to glycogen through the inhibition of GSK3 and subsequent activation of glycogen synthase. Even though glycogen determination has not been directly addressed, increased GSK3 phosphorylation is observed in MASTL depleted cells (**Figure 36c**). HIF1α protein levels are increased upon MASTL depletion in an AKT-dependent manner, as they are restored by treatment with AKT inhibitors. It has been recently published that PP2A/B55α prevents HIF1α from degradation through a different mechanism and favor survival under hipoxia and glucose deprivation in breast cancer cell lines. In this scenario PP2A/B55α counteracts S6K1-mediated PHD2 phosphorylation, suggesting additional mechanisms of B55-mediated control of metabolism (Di Conza et al., 2017).

Chronic mTORC1 activation as consequence of over nutrition and excess of nutrients in the blood renders cells insensitive to insulin and impairs GLUT4-mediated glucose uptake. Therefore mTORC1/S6K1-dependent feedback modulation of AKT activity has implications *in vivo* in obesity and metabolic disorders involving insulin resistance, such as type 2 diabetes. Interestingly, ablation of Mastl *in vivo* improves glucose tolerance in a model of high fat diet (HFD)-induced obesity without affecting glucose-stimulated insulin secretion. Ablation of Mastl did not improved insulin sensitivity, although HFD-fed control mice did not develop insulin resistance

either. Nevertheless, the fact that Mastl null mice are not hyperinsulinemic might suggest that the improved glucose tolerance is consequence of better glucose uptake in Mastl depleted tissues. The effect of Mastl ablation is likely mediated by increased PI3K/AKT signaling in the muscle and concomitant glucose uptake, as the effect is rescued upon treatment with a PI3K inhibitor (PI3Ki). Muscle is likely the tissue of Mastl function, although we cannot rule out a contribution of WAT or liver. Deletion of Mastl in old mice lowers basal glycaemia in *ad libitum* conditions, suggesting that Mastl might improve glucose tolerance upon challenging conditions of either HFD or aging. It has just been published a new glucose sensing mechanism in the skeletal muscle that is essential to maintain postprandial glucose homeostasis independently on insulin signaling (Meng et al., 2017). This mechanism involves glucose sensing by K_{ATP} channels and insulin-independent activation of AKT through Baf60c-dependent transcription of DEPTOR. This highlights the necessity of inhibition of the mTORC1-dependent feedback loop to relieve inhibition of AKT signaling and maintain whole body glucose homeostasis, suggesting that Mastl could play a role in skeletal muscle independently on insulin signaling.

Of note, Ensa knockout mice have improved glucose tolerance, despite having defective insulin secretion, and are more insulin sensitive (Wiles et al., 2002), suggesting that lack of Ensa increases glucose uptake. Whether Ensa depletion affects insulin signaling *in vivo* has not been explored, but fit in a model where Mastl phosphorylates Ensa to inhibit PP2A/B55 and AKT signaling. In the same direction, haploinsuficiency of the B55α subunit of PP2A causes insulin resistance likely due to the defective insulin-induced AKT stimulation in insulin-responsive tissues (Goldsworthy et al., 2016).

4.3 Uncoupling the MASTL-ENSA/ARPP19-PP2A/B55 pathway

The only molecular pathway attributed so far to the kinase MASTL is the inhibition of PP2A/B55 phosphatase complexes through the phosphorylation of ENSA and ARPP19 proteins. With the exception of a recent work in which it was proposed that MASTL induced GSK3 dephosphorylation independent of endosulfines, through an unknown mechanism (Vera et al., 2015), all functions ascribed for MASTL operate through the same molecular pathway. That is the case of its well-studied function in mitosis, as well as its new function in metabolism. PP2A/B55 phosphatase complexes and endosulfines function in many different pathways in the cell and, as such, control other cellular and physiological functions in addition to mitosis and the mTORC1/S6K1-dependent feedback loop. Nevertheless, it is not known to what extent all of these endosulfine- and PP2A/B55-dependent functions are also mediated by MASTL.

As stated above, ENSA and ARPP19 are able to regulate PP2A/B55 complexes at M entry even when MASTL is inactive, and this is achieved through ENSA/ARPP19 phosphorylation by CDK1. This raises the possibility that there might exist some cellular contexts, such as those where MASTL activity is irrelevant, where ENSA/ARPP19-mediated inhibition of PP2A is independent of MASTL. ENSA/ARPP19 proteins are known to be involved in several biological processes in addition to the cell cycle. In the murine brain, suppression of ARPP19 expression increases neurite length (White & Giffard, 2013), and this is consistent with previous reports that showed that PP2A/B55γ activity induces neurite outgrowth (Strack, 2002), although whether ARPP19 modulates PP2A/B55γ activity in this context has not been addressed. Interestingly, ARPP19 is a major substrate for cAMP activated protein kinase (PKA) in postsynaptic neurons, whether PKA-mediated ARPP19 phosphorylation contributes to PP2A/B55 inhibition in this context is unknown. Interestingly, in some cellular scenarios such as meiosis, PKA-mediated phosphorylation of ENSA/ARPP19 antagonizes the effect of MASTL phosphorylation (Dupré et al., 2013).

ENSA was identified as an endogenous ligand and regulator of the sulfonylurea-binding site of K_{ATP} channels in pancreatic β-cells and ovine brain (Virsolvy-Vergine et al., 1992). ENSA binding mediates the closure of the K_{ATP} channels, and stimulates insulin secretion in β-cells, although the precise mechanism and ENSA regulation is unknown. The involvement of PP2A/B55, as target of ENSA, in insulin secretion has not been directly addressed either. A recently published work showed that haploinsuficiency of B55α in mice causes insulin resistance and highly compensatory increase in β-cell mass and hyperinsulemia (Goldsworthy et al., 2016).

Although diminished PP2A/B55α activity would fit in a model of ENSA promoting insulin secretion through inhibition of phosphatase complexes, the hyperinsulemia phenotype and increased β-cell mass in B55α heterozygous mice were most likely adaptive responses to insulin resistance caused by defective insulin-induced AKT stimulation in metabolic tissues. As mentioned above, ENSA acts as an endogenous counterpart to sulfonylureas; drugs that are used in type 2 diabetic patients for triggering insulin secretion. PKA is also known to be involved in the process of insulin secretion, since treatment of cells with the PKA activator, forskolin, enhances insulin secretion (F. Wei et al., 2005). However, the potential contribution of PKA to the regulation of ENSA has not been addressed. According to our data, ablation of MASTL in mice does not impair insulin secretion either in fasting or after glucose-stimulation (**Figure 32**). Since ENSA ablation blunts insulin secretion it is unlikely that MASTL positively regulates ENSA in β-cells to trigger insulin secretion, pointing to a MASTL-independent function of ENSA in cellular metabolism.

PP2A/B55 complexes target many different signaling pathways and have also been linked to several cell cycle and metabolic functions but little is known about their regulation in specific cellular contexts. Here we present a mechanism of PP2A/B55 regulation mediated by MASTL that is relevant for mitosis and the control mTORC1/S6K1-mediated feedback loop. Further there exist another mechanism driven by the inhibitory protein α4, which binds PP2A catalytic subunit and impairs assembly with the B regulatory subunits and that might regulate PP2A/B55 activity independently on MASTL. Such is the case of PP2A/B55α driving a p53-dependent metabolic adaptation to glutamine deprivation, where PP2A/B55α activity is controlled by α4 protein, as glutamine deprivation induces dissociation of PP2A from its inhibitor α4 (Reid et al., 2013). Similarly, PP2A/B55α is activated upon amino acid and serum starvation, but not rapamycin treatment, through a similar mechanism to activate autophagy (Wong et al., 2015). As mentioned above, PP2A/B55 complexes also regulate G0-G1 and G1/S transitions through phosphorylation of Rb family of pocket proteins (Kurimchak & Graña, 2012), and this function was regulated in a MASTL-independent manner, suggesting additional levels of regulation of PP2A/B55.

In summary, even though the MASTL-ENSA/ARPP19-PP2A/B55 module is evolutionary conserved from yeast to mammals, and MASTL has emerged as a PP2A/B55-inhibitory kinase, not all the functions attributed to the different components of the pathway seem to be controlled by MASTL. Thus, there must be additional mechanism of regulation of endosulfines and PP2A/B55 complexes to meet specific necessities in a cell context and cell type specific manner.

4.4 Therapeutic implications of MASTL regulation

Based on its mitotic function and the antiproliferative response of MASTL depletion, MASTL has been proposed as a potential new target for cancer therapy. As such MASTL is overexpressed is breast tumors and its expression correlates with poor prognosis, and MASTL depletion impairs proliferation of breast tumor cells *in vitro* and *in vivo* (Álvarez-Fernández et al., submitted). Current efforts are based in the identification of those tumors that might benefit of MASTL-based therapies.

With the newly identified role of MASTL in the mTORC1-dependent feedback loop, MASTL also emerges as a new potential therapeutic target for metabolic diseases. That mTORC1 hyperactivation from genetic or dietary manipulation results in insulin resistance, and mice lacking S6K1 are protected from obesity-induced insulin resistance, has led to speculate that mTORC1 or S6K1 inhibitors could improve glucose tolerance and protect against type 2 diabetes (Um et al., 2004). Pharmacological inhibition of mTORC1 using rapamycin has the opposite effect, causing insulin resistance and impaired glucose homeostasis (Fang et al., 2013). This result is explained at least in part by the fact that prolonged rapamycin treatment also inhibits mTORC2 signaling *in vivo*. As mTORC2 directly activates AKT downstream of insulin/PI3K signaling, it is not surprising that mTORC2 inhibition disrupts the physiological response to insulin. A selective S6K1 inhibitor improves glucose tolerance in HFD-fed mice and enhance insulin signaling in metabolic tissues, overcoming the limitations of rapamycin (Shum et al., 2016). Targeting regulators of the feedback loop downstream of mTORC1 might be *bona fide* targets to improve glucose disposal in obese diabetic individuals while avoiding toxicity associated with inhibition of mTOR. In this line, MASTL appears as a new potential target given the low toxicity associated with Mastl inhibition in adult mice, whereas improves glucose tolerance and insulin signaling in mice.

The mTORC1/S6K1-dependent feedback loop also influences therapeutic responses to mTOR inhibitors in cancer therapy, as PI3K/AKT and ERK/MAPK activation attenuates antitumor effect of mTORC1 inhibition (Carracedo et al., 2008; O'Reilly et al., 2006). In addition to insulin and IGF-I signaling, mTOR inhibitors also enhance the activation of other receptor tyrosine kinases (RTKs) upstream of PI3K and AKT. This includes members of the EGF Receptor family (EGFR, ErbB2 [also known as Her2], ErbB3 [Her3], and ErbB4 [Her4]), which are acutely activated upon mTOR inhibition, without having immediate effects on receptor levels (O'Reilly et al., 2006; Rodrik-Outmezguine et al., 2011). While the post-translational mechanisms underlying this regulation are not currently known, the effects are most prominently seen with mTOR kinase

inhibitors, rather than the allosteric inhibitor rapamycin. As this class of compounds inhibits mTORC1 and mTORC2 equally, some of this feedback regulation could be mediated by mTORC2 signaling. Microarray analyses showed that MASTL depleted cells have strong upregulation of the ERBB pathway and its downstream effectors, including the MAPK pathway, suggesting that the effect of MASTL in the feedback is not restricted to the insulin pathway (data not shown). MASTL inhibition might affect the status of other adaptor proteins of the ERBB receptors although this has not been addressed, or there might be crosstalk among insulin receptor and other RTKs. Furthermore, MASTL nulls cells are more sensitive to human epidermal growth factor (hEGF) stimulation, as shown by increased autophosphorylation of EGFR, and although signal transduction to AKT is not largely enhanced, treatment with and EGFR inhibitor partially rescued AKT T308 phosphorylation in MASTL null cells (**Figure 20**). Whereas GRB10 has been found bound to EGFR (He et al., 1998), GRB10 depletion does not restore sensitivity to hEGF in TSC2-/- MEFs (Hsu et al., 2011a). These results are still controversial, so we cannot rule out whether MASTL might regulate EGFR activity by another mechanism independent on GRB10. MASTL depleted cells also present higher EGFR total levels (**Figure 20b**), and it has been proposed that mTORC1 activity protects EGFR from lysosomal degradation (Kim et al., 2015), raising another plausible explanation for the enhanced EGFR signaling in MASTL depleted cells. In any case, these results should be taken into account for future anti-tumoral therapies targeting MASTL kinase, as combined treatments of MASTL inhibitors along with RTK inhibitors, which are already use in clinics, may help for finding synergies and enhance therapeutic response in tumors.

Implications of MASTL in AKT-driven metabolism could also be relevant to find metabolic dependencies to MASTL inhibition in tumor cells. For instance, MASTL depleted cells might rely more on glucose metabolism and, as such, be more sensitive to glucose availability.

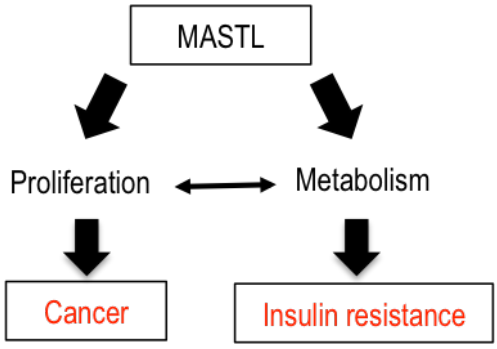

Figure 46. MASTL is an essential mitotic regulator with metabolic implications. MASTL is a recently discovered mitotic kinase with critical implications in proliferation and cancer. Other functions of MASTL and its physiological relevance are just starting to emerge. We have described a new role of MASTL in the control of AKT and mTORC1 signaling and its metabolic implications. This dual role of MASTL might be exploited for treating glucose intolerance disorders and might contribute to find more effective antitumoral therapies.

Altogether, the work herein presented supports a new role of MASTL in the modulation of mTORC1/S6K1-dependent feedback loop to potentiate PI3K/AKT inhibition and contributed to further understand the role of MASTL kinase in mammals. Given that MASTL is a druggable kinase whose deletion presents low toxicity in adult mice, these findings might hopefully expand its potential therapeutic applicability for the treatment of glucose intolerance, and contribute to the development of more accurate antitumoral responses (**Figure 46**).

Conclusions

1. MASTL is an essential mitotic kinase required for proper chromosome condensation and segregation in mammals. MASTL prevents premature dephosphorylation of CDK-dependent phosphosites in mitosis through inhibition of the PP2A/B55 phosphatase.
2. Mastl is not essential for S-phase entry from quiescence, neither for entry or maintenance of cellular quiescence.
3. MASTL-ENSA/ARPP19-PP2A/B55 pathway participates in the mTORC1/S6K1-dependent negative feedback loop that limits AKT activity.
4. MASTL, through ENSA/ARPP19-mediated inhibition of PP2A/B55, prevents the dephosphorylation of two targets of the feedback, the adaptor proteins IRS and GRB10, to allow fine-tune of PI3K/AKT pathway in response to nutrients (e.g. glucose) and growth factors. Deregulation of this axis has metabolic consequences in glucose uptake in cells.
5. MASTL activity is positively modulated in feedback conditions downstream of the mTORC1/S6K1 pathway.
6. Mastl plays a physiological role in proliferation *in vivo*. Whereas ablation of Mastl in young mice leads to severe proliferative defects that compromise survival, adult mice are more tolerant to Mastl depletion. However, Mastl ablation impaired tissue regeneration and altered tissue homeostasis in the long term, eventually leading to premature death.
7. Mastl controls glucose homeostasis *in vivo*, and improves glucose tolerance in conditions of high fat diet-induced obesity, in a PI3K-dependent manner, without affecting glucose-stimulated-insulin secretion.

References

Álvarez-Fernández, M., & Malumbres, M. (2014). Preparing a cell for nuclear envelope breakdown: Spatio-temporal control of phosphorylation during mitotic entry. *BioEssays*, *36*(8), 757–765.

Álvarez-Fernández, M., Sánchez-Martínez, R., Sanz-Castillo, B., Gan, P. P., Sanz-Flores, M., Trakala, M., Ruiz-Torres, M., Lorca, T., Castro, A., & Malumbres, M. (2013). Greatwall is essential to prevent mitotic collapse after nuclear envelope breakdown in mammals. *Proceedings of the National Academy of Sciences of the United States of America*, *110*(43), 17374–9.

Álvarez-Fernández, M., Sanz-Flores, M., Sanz, B., Salazar-Roa, M., Partida, D., Ali, H. R., Manchado, E., Lowe, S., VanArsdale, T., Shields, D., Caldas, C., & Quintela-Fandino, Miguel Malumbres, M. (n.d.). MASTL/Greatwall kinase activity as a new therapeutic target in breast cancer. *Submitted*.

Anania, M., Gasparri, F., Cetti, E., Fraietta, I., Todoerti, K., Miranda, C., Mazzoni, M., Re, C., Colombo, R., Ukmar, G., Camisasca, S., Pagliardini, S., Pierotti, M., … Greco, A. (2015). Identification of thyroid tumor cell vulnerabilities through a siRNA-based functional screening. *Oncotarget*, *6*(33), 34629–34648.

Annicotte, J.-S., Blanchet, E., Chavey, C., Iankova, I., Costes, S., Assou, S., Teyssier, J., Dalle, S., Sardet, C., & Fajas, L. (2009). The CDK4-pRB-E2F1 pathway controls insulin secretion. *Nature Cell Biology*, *11*(8), 1017–1023.

Archambault, V., Zhao, X., White-Cooper, H., Carpenter, A. T. C., & Glover, D. M. (2007). Mutations in Drosophila Greatwall/scant reveal its roles in mitosis and meiosis and interdependence with polo kinase. *PLoS Genetics*, *3*(11), 2163–2179.

Bai, L., Wang, Y., Fan, J., Chen, Y., Ji, W., Qu, A., Xu, P., James, D. E., & Xu, T. (2007). Dissecting Multiple Steps of GLUT4 Trafficking and Identifying the Sites of Insulin Action. *Cell Metabolism*, *5*(1), 47–57.

Bai, Y., Xuan, B., Liu, H., Zhong, J., Yu, D., & Qian, Z. (2015). Tuberous Sclerosis Complex Protein 2-Independent Activation of mTORC1 by Human Cytomegalovirus pUL38. *J Virol*, *89*(15), 7625–7635.

Bernal-Mizrachi, E., Fatrai, S., Johnson, J. D., Ohsugi, M., Otani, K., Han, Z., Polonsky, K. S., & Permutt, M. A. (2004). Defective insulin secretion and increased susceptibility to experimental diabetes are induced by reduced Akt activity in pancreatic islet ?? cells. *Journal of Clinical Investigation*, *114*(7), 928–936.

Bernard, A., Jin, M., González-Rodríguez, P., Füllgrabe, J., Delorme-Axford, E., Backues, S. K., Joseph, B., & Klionsky, D. J. (2015). Rph1/KDM4 mediates nutrient-limitation signaling that

leads to the transcriptional induction of autophagy. *Current Biology*, *25*(5), 546–555.

Betz, C., & Hall, M. N. (2013). Where is mTOR and what is it doing there? *Journal of Cell Biology*, *203*(4), 563–574.

Blake-hodek, K. A., Williams, B. C., Zhao, Y., Castilho, P. V, Chen, W., Mao, Y., & Yamamoto, T. M. (2012). Determinants for Activation of the Atypical AGC Kinase Greatwall. *Molecular and Cellular Biology*, 1337–1353.

Blake-Hodek, K. a, Williams, B. C., Zhao, Y., Castilho, P. V, Chen, W., Mao, Y., Yamamoto, T. M., & Goldberg, M. L. (2012). Determinants for activation of the atypical AGC kinase Greatwall during M phase entry. *Molecular and Cellular Biology*, *32*(8), 1337–53.

Bontron, S., Jaquenoud, M., Vaga, S., Talarek, N., Bodenmiller, B., Aebersold, R., & De Virgilio, C. (2013). Yeast Endosulfines Control Entry into Quiescence and Chronological Life Span by Inhibiting Protein Phosphatase 2A. *Cell Reports*, *3*(1), 16–22.

Bradley, H., Shaw, C. S., Worthington, P. L., Shepherd, S. O., Cocks, M., & Wagenmakers, A. J. M. (2014). Quantitative immunofluorescence microscopy of subcellular GLUT4 distribution in human skeletal muscle: effects of endurance and sprint interval training. *Physiological Reports*, *2*(7), 1–16.

Briaud, I., Dickson, L. M., Lingohr, M. K., McCuaig, J. F., Lawrence, J. C., & Rhodes, C. J. (2005). Insulin receptor substrate-2 proteasomal degradation mediated by a mammalian target of rapamycin (mTOR)-induced negative feedback down-regulates protein kinase B-mediated signaling pathway in ??-cells. *Journal of Biological Chemistry*, *280*(3), 2282–2293.

Brugarolas, J., Lei, K., Hurley, R. L., Manning, B. D., Reiling, J. H., Hafen, E., Witters, L. A., Ellisen, L. W., Kaelin, W. G., & Jr, W. G. K. (2004). Regulation of mTOR function in response to hypoxia by REDD1 and the TSC1 / TSC2 tumor suppressor complex. *Genes and Development*, *18*(23), 1–12.

Brunet, A., Bonni, A., Zigmond, M. J., Lin, M. Z., Juo, P., Hu, L. S., Anderson, M.J., Arden, K. C., Blenis, J., & Greenberg, M. E. (1999). Akt promotes cell survival by phosphorylating and inhibiting a Forkhead transcription factor. *Cell*, *96*, 857–868.

Burgess, A., Vigneron, S., Brioudes, E., Labbé, J.-C., Lorca, T., & Castro, A. (2010). Loss of human Greatwall results in G2 arrest and multiple mitotic defects due to deregulation of the cyclin B-Cdc2/PP2A balance. *Proceedings of the National Academy of Sciences of the United States of America*, *107*(28), 12564–9.

Cameroni, E., Hulo, N., Roosen, J., Winderickx, J., & De Virgilio, C. (2004). The novel yeast PAS kinase Rim15 orchestrates G0-associated antioxidant defense mechanisms. *Cell Cycle*, *3*(4), 462–468.

Carlson, C. J., White, M. F., & Rondinone, C. M. (2004). Mammalian target of rapamycin regulates IRS-1 serine 307 phosphorylation. *Biochemical and Biophysical Research Communications*, *316*(2), 533–539.

Carracedo, A., Ma, L., Rojo, F., Teruya-Feldstein, J., Salmena, L., Alimonti, A., Egia, A., Sasaki, A. T., Thomas, G., Kozma, S. C., Papa, A., Nardella, C., Cantley, L. C., … Pandolfi, P. P. (2008). Inhibition of mTORC1 leads to MAPK pathway activation through a PI3K-dependent feedback loop in human cancer. *Journal of Clinical Investigation*, *118*(9), 3065–3074.

Castilho, P. V., Williams, B. C., Mochida, S., Zhao, Y., & Goldberg, M. L. (2009). The M Phase Kinase Greatwall (Gwl) Promotes Inactivation of PP2A/B55?, a Phosphatase Directed Against CDK Phosphosites. *Molecular Biology of the Cell*, *20*, 4777–4789.

Chen, R. Q., Yang, Q. K., Lu, B. W., Yi, W., Cantin, G., Chen, Y. L., Fearns, C., Yates, J. R., & Lee, J. D. (2009). CDC25B mediates rapamycin-induced oncogenic responses in cancer cells. *Cancer Research*, *69*(6), 2663–2668.

Chica, N., Rozalén, A. E., Pérez-Hidalgo, L., Rubio, A., Novak, B., & Moreno, S. (2016). Nutritional control of cell size by the greatwall-endosulfine-PP2A·B55 pathway. *Current Biology*, *26*(3), 319–330.

Choi, E., Zhang, X., Xing, C., & Yu, H. (2016). Mitotic Checkpoint Regulators Control Insulin Article Mitotic Checkpoint Regulators Control Insulin Signaling and Metabolic Homeostasis. *Cell*, 1–15.

Clark, S. F., Molero, J. C., & James, D. E. (2000). Release of insulin receptor substrate proteins from an intracellular complex coincides with the development of insulin resistance. *Journal of Biological Chemistry*, *275*(6), 3819–3826.

Clarke, J. F., Young, P. W., Yonezawa, K., Kasuga, M., & Holman, G. D. (1994). Inhibition of the translocation of GLUT1 and GLUT4 in 3T3-L1 cells by the phosphatidylinositol 3-kinase inhibitor, wortmannin. *The Biochemical Journal*, *300 (Pt 3*, 631–5.

Cross, D. A., Alessi, D. R., Cohen, P., Andjelkovich, M., & Hemmings, B. A. (1995). Inhibition of glycogen synthase kinase-3 by insulin mediated by protein kinase B. *Nature*, *378*, 785–789.

Cross, D. A., Alessi, D. R., Vandenheede, J. R., McDowell, H. E., Hundal, H. S., & Cohen, P. (1994). The inhibition of glycogen synthase kinase-3 by insulin or insulin-like growth factor 1 in the rat skeletal muscle cell line L6 is blocked by wortmannin, but not by rapamycin: evidence that wortmannin blocks activation of the mitogen-activated protein kin. *The Biochemical Journal*, *303 (Pt 1*(1994), 21–6.

Cundell, M. J., Bastos, R., Zhang, T., Holder, J., Gruneberg, U., Novak, B., & Barr, F. A. (2013).

The BEG (PP2A-B55/ENSA/Greatwall) Pathway Ensures Cytokinesis follows Chromosome Separation. *Molecular Cell*, *52*(3), 393–405.

Curtis, C., Shah, S., SF, C., G, T., OM, R., MJ, D., D, S., AG, L., S, S., Y, Y., S, G., G, H., Haffari G, Bashashati A, Russell R, McKinney S; METABRIC Group, Langerød A, Green A, Provenzano E, Wishart G, Pinder S, Watson P, M. F., … S., A. (2012). The genomic and transcriptomic architecture of 2,000 breast tumours reveals novel subgroups. *Nature*, *486*, 346–352.

Dahlhaus, M., Burkovski, A., Hertwig, F., Mussel, C., Volland, R., Fischer, M., Debatin, K., Kestler, H., & Beltinger, C. (2016). Boolean modeling identifies Greatwall/MASTL as an important regulator in the AURKA network of neuroblastoma. *Cancer Letters*, *371*, 79–89.

de Cárcer, G., Wachowicz, P., Sara Martínez-Martínez, J. O., Nerea Méndez-Barbero, Beatriz Escobar, Alejandra González, Tohru Takaki, A., El Bakkali, 1 Juan Antonio Cámara, 4 Luis J. Jiménez-Borreguero5, Xosé Bustelo, 7 Marta, 7 Cañamero, 8 Francisca Mulero, Sevilla, M. de los A., Montero, M. J., Redondo, J. M., & Malumbres, M. (2017). Plk1 regulates contraction of postmitotic smooth muscle cells and vascular homeostasis. *Nature Medicine*, *in press*.

de Virgilio, C. (2012). The essence of yeast quiescence. *FEMS Microbiology Reviews*, *36*(2), 306–339.

Di Conza, G., Cafarello, S. T., Loroch, S., Kietzmann, T., Moretti, F., Mazzone, M., Conza, G. Di, Cafarello, S. T., Loroch, S., Mennerich, D., & Deschoemaeker, S. (2017). The mTOR and PP2A Pathways Regulate PHD2 Phosphorylation to Fine-Tune HIF1 a Levels and Colorectal Cancer Cell Survival under Hypoxia Article The mTOR and PP2A Pathways Regulate PHD2 Phosphorylation to Fine-Tune HIF1 a Levels and Colorectal Cancer Cell Su. *CellReports*, *18*(7), 1699–1712.

Di Conza, G., Trusso Cafarello, S., Zheng, X., Zhang, Q., & Mazzone, M. (2017). PHD2 Targeting Overcomes Breast Cancer Cell Death upon Glucose Starvation in a PP2A/B55α-Mediated Manner. *Cell Reports*, *18*(12), 2836–2844.

Dibble, C. C., Asara, J. M., & Manning, B. D. (2009). Characterization of Rictor Phosphorylation Sites Reveals Direct Regulation of mTOR Complex 2 by S6K1 † †. *Molecular and Cellular Biology*, *29*(21), 5657–5670.

Dibble, C. C., & Manning, B. D. (2013). Signal integration by mTORC1 coordinates nutrient input with biosynthetic output. *Nature Cell Biology*, *15*(6), 555–64.

Ding, M., Bruick, R. K., & Yu, Y. (2016). Secreted IGFBP5 mediates mTORC1-dependent feedback inhibition of IGF-1 signalling. *Nature Cell Biology*, *18*(3).

Dupré, A., Buffin, E., Roustan, C., Nairn, A. C., Jessus, C., & Haccard, O. (2013). The phosphorylation of ARPP19 by Greatwall renders the auto-amplification of MPF independently of PKA in Xenopus oocytes. *Journal of Cell Science*, *126*, 3916–3926.

Dupre, A., Daldello, E. M., Nairn, A. C., Jessus, C., & Haccard, O. (2014). Phosphorylation of ARPP19 by protein kinase A prevents meiosis resumption in Xenopus oocytes. *Nat Commun*, *5*, 3318.

Efeyan, A., Comb, W. C., & Sabatini, D. M. (2015). Nutrient-sensing mechanisms and pathways. *Nature*, *517*(7534), 302–310.

Efeyan, A., & Sabatini, D. M. (2010). MTOR and cancer: Many loops in one pathway. *Current Opinion in Cell Biology*, *22*(2), 169–176.

Efeyan, A., Zoncu, R., Chang, S., Gumper, I., Snitkin, H., Wolfson, R. L., Kirak, O., Sabatini, D. D., & Sabatini, D. M. (2013). Regulation of mTORC1 by the Rag GTPases is necessary for neonatal autophagy and survival. *Nature*, *493*(7434), 679–83.

Eichhorn PJ, MP, C., & R., B. (2009). Protein phosphatase 2A regulatory subunits and cancer. *Biochimica et Biophysica Acta - Molecular Cell Research*, *1795*, 1–15.

Elstrom, R. L., Bauer, D. E., Buzzai, M., Karnauskas, R., Harris, M. H., Plas, D. R., Zhuang, H., Cinalli, R. M., Alavi, A., Rudin, C. M., & Thompson, C. B. (2004). Akt stimultes aerobic glycolysis in cancer cells. *Cancer Research*, *64*(11), 3892–3899.

Fabrizio, P., Pozza, F., Pletcher, S., Gendron, C., & Longo. (2001). Regulation of longevity and stress resistance by Sch9 in yeast. *Science*, *292*, 288–290.

Fang, Y., Westbrook, R., Hill, C., Boparai, R. K., Arum, O., Spong, A., Wang, F., Javors, M. A., Chen, J., Sun, L. Y., & Bartke, A. (2013). Duration of rapamycin treatment has differential effects on metabolism in mice. *Cell Metabolism*, *17*(3), 456–462.

Franco, J., Balaji, U., Freinkman, E., Witkiewicz, A. K., & Knudsen, E. S. (2016). Metabolic Reprogramming of Pancreatic Cancer Mediated by CDK4/6 Inhibition Elicits Unique Vulnerabilities. *Cell Reports*, *14*(5), 979–990.

Gandhi M.J., C.L., C., & J.G., D. (2003). 10, FLJ14813 Missense Mutation: A Candidate for Autosomal Dominant Thrombocytopenia on Human Chromosome. *Human Heredity*, *55*, 66–70.

Gao, T., Furnari, F., & Newton, A. C. (2005). PHLPP: A phosphatase that directly dephosphorylates Akt, promotes apoptosis, and suppresses tumor growth. *Molecular Cell*, *18*(1), 13–24.

Gharbi-Ayachi, A., Labbé, J.-C., Burgess, A., Vigneron, S., Strub, J.-M., Brioudes, E., Van-Dorsselaer, A., Castro, A., & Lorca, T. (2010a). The Substrate of Greatwall Kinase, Arpp19,

Controls Mitosis by Inhibiting Protein Phosphatase 2A. *Science*, *330*(December), 1673–1677.

Gharbi-Ayachi, A., Labbé, J.-C., Burgess, A., Vigneron, S., Strub, J.-M., Brioudes, E., Van-Dorsselaer, A., Castro, A., & Lorca, T. (2010b). The substrate of Greatwall kinase, Arpp19, controls mitosis by inhibiting protein phosphatase 2A. *Science (New York, N.Y.)*, *330*(6011), 1673–7.

Goldsworthy, M., Bai, Y., Li, C. M., Ge, H., Lamas, E., Hilton, H., Esapa, C. T., Baker, D., Baron, W., Juan, T., V??niant, M. M., Lloyd, D. J., & Cox, R. D. (2016). Haploinsufficiency of the insulin receptor in the presence of a splice-site mutation in PPP2R2A results in a novel digenic mouse model of type 2 diabetes. *Diabetes*, *65*(5), 1434–1446.

Greene, M. W., Sakaue, H., Wang, L., Alessi, D. R., & Roth, R. A. (2003). Modulation of insulin-stimulated degradation of human insulin receptor substrate-1 by serine 312 phosphorylation. *Journal of Biological Chemistry*, *278*(10), 8199–8211.

Gwinn, D. M., Shackelford, D. B., Egan, D. F., Mihaylova, M. M., Mery, A., Vasquez, D. S., Turk, B. E., & Shaw, R. J. (2008). AMPK Phosphorylation of Raptor Mediates a Metabolic Checkpoint. *Molecular Cell*, *30*(2), 214–226.

Hara, M., Abe, Y., Tanaka, T., Yamamoto, T., Okumura, E., & Kishimoto, T. (2012). Greatwall kinase and cyclin B-Cdk1 are both critical constituents of M-phase-promoting factor. *Nature Communications*, *3*(w), 1059.

Harrington, L. S., Findlay, G. M., Gray, A., Tolkacheva, T., Wigfield, S., Rebholz, H., Barnett, J., Leslie, N. R., Cheng, S., Shepherd, P. R., Gout, I., Downes, C. P., & Lamb, R. F. (2004). The TSC1-2 tumor suppressor controls insulin-PI3K signaling via regulation of IRS proteins. *Journal of Cell Biology*, *166*(2), 213–223.

Hartley, D., & Cooper, G. M. (2002). Role of mTOR in the degradation of IRS-1: Regulation of PP2A activity. *Journal of Cellular Biochemistry*, *85*(2), 304–314.

Haruta, T., Uno, T., Kawahara, J., Takano, A., Egawa, K., Sharma, P. M., Olefsky, J. M., & Kobayashi, M. (2000). A Rapamycin-Sensitive Pathway Down-Regulates Insulin Signaling via Phosphorylation and Proteasomal Degradation of Insulin Receptor Substrate-1. *Molecular Endocrinology*, (July), 783–794.

He, W., Rose, D. W., Olefsky, J. M., & Gustafson, T. A. (1998). Grb10 interacts differentially with the insulin receptor, insulin-like growth factor I receptor, and epidermal growth factor receptor via the Grb10 src hamology 2 (SH2) domain and a second novel domain located between the pleckstrin hamology and SH2 domai. *Journal of Biological Chemistry*, *273*(12), 6860–6867.

Hegarat, N., Vesely, C., Vinod, P. K., Ocasio, C., Peter, N., Gannon, J., Oliver, A. W., Nov??k, B., & Hochegger, H. (2014). PP2A/B55 and Fcp1 Regulate Greatwall and Ensa Dephosphorylation during Mitotic Exit. *PLoS Genetics*, *10*(1).

Hein, A. L., Seshacharyulu, P., Rachagani, S., Sheinin, Y. M., Ouellette, M. M., Ponnusamy, M. P., Mumby, M. C., Batra, S. K., & Yan, Y. (2016). PR55?? subunit of protein phosphatase 2A supports the tumorigenic and metastatic potential of pancreatic cancer cells by sustaining hyperactive oncogenic signaling. *Cancer Research*, *76*(8), 2243–2253.

Henry, B. (2003). Loss of Tsc1 / Tsc2 activates mTOR and disrupts PI3K-Akt signaling through downregulation of PDGFR, *112*(8), 1223–1233.

Hsu, P. P., Kang, S. A., Rameseder, J., Zhang, Y., Ottina, K. A., Lim, D., Peterson, T. R., Choi, Y., Gray, N. S., Yaffe, M. B., Marto, J. A., & Sabatini, D. M. (2011a). Reveals a Mechanism of mTORC1-Mediated Inhibition of Growth Factor Signaling. *Science*, *926*(June).

Hsu, P. P., Kang, S. A., Rameseder, J., Zhang, Y., Ottina, K. A., Lim, D., Peterson, T. R., Choi, Y., Gray, N. S., Yaffe, M. B., Marto, J. A., & Sabatini, D. M. (2011b). The mTOR-regulated phosphoproteome reveals a mechanism of mTORC1-mediated inhibition of growth factor signaling. *Science (New York, N.Y.)*, *332*(6035), 1317–22.

Huang, J., Dibble, C. C., Matsuzaki, M., & Manning, B. D. (2008). The TSC1-TSC2 complex is required for proper activation of mTOR complex 2. *Molecular and Cellular Biology*, *28*(12), 4104–15.

Huang, J., & Manning, B. D. (2009). A complex interplay between Akt, TSC2 and the two mTOR complexes. *Biochemical Society Transactions*, *37*(Pt 1), 217–22.

Inoki, K., Li, Y., Zhu, T., Wu, J., & Guan, K.-L. (2002). TSC2 is phosphorylated and inhibited by Akt and suppresses mTOR signalling. *Nature Cell Biology*, *4*(9), 648–57.

Inoki, K., Zhu, T., & Guan, K.-L. (2003). TSC2 Mediates Cellular Energy Response to Control Cell Growth and Survival. *Cell*, *115*(5), 577–590.

Izumiya, Y., Hopkins, T., Morris, C., Sato, K., Zeng, L., Viereck, J., Hamilton, J. A., Ouchi, N., LeBrasseur, N. K., & Walsh, K. (2008). Fast/Glycolytic Muscle Fiber Growth Reduces Fat Mass and Improves Metabolic Parameters in Obese Mice. *Cell Metabolism*, *7*(2), 159–172.

Jones, R. G., Plas, D. R., Kubek, S., Buzzai, M., Mu, J., Xu, Y., Birnbaum, M. J., & Thompson, C. B. (2005). AMP-activated protein kinase induces a p53-dependent metabolic checkpoint. *Molecular Cell*, *18*(3), 283–293.

Juanes, M. A., Khoueiry, R., Kupka, T., Castro, A., Mudrak, I., Ogris, E., Lorca, T., & Piatti, S. (2013). Budding Yeast Greatwall and Endosulfines Control Activity and Spatial Regulation of PP2ACdc55 for Timely Mitotic Progression. *PLoS Genetics*, *9*(7), 1–14.

Kalender, A., Selvaraj, A., Kim, S. Y., Gulati, P., Brûlé, S., Viollet, B., Kemp, B. E., Bardeesy, N., Dennis, P., Schlager, J. J., Marette, A., Kozma, S. C., & Thomas, G. (2010). Metformin, independent of AMPK, inhibits mTORC1 in a rag GTPase-dependent manner. *Cell Metabolism*, *11*(5), 390–401.

Kang, S. A., Pacold, M. E., Cervantes, C. L., Lim, D., Lou, H. J., Ottina, K., Gray, N. S., Turk, B. E., Yaffe, M. B., Sabatini, D. M., Kang, S. A., Pacold, M. E., Cervantes, C. L., … Sabatini, D. M. (2013). mTORC1 Phosphorylation Sites Encode Their Sensitivity to Starvation and Rapamycin. *Science*, *341*(July).

Kim, M. Y., Bucciarelli, E., Morton, D. G., Williams, B. C., Blake-Hodek, K., Pellacani, C., Von Stetina, J. R., Hu, X., Somma, M. P., Drummond-Barbosa, D., & Goldberg, M. L. (2012). Bypassing the Greatwall-Endosulfine pathway: Plasticity of a pivotal cell-cycle regulatory module in Drosophila melanogaster and caenorhabditis elegans. *Genetics*, *191*(4), 1181–1197.

Kim, Y. M., Jung, C. H., Seo, M., Kim, E. K., Park, J. M., Bae, S. S., & Kim, D. H. (2015). MTORC1 phosphorylates UVRAG to negatively regulate autophagosome and endosome maturation. *Molecular Cell*, *57*(2), 207–218.

Kuo, Y. C., Huang, K. Y., Yang, C. H., Yang, Y. S., Lee, W. Y., & Chiang, C. W. (2008). Regulation of phosphorylation of Thr-308 of Akt, cell proliferation, and survival by the B55α regulatory subunit targeting of the protein phosphatase 2A holoenzyme to Akt. *Journal of Biological Chemistry*, *283*(4), 1882–1892.

Kurimchak, A., & Graña, X. (2012). PP2A Counterbalances Phosphorylation of pRB and Mitotic Proteins by Multiple CDKs: Potential Implications for PP2A Disruption in Cancer. *Genes & Cancer*, *3*(11–12), 739–48.

Kwiatkowski, D., Zhang, H., Bandura, J., Heiberger, K., Glogauer, M., El-Hashemite, N., & Onda, H. (2002). A mouse model of TSC1 reveals sex-dependent lethality from liver hemangiomas, and up-regulation of p70S6 kinase activity in Tsc1 null cells. *Human Molecular Genetics*, *11*(5), 525–534.

Lagarrigue, S., Lopez-Mejia, I. C., Denechaud, P. D., Escoté, X., Castillo-Armengol, J., Jimenez, V., Chavey, C., Giralt, A., Lai, Q., Zhang, L., Martinez-Carreres, L., Delacuisine, B., Annicotte, J. S., … Fajas, L. (2016). CDK4 is an essential insulin effector in adipocytes. *Journal of Clinical Investigation*, *126*(1), 335–348.

Lee, Y., Dominy, J. E., Choi, Y. J., Jurczak, M., Tolliday, N., Camporez, J. P., Chim, H., Lim, J., Ruan, H., Yang, X., Vazquez, F., Sicinski, P., Shulman, G. I., & Puigserver, P. (2014). Cyclin D1-Cdk4 controls glucose metabolism independently of cell cycle progression.

Nature, *510*(7506), 547–551.

Leto, D., & Saltiel, A. R. (2012). Regulation of glucose transport by insulin: traffic control of GLUT4. *Nature Reviews. Molecular Cell Biology*, *13*(6), 383–96.

Lindqvist, A., Rodríguez-Bravo, V., & Medema, R. H. (2009). The decision to enter mitosis: feedback and redundancy in the mitotic entry network. *Journal of Cell Biology*, *185*(2), 193–202.

Llanos, S., García-Pedrero, J. M., Morgado-Palacin, L., Rodrigo, J. P., & Serrano, M. (2016). Stabilization of p21 by mTORC1/4E-BP1 predicts clinical outcome of head and neck cancers. *Nature Communications*, *7*, 10438.

Lorca, T., & Castro, A. (2012). Deciphering the New Role of the Greatwall/PP2A Pathway in Cell Cycle Control. *Genes Cancer*, *3*(11–12), 712–720.

Lum, J. J., Bui, T., Gruber, M., Gordan, J. D., DeBerardinis, R. J., Covello, K. L., Simon, M. C., & Thompson, C. B. (2007). The transcription factor HIF-1 alpha plays a critical role in the growth factor-dependent regulation of both aerobic and anaerobic glycolysis. *Genes & Development*, *21*(9), 1037–1049.

Luo, X., Talarek, N., & De Virgilio, C. (2011). Initiation of the yeast G0 program requires Igo1 and Igo2, which antagonize activation of decapping of specific nutrient-regulated mRNAs. *RNA Biology*, *8*(1), 14–17.

Majumder, P. K., Febbo, P. G., Bikoff, R., Berger, R., Xue, Q., McMahon, L. M., Manola, J., Brugarolas, J., McDonnell, T. J., Golub, T. R., Loda, M., Lane, H. A., & Sellers, W. R. (2004). mTOR inhibition reverses Akt-dependent prostate intraepithelial neoplasia through regulation of apoptotic and HIF-1-dependent pathways. *Nature Medicine*, *10*(6), 594–601.

Malumbres, M., & Barbacid, M. (2001). To cycle or not to cycle: a critical decision in cancer. *Nature Reviews. Cancer*, *1*(3), 222–31.

Manchado, E., Guillamot, M., de Cárcer, G., Eguren, M., Trickey, M., García-Higuera, I., Moreno, S., Yamano, H., Cañamero, M., & Malumbres, M. (2010). Targeting Mitotic Exit Leads to Tumor Regression In Vivo: Modulation by Cdk1, Mastl, and the PP2A/B55??,?? Phosphatase. *Cancer Cell*, *18*(6), 641–654.

Manning, B. D., & Cantley, L. C. (2007). AKT/PKB Signaling: Navigating Downstream. *Cell*, *129*(7), 1261–1274.

Manning, B. D., Tee, A. R., Logsdon, M. N., Blenis, J., & Cantley, L. C. (2002). The PI3K-Akt Pathway Regulates Tuberin Identification of the Tuberous Sclerosis Complex-2 Tumor Suppressor Gene Product Tuberin as a Target of the Phosphoinositide 3- Kinase / Akt Pathway An Approach to Determine Substrates of Protein Kinases a PI3K-Depen. *Cell*, *10*,

151–162.

Manning, B. D., & Toker, A. (2017). AKT/PKB Signaling: Navigating the Network. *Cell*, *169*(3), 381–405.

Martínez González, S., Hernández, A. I., Varela, C., Lorenzo, M., Ramos-Lima, F., Cendón, E., Cebrián, D., Aguirre, E., Gomez-Casero, E., Albarrán, M. I., Alfonso, P., García-Serelde, B., Mateos, G., … Pastor, J. (2012). Rapid identification of ETP-46992, orally bioavailable PI3K inhibitor, selective versus mTOR. *Bioorganic and Medicinal Chemistry Letters*, *22*(16), 5208–5214.

Meng, Z.-X., Gong, J., Chen, Z., Sun, J., Xiao, Y., Wang, L., Li, Y., Liu, J., Xu, X. Z. S., & Lin, J. D. (2017). Glucose Sensing by Skeletal Myocytes Couples Nutrient Signaling to Systemic Homeostasis. *Molecular Cell*, *66*(3), 332–344.e4.

Menon, S., Dibble, C. C., Talbott, G., Hoxhaj, G., Valvezan, A. J., Takahashi, H., Cantley, L. C., & Manning, B. D. (2014). Spatial control of the TSC complex integrates insulin and nutrient regulation of mtorc1 at the lysosome. *Cell*, *156*(4), 1771–1785.

Mochida, S. (2014). Regulation of a – endosulfine , an inhibitor of protein phosphatase 2A , by multisite phosphorylation. *The FEBS Journal*, *281*, 1159–1169.

Mochida, S., Ikeo, S., Gannon, J., & Hunt, T. (2009). Regulated activity of PP2A-B55 delta is crucial for controlling entry into and exit from mitosis in Xenopus egg extracts. *The EMBO Journal*, *28*(18), 2777–85.

Mochida, S., Maslen, S. L., Skehel, M., & Hunt, T. (2010). Greatwall phosphorylates an inhibitor of protein phosphatase 2A that is essential for mitosis. *Science (New York, N.Y.)*, *330*(6011), 1670–3.

Moreno-torres, M., Jaquenoud, M., & Virgilio, C. De. (2015). TORC1 controls G1–S cell cycle transition in yeast via Mpk1 and the greatwall kinase pathway. *Nature Communications*, *6*, 1–10.

Nagel, R., Stigter-Van Walsum, M., Buijze, M., van den Berg, J., van der Meulen, I. H., Hodzic, J., Piersma, S. R., Pham, T. V, Jim Enez, C. R., van Beusechem, V. W., Brakenhoff, R. H., Jimenez, C. R., van Beusechem, V. W., … Brakenhoff, R. H. (2015). Cancer Biology and Signal Transduction Genome-wide siRNA Screen Identifies the Radiosensitizing Effect of Downregulation of MASTL and FOXM1 in NSCLC. *Mol Cancer Ther*, *14*(6), 1–11.

O'Reilly, K. E., Rojo, F., She, Q. B., Solit, D., Mills, G. B., Smith, D., Lane, H., Hofmann, F., Hicklin, D. J., Ludwig, D. L., Baselga, J., & Rosen, N. (2006). mTOR inhibition induces upstream receptor tyrosine kinase signaling and activates Akt. *Cancer Research*, *66*(3), 1500–1508.

O'Shea, C., Klupsch, K., Choi, S., Bagus, B., Soria, C., Shen, J., McCormick, F., & Stokoe, D. (2005). Adenoviral proteins mimic nutrient/growth signals to activate the mTOR pathway for viral replication. *The EMBO Journal*, *24*(6), 1211–21.

Okumura, E., Morita, A., Wakai, M., Mochida, S., Hara, M., & Kishimoto, T. (2014). Cyclin B-Cdk1 inhibits protein phosphatase PP2A-B55 via a greatwall kinase-independent mechanism. *Journal of Cell Biology*, *204*(6), 881–889.

Pedruzzi, I., Dubouloz, F., Cameroni, E., Wanke, V., Roosen, J., Winderickx, J., & De Virgilio, C. (2003). TOR and PKA Signaling Pathways Converge on the Protein Kinase Rim15 to Control Entry into G0. *Molecular Cell*, *12*(6), 1607–1613.

Peng, A., Yamamoto, T. M., Goldberg, M. L., & Maller, J. L. (2010). A novel role for greatwall kinase in recovery from DNA damage. *Cell Cycle*, *9*(21), 4364–4369.

Peterson, R. T., Desai, B. N., Hardwick, J. S., & Schreiber, S. L. (1999). Protein phosphatase 2A interacts with the 70-kDa S6 kinase and is activated by inhibition of FKBP12-rapamycinassociated protein. *Proceedings of the National Academy of Sciences of the United States of America*, *96*(8), 4438–4442.

Quon, M. J., Butte, A. J., Zarnowski, M. J., Sesti, G., Cushman, S. W., & Taylor, S. I. (1994). Insulin-Receptor Substrate-1 Mediates the Stimulatory Effect of Insulin on Glut4 Translocation in Transfected Rat Adipose-Cells. *Journal of Biological Chemistry*, *269*(45), 27920–27924.

Rachdi, L., Balcazar, N., Osorio-Duque, F., Elghazi, L., Weiss, A., Gould, A., Chang-Chen, K. J., Gambello, M. J., & Bernal-Mizrachi, E. (2008). Disruption of Tsc2 in pancreatic beta cells induces beta cell mass expansion and improved glucose tolerance in a TORC1-dependent manner. *Proceedings of the National Academy of Sciences of the United States of America*, *105*(27), 9250–9255.

Reid, M. A., Wang, W. I., Rosales, K. R., Welliver, M. X., Pan, M., & Kong, M. (2013). The B55α Subunit of PP2A Drives a p53-Dependent Metabolic Adaptation to Glutamine Deprivation. *Molecular Cell*, *50*(2), 200–211.

Reinders, A., Bürckert, N., Boller, T., & Bu, N. (1998). Saccharomyces cerevisiae cAMP-dependent protein kinase controls entry into stationary phase through the Rim15p protein kinase, 2943–2955.

Rodrik-Outmezguine, V. S., Chandarlapaty, S., Pagano, N. C., Poulikakos, P. I., Scaltriti, M., Moskatel, E., Baselga, J., Guichard, S., & Rosen, N. (2011). mTOR kinase inhibition causes feedback-dependent biphasic regulation of AKT signaling. *Cancer Discovery*, *1*(3), 248–259.

Rosner, M., & Hengstschläger, M. (2008). Cytoplasmic and nuclear distribution of the protein complexes mTORC1 and mTORC2: Rapamycin triggers dephosphorylation and delocalization of the mTORC2 components rictor and sin1. *Human Molecular Genetics*, *17*(19), 2934–2948.

Roux, P. P., Ballif, B. A., Anjum, R., Gygi, S. P., & Blenis, J. (2004). Tumor-promoting phorbol esters and activated Ras inactivate the tuberous sclerosis tumor suppressor complex via p90 ribosomal S6 kinase. *Proceedings of the National Academy of Sciences of the United States of America*, *101*(37), 13489–94.

Rui, L., Aguirre, V., Kim, J. K., Shulman, G. I., Lee, A., Corbould, A., Dunaif, A., & White, M. F. (2001). Insulin / IGF-1 and TNF-α stimulate phosphorylation of IRS-1 at inhibitory Ser 307 via distinct pathways. *Journal of Clinical Investigation*, *107*(2), 181–189.

Rui, L., Fisher, T. L., Thomas, J., & White, M. F. (2001). Regulation of Insulin/Insulin-like Growth Factor-1 Signaling by Proteasome-mediated Degradation of Insulin Receptor Substrate-2. *Journal of Biological Chemistry*, *276*(43), 40362–40367.

Saltiel, A. R., & Kahn, C. R. (2001). Insulin signalling and the regulation of glucose and lipid metabolism. *Nature*, *414*(6865), 799–806.

Sano, H., Kane, S., Sano, E., Miinea, C., Asara, J., Lane, W., Garner, C., & Lienhard, G. (2003). Insulin-stimulated Phosphorylation of a Rab GTPase-activating Protein Regulates GLUT4 Translocation. *Journal of Biological Chemistry*, *278*(17), 14599–14602.

Saxton, R. A., & Sabatini, D. M. (2017). mTOR Signaling in Growth, Metabolism, and Disease. *Cell*, *168*(6), 960–976.

Schalm, S. S., & Blenis, J. (2002). Identification of a conserved motif required for mTOR signaling. *Current Biology*, *12*(8), 632–639.

Schalm, S. S., Fingar, D. C., Sabatini, D. M., & Blenis, J. (2003). TOS Motif-Mediated Raptor Binding Regulates 4E-BP1 Multisite Phosphorylation and Function. *Current Biology*, *12*, 797–806.

Schmitz, M. H. A., Held, M., Janssens, V., Hutchins, J. R. A., Hudecz, O., Ivanova, E., Goris, J., Trinkle-Mulcahy, L., Lamond, A. I., Poser, I., Hyman, A. A., Mechtler, K., Peters, J.-M., & Gerlich, D. W. (2010). Live-cell imaging RNAi screen identifies PP2A-B55alpha and importin-beta1 as key mitotic exit regulators in human cells. *Nature Cell Biology*, *12*(9), 886–93.

Schuler, M., Dierich, A., Chambon, P., & Metzger, D. (2004). Efficient temporally controlled targeted somatic mutagenesis in hepatocytes of the mouse. *Genesis*, *39*(3), 167–172.

Semenza, G. L., Roth, P. H., Fang, H. M., & Wang, G. L. (1994). Transcriptional regulation of

genes encoding glycolytic enzymes by hypoxia-inducible factor 1. *The Journal of Biological Chemistry*, *269*(38), 23757–63.

Shah, O. J., & Hunter, T. (2006). Turnover of the Active Fraction of IRS1 Involves Raptor-mTOR- and S6K1-Dependent Serine Phosphorylation in Cell Culture Models of Tuberous Sclerosis. *Molecular and Cellular Biology*, *26*(17), 6425–6434.

Shah, O. J., Wang, Z., & Hunter, T. (2004). Inappropriate activation of the TSC/Rheb/mTOR/S6K cassette induces IRS1/2 depletion, insulin resistance, and cell survival deficiencies. *Current Biology*, *14*(18), 1650–1656.

Shaw, R. J., Bardeesy, N., Manning, B. D., Lopez, L., Kosmatka, M., DePinho, R. A., & Cantley, L. C. (2004). The LKB1 tumor suppressor negatively regulates mTOR signaling. *Cancer Cell*, *6*(1), 91–99.

Shimobayashi, M., & Hall, M. N. (2014). Making new contacts: the mTOR network in metabolism and signalling crosstalk. *Nature Reviews. Molecular Cell Biology*, *15*(3), 155–62.

Shirakawa, J., Fernandez, M., Takatani, T., El Ouaamari, A., Jungtrakoon, P., Okawa, E. R., Zhang, W., Yi, P., Doria, A., & Kulkarni, R. N. (2017). Insulin Signaling Regulates the FoxM1/PLK1/CENP-A Pathway to Promote Adaptive Pancreatic β Cell Proliferation. *Cell Metabolism*, 1–15.

Shum, M., Bellmann, K., St-Pierre, P., & Marette, A. (2016). Pharmacological inhibition of S6K1 increases glucose metabolism and Akt signalling in vitro and in diet-induced obese mice. *Diabetologia*, *59*(3), 592–603.

Sofer, A., Lei, K., Johannessen, C. M., & Ellisen, L. W. (2005). Regulation of mTOR and Cell Growth in Response to Energy Stress by REDD1 Regulation of mTOR and Cell Growth in Response to Energy Stress by REDD1, *25*(14), 5834–5845.

Strack, S. (2002). Overexpression of the protein phosphatase 2A regulatory subunit Bgamma promotes neuronal differentiation by activating the MAP kinase (MAPK) cascade. *The Journal of Biological Chemistry*, *277*(44), 41525–32.

Sun, X., Goldberg, J., Qiao, L., & Mitchell, J. (1999). Insulin-induced insulin receptor substrate-1 degradation is mediated by the proteasome degradation pathway. *Diabetes*, *48*(7), 1359–1364.

Taha, C., Liu, Z., Jin, J., Al-hasani, H., Sonenberg, N., & Klip, A. (1999). Opposite Translational Control of GLUT1 and GLUT4 Glucose Transporter mRNAs in Response to Insulin. *Journal of Biological Chemistry*, *274*(46), 33085–33091.

Takano, A., Usui, I., Haruta, T., Kawahara, J., Uno, T., Iwata, M., & Kobayashi, M. (2001). Mammalian target of rapamycin pathway regulates insulin signaling via subcellular

redistribution of insulin receptor substrate 1 and integrates nutritional signals and metabolic signals of insulin. *Molecular and Cellular Biology*, *21*(15), 5050–62.

Talarek, N., Cameroni, E., Jaquenoud, M., Luo, X., Bontron, S., Lippman, S., Devgan, G., Snyder, M., Broach, J. R., & De Virgilio, C. (2010). Initiation of the TORC1-Regulated G0 Program Requires Igo1/2, which License Specific mRNAs to Evade Degradation via the 5′-3′ mRNA Decay Pathway. *Molecular Cell*, *38*(3), 345–355.

Tan, J., Lee, P., Z, L., X, J., YC, L., SC, H., & Q., Y. (2010). B55β-associated PP2A complex controls PDK1-directed myc signaling and modulates rapamycin sensitivity in colorectal cancer. *Cancer Cell*, *18*, 459–471.

Tremblay, F., & Marette, a. (2001). Amino acid and insulin signaling via the mTOR/p70 S6 kinase pathway: A negative feedback mechanism leading to insulin resistance in skeletal muscle cells. *The Journal of Biological Chemistry*, *276*(41), 38052–38060.

Um, S. H., Frigerio, F., Watanabe, M., Picard, F., Joaquin, M., Sticker, M., Fumagalli, S., Allegrini, P. R., Kozma, S. C., Auwerx, J., & Thomas, G. (2004). Absence of S6K1 protects against age- and diet-induced obesity while enhancing insulin sensitivity. *Nature*, *431*(7005), 200–205.

Vander Haar, E., Lee, S.-I., Bandhakavi, S., Griffin, T. J., & Kim, D.-H. (2007). Insulin signalling to mTOR mediated by the Akt/PKB substrate PRAS40. *Nature Cell Biology*, *9*(3), 316–23.

Vera, J., Lartigue, L., Vigneron, S., Gadea, G., Gire, V., Del Rio, M., Soubeyran, I., Chibon, F., Lorca, T., & Castro, A. (2015). Greatwall promotes cell transformation by hyperactivating AKT in human malignancies. *eLife*, *4*(NOVEMBER2015), 1–24.

Vigneron, S., Brioudes, E., Burgess, A., Labbé, J.-C., Lorca, T., & Castro, A. (2009). Greatwall maintains mitosis through regulation of PP2A. *The EMBO Journal*, *28*(18), 2786–93.

Vigneron, S., Gharbi-ayachi, A., Burgess, A., Labbe, J., Labesse, G., Monsarrat, B., Lorca, T., & Castro, A. (2011). Characterization of the Mechanisms Controlling Greatwall Activity . *Molecular and Cellular Biology*, *31*(11), 2262–2275.

Vigneron, S., Gharbi-Ayachi, A., Raymond, A.-A., Burgess, A., Labbé, J.-C., Labesse, G., Monsarrat, B., Lorca, T., & Castro, A. (2011). Characterization of the mechanisms controlling Greatwall activity. *Molecular and Cellular Biology*, *31*(11), 2262–75.

Vigneron, S., Robert, P., Hached, K., Sundermann, L., Charrasse, S., Labbé, J., Castro, A., & Lorca, T. (2016). The master Greatwall kinase , a critical regulator of mitosis and meiosis. *The International Journal of Developmental Biology*, *254*(May), 245–254.

Virsolvy-Vergine, A., Leray, H., Kuroki, S., Lupo, B., Dufour, M., & Bataille, D. (1992). Endosulfine, an endogenous peptidic ligand for the sulfonylurea receptor: purification and

partial characterization from ovine brain. *Proceedings of the National Academy of Sciences of the United States of America*, *89*(14), 6629–33.

Voets, E., & Wolthuis, R. M. F. (2010). MASTL is the human orthologue of Greatwall kinase that facilitates mitotic entry, anaphase and cytokinesis. *Cell Cycle*, *9*(17), 3591–3601.

Wang, L., Balas, B., Christ-Roberts, C. Y., Kim, R. Y., Ramos, F. J., Kikani, C. K., Li, C., Deng, C., Reyna, S., Musi, N., Dong, L. Q., DeFronzo, R. a, & Liu, F. (2007). Peripheral disruption of the Grb10 gene enhances insulin signaling and sensitivity in vivo. *Molecular and Cellular Biology*, *27*(18), 6497–6505.

Wang, L., Vivian Q. Luong, Giannini, P. J., & Peng, A. (2014). Mastl kinase, a promising therapeutic target, promotes cancer recurrence. *Oncotarget*, *5*, 11479–11489.

Wang, P., Galan, J. A., Normandin, K., Bonneil, É., Hickson, G. R., Roux, P. P., Thibault, P., & Archambault, V. (2013). Cell cycle regulation of Greatwall kinase nuclear localization facilitates mitotic progression. *Journal of Cell Biology*, *202*(2), 277–293.

Wanke, V., Pedruzzi, I., Cameroni, E., Dubouloz, F., & De Virgilio, C. (2005). Regulation of G0 entry by the Pho80-Pho85 cyclin-CDK complex. *The EMBO Journal*, *24*(24), 4271–4278.

Wei, F., Nagashima, K., Ohshima, T., Saheki, Y., Lu, Y., Matsushita, M., Yamada, Y., Mikoshiba, K., Seino, Y., Matsui, H., & Tomizawa, K. (2005). Cdk5-dependent regulation of glucose-stimulated insulin secretion, *11*(10), 1104–1108.

Wei, M., Fabrizio, P., Hu, J., Ge, H., Cheng, C., Li, L., & Longo, V. D. (2008). Life span extension by calorie restriction depends on Rim15 and transcription factors downstream of Ras/PKA, Tor, and Sch9. *PLoS Genetics*, *4*(1), 0139–0149.

White, R. E., & Giffard, R. G. (2013). MicroRNA-320 Induces Neurite Outgrowth by Targeting ARPP-19. *Neuroreport*, *23*, 590–595.

Wiles, V. M., Baribault, H., & Zhang, Q. (2002). Transgenic mice containing Alpha-endosulfine gene disruptions.

Williams, B. C., Filter, J. J., Blake-Hodek, K. A., Wadzinski, B. E., Fuda, N. J., Shalloway, D., & Goldberg, M. L. (2014). Greatwall-phosphorylated Endosulfine is both an inhibitor and a substrate of PP2A-B55 heterotrimers. *eLife*, *2014*(3), 1–34.

Wlodarchak, N., & Xing, Y. (2016). PP2a as a master regulator of cell cycle, *51*(3), 162–184.

Wong, P.-M., Feng, Y., Wang, J., Shi, R., & Jiang, X. (2015). Regulation of autophagy by coordinated action of mTORC1 and protein phosphatase 2A. *Nature Communications*, *6*, 8048.

Wong, P. Y., Ma, H. T., Lee, H., & Poon, R. Y. C. (2016). MASTL(Greatwall) regulates DNA damage responses by coordinating mitotic entry after checkpoint recovery and APC/C

activation. *Scientific Reports*, *6*, 22230.

Wurzenberger, C., & Gerlich, D. W. (2011). Phosphatases: providing safe passage through mitotic exit. *Nature Reviews. Molecular Cell Biology*, *12*(8), 469–82.

Yan, L., Mieulet, V., Burgess, D., Findlay, G. M., Sully, K., Procter, J., Goris, J., Janssens, V., Morrice, N. A., & Lamb, R. F. (2010). PP2AT61?? Is an Inhibitor of MAP4K3 in Nutrient Signaling to mTOR. *Molecular Cell*, *37*(5), 633–642.

Yonghao, Y., Sang-Oh, Y., Poulogiannis, G., Yang, Q., Ma, X. M., Villén, J., Kubica, N., Hoffman, G. R., Cantley, L. C., Gygi, S. P., & Blenis, J. (2011). Phosphoproteomic analysis identifies Grb10 as an mTORC1 substrate that negatively regulates insulin signaling. *Science (New York, N.Y.)*, *332*(6035), 1322–6.

Yoo, S. J. S., Jimenez, R. H., Sanders, J. A., Boylan, J. M., Brautigan, D. L., & Gruppuso, P. A. (2008). The ??4-containing form of protein phosphatase 2A in liver and hepatic cells. *Journal of Cellular Biochemistry*, *105*(1), 290–300.

Yu, J., Fleming, S. L., Williams, B., Williams, E. V., Li, Z., Somma, P., Rieder, C. L., & Goldberg, M. L. (2004). Greatwall kinase: A nuclear protein required for proper chromosome condensation and mitotic progression in Drosophila. *Journal of Cell Biology*, *164*(4), 487–492.

Yu, J., Zhao, Y., Li, Z., Galas, S., & Goldberg, M. L. (2006). Greatwall Kinase Participates in the Cdc2 Autoregulatory Loop in Xenopus Egg Extracts. *Molecular Cell*, *22*(1), 83–91.

Zacharek, S. J., Xiong, Y., & Shumway, S. D. (2005). Negative regulation of TSC1-TSC2 by mammalian D-type cyclins. *Cancer Research*, *65*(24), 11354–11360.

Zelzer, E., Levy, Y., Kahana, C., Shilo, B. Z., Rubinstein, M., & Cohen, B. (1998). Insulin induces transcription of target genes through the hypoxia- inducible factor HIF-1alpha/ARNT. *Embo J*, *17*(17), 5085–5094.

Zhang, H., Bajraszewski, N., Wu, E., Wang, H., Moseman, A. P., Dabora, S. L., Griffin, J. D., & Kwiatkowski, D. J. (2007). PDGFRs are critical for PI3K/Akt activation and negatively regulated by mTOR. *Journal of Clinical Investigation*, *117*(3), 730–738.

Zhang, H. H., Lipovsky, A. I., Dibble, C. C., Sahin, M., & Manning, B. D. (2006). S6K1 Regulates GSK3 under Conditions of mTOR-Dependent Feedback Inhibition of Akt. *Molecular Cell*, *24*(2), 185–197.

Zhang, X., Shu, L., Hosoi, H., Gopal Murti, K., & Houghton, P. J. (2002). Predominant nuclear localization of mammalian target of rapamycin in normal and malignant cells in culture. *Journal of Biological Chemistry*, *277*(31), 28127–28134.

Zheng, M., Wang, Y.-H., Wu, X.-N., Wu, S.-Q., Lu, B.-J., Dong, M.-Q., Zhang, H., Sun, P., Lin, S.-

C., Guan, K.-L., & Han, J. (2011). Inactivation of Rheb by PRAK-mediated phosphorylation is essential for energy-depletion-induced suppression of mTORC1. *Nature Cell Biology*, *13*(3), 263–272.

Zinzalla, V., Stracka, D., Oppliger, W., & Hall, M. N. (2011). Activation of mTORC2 by association with the ribosome. *Cell*, *144*(5), 757–768.

Zoncu, R., Efeyan, A., & Sabatini, D. M. (2011). mTOR: from growth signal integration to cancer, diabetes and ageing. *Nature Reviews. Molecular Cell Biology*, *12*(1), 21–35.

Annex

Álvarez-Fernández, M., Sánchez-Martínez, R., **Sanz-Castillo, B**., Gan, P.P., Sanz-Flores, M., Trakala, M., Ruiz-Torres, M., Lorca, T., Castro, A., and Malumbres, M. (2013). Greatwall is essential to prevent mitotic collapse after nuclear envelope breakdown in mammals. *Proc. Natl. Acad. Sci. 110*, 17374–17379.

Mónica Álvarez-Fernández, María Sanz-Flores, Belén Sanz-Castillo, María Salazar-Roa, David Partida, H. Raza Ali, Eusebio Manchado, Scott Lowe, Todd VanArsdale, David Shields, Carlos Caldas, Miguel Quintela-Fandino and Marcos Malumbres. MASTL/Greatwall kinase activity as a new therapeutic target in breast cancer. *Submitted*